A STUDY OF THE MOLECULAR PROPERTIES OF RAT-TAIL TENDON COLLAGEN AND AN INVESTIGATION OF THE STRUCTURE OF FEATHER KERATIN

Thesis by

Joseph Kraut

In Partial Fulfillment of the Requirements

for the Degree of

Doctor of Philosophy

California Institute of Technology

Pasadena, California

1954

ACKNOWLEDGEMENT

The author wishes to express his gratitude to Professor D. H. Campbell for his introduction to the technique of light scattering, to Dr. J. R. Vinograd for many hours of helpful discussion during the course of the investigation of collagen and gelatin, and to Professor Linus Pauling , Professor R. B. Corey and Dr. R. E. Marsh for their indispensable advice and assistance in connection with the study of feather keratin.

The author is also grateful to the National Science Foundation for the fellowship awarded him during the course of this work.

ABSTRACT

Some experimental aspects of the study of large molecules by the technique of light scattering are examined.

The application of this technique to the study of rat-tail tendon collagen is then discussed. Investigations of this protein dissolved in dilute acetic acid and in concentrated urea, and a study of its transformation to "parent" gelatin lead to the suggestion of a schematic picture of the collagen molecule.

A brief study of a fractionated gelatin is then described, and its molecular weight and some conclusions concerning possible molecular sizes are reported. The difficulties inherent in the investigation of gelatin solutions are examined.

The final Part is concerned with a study of the structure of feather keratin by x-ray diffraction methods. The known meridional and equatorial spacings are revised and extended on the basis of measurements made on newly obtained diffraction photographs. Observed intensities are compared with those predicted for a structure which has been recently suggested.

TABLE OF CONTENTS

PART I - THE TECHNIQUE OF LIGHT SCATTERING

A) Introduction.

The use of the technique of light scattering in its present form, by means of which the molecular properties of proteins, high-polymers, and other large molecules are determined from the behavior of a parallel beam of light upon passing through a solution containing such molecules, may be considered to have had its beginning in 1944. In that year, Debye (1) showed that molecular weights, shapes and thermodynamic properties of large molecules could be obtained exclusively from an analysis of the light-scattering behavior of their solutions. The theoretical background upon which Debye based his conclusions had been elucidated much earlier, however. In 1871 Lord Rayleigh (2) presented his theory of the molecular scattering of light, and in 1910 Einstein (3) showed its connection with thermodynamics by application of the theory of statistical fluctuations. This theoretical background has been reviewed elsewhere, (4), (5), (6), (7), and will not be summarized here.

Since 1944, the technique of light scattering has undergone a rapid evolution which is continuing at present. Being thus still in a developmental stage, its methods have not yet become standardized and vary widely from one investigator to another. Hence it is necessary to devote

Part I of this dissertation to a discussion of the techniques which have been developed, adapted and adopted by the author before presenting the results which have been obtained from an investigation of the light-scattering properties of collagen and gelatin solutions employing these techniques.

B) Modification of the apparatus.

The light-scattering instrument used in these investigations is a commercial model of the Brice type (8) manufactured by the Process and Instruments Corporation, Brooklyn, New York. As originally constructed, it was equipped to employ a square cell for measuring transverse scattering and an hexagonal cell for measuring scattering at angles of 45 degrees and 135 degrees to the direction of the incident beam. The former required about 35 $cm.^3$ of solution, and the latter about 50 $cm.^3$ Two limitations inherent in this arrangement are apparent. First, a large quantity of optically clear solution is required, and second, it is impossible to obtain complete angular scattering data. The latter are necessary to determine the family of Zimm curves (9) characteristic of the molecule under investigation, and it has become increasingly evident that only when these curves are available can the interpretation of the data be considered completely reliable for molecules which are comparable in size to

the wavelength of light.

For these reasons it was deemed advisable to modify somewhat the original design of the apparatus. A new type of light-scattering cell was obtained from the Pyrocell Corporation, New York City. Since this cell had not yet been described in the literature, it was necessary to investigate its utility for light-scattering measurements rather completely. The cell consists of an half cylinder divided by a partition into a solution compartment and a compartment for the pure solvent, as shown in figure 1. The solution compartment has a capacity of about 10 $cm.^3$ This design has the advantages of employing a small quantity of scattering solution while retaining a long illuminated path, and of allowing the scattered intensity to be measured at any angle to the direction of the incident beam.

Since the width of the solution compartment is only 5 mm. and the width of the incident light beam in the instrument was originally 12 mm., it was necessary to alter the collimating system. The lenses and apertures between the mercury arc lamp and the cell holder were replaced by the system shown in schematic outline in figure 2. The aperture A_1 has a width of 22 mm. A_2 is adjustable and is normally set at 5 mm. A_3 and A_4 have widths of 15 mm. and 10 mm. respectively. M is an AH-4 mercury arc lamp. L is a convex lens of diameter 29 mm.

and focal length 45 mm. The lens is placed about 50 mm. from the center of the lamp. H is the housing for the neutral-filter carriage. F represents the monochromatizing filter for isolating a single line in the spectrum of the mercury arc. This arrangement was found to give substantially the same total illumination of the scattering solution as the original design, but a narrower beam of adjustable width and with a divergence of less than two degrees horizontally and less than one degree in the vertical direction. The divergence can be further reduced, if desired, by stopping down the circular diaphragm on the shutter mounting. It was not found necessary to do so in any of the work described in this dissertation.

The path of the incident light beam through the cell, and the field of vision of the photomultiplier when set at ninety degrees to the direction of the incident beam are illustrated in figure 3. The diagram is drawn as though no change in refractive index occurs at any of the glass-air or water-glass interfaces. In fact such refractive index changes will slightly alter the readings obtained when measuring scattering intensities, and this effect must be compensated by application of the appropriate correction factor. This correction is discussed in Section D, subsection 2.

A minor change was also made in the nosepiece of the photomultiplier housing. This device acts not only as

part of the aperture system of the photomultiplier, but also functions as a mounting for the removable polaroid filter. As this nosepiece was originally constructed, the polaroid could be rotated through an angle of ninety degrees. A slight change of the nosepiece, however, permitted a rotation of the polaroid filter through 180 degrees, thereby making it possible to adjust the polaroid for the maximum galvanometer deflection when viewing the transversely scattered light. In this position, the polaroid axis is aligned so as to transmit the vertically polarized component of the scattered light. Rotation of the polaroid, then, through ninety degrees, or until the galvanometer deflection is a minimum, places the polaroid in the position to transmit the horizontally polarized component of the scattered light. The relative intensities of these two components are needed to determine the "depolarization factor", which will be discussed in Section D, subsection 2. This slight modification enables one to obtain an accurate measurement of this quantity without first placing the polaroid axis in a special position relative to its holder, as was previously necessary.

One further modification was necessary in order to eliminate a small amount of residual reflection from the incident beam trap. Covering its rear surface with a piece of black velvet proved to be satisfactory for this purpose.

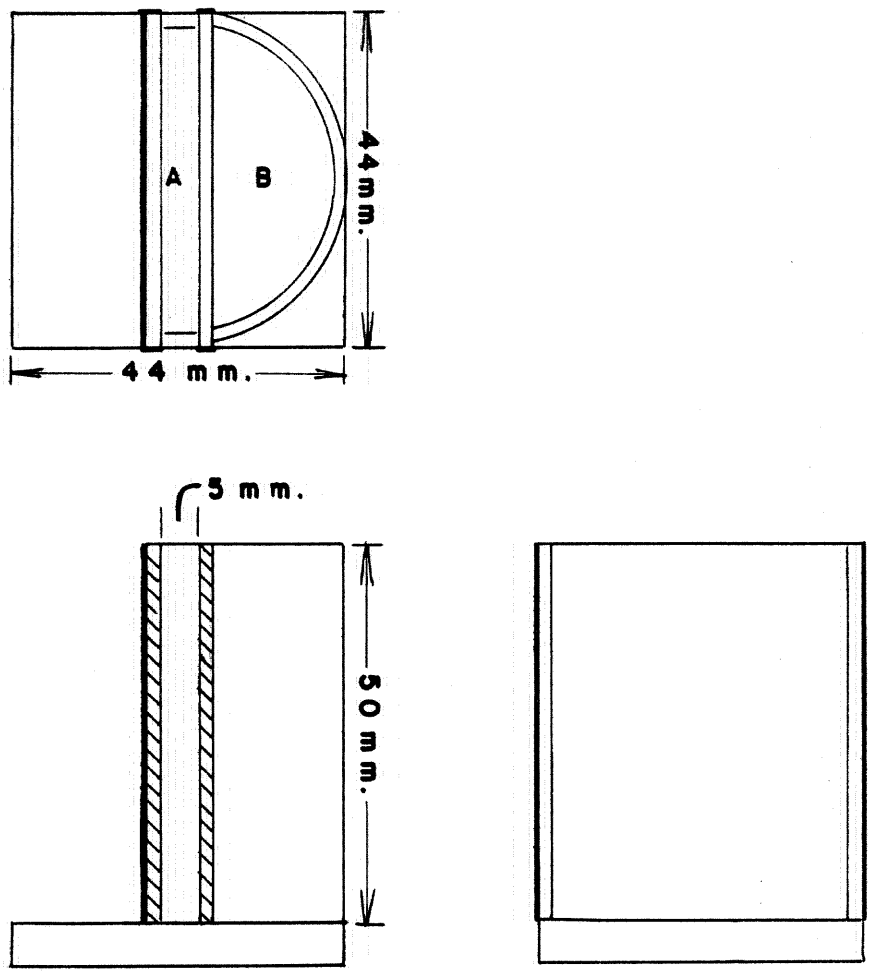

FIGURE I

LIGHT SCATTERING CELL

A. solution compartment
B. solvent compartment

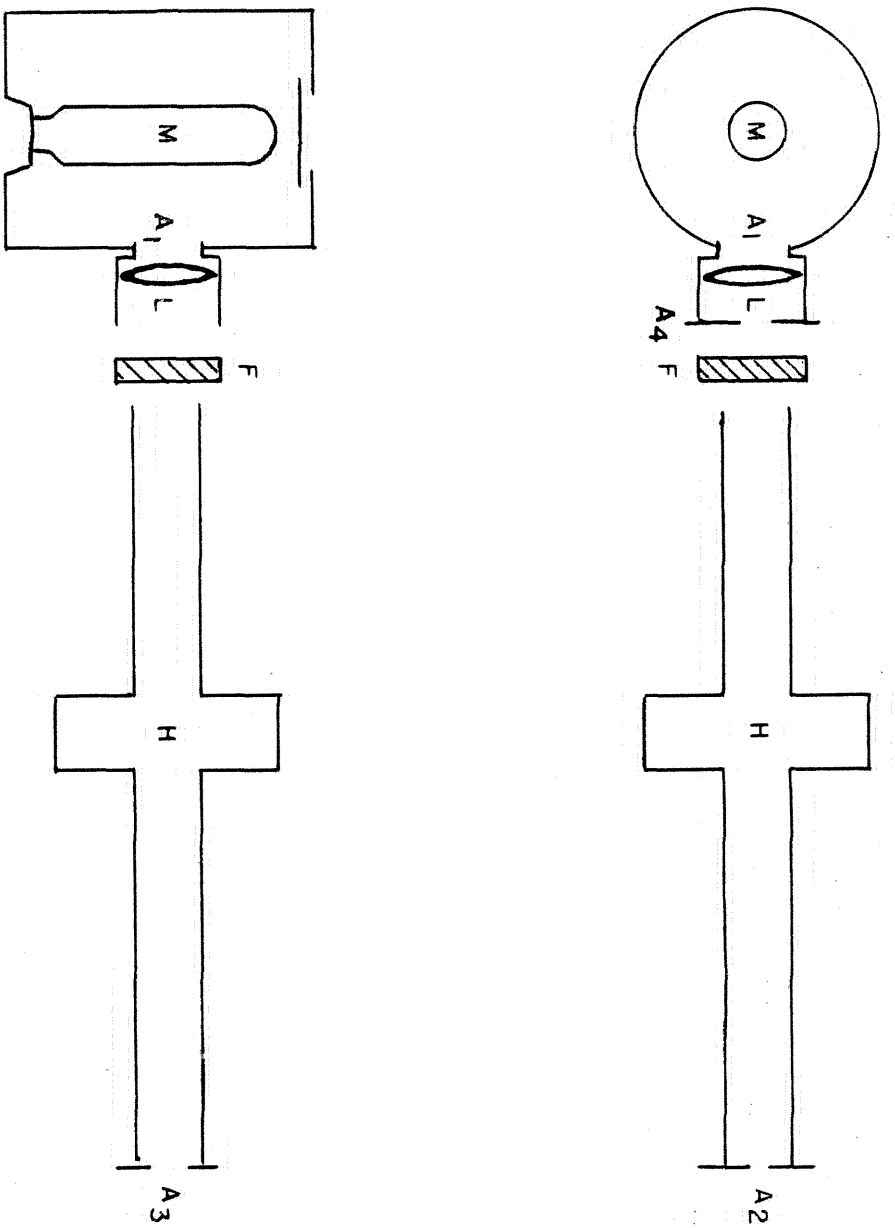

FIGURE 2

COLLIMATING SYSTEM

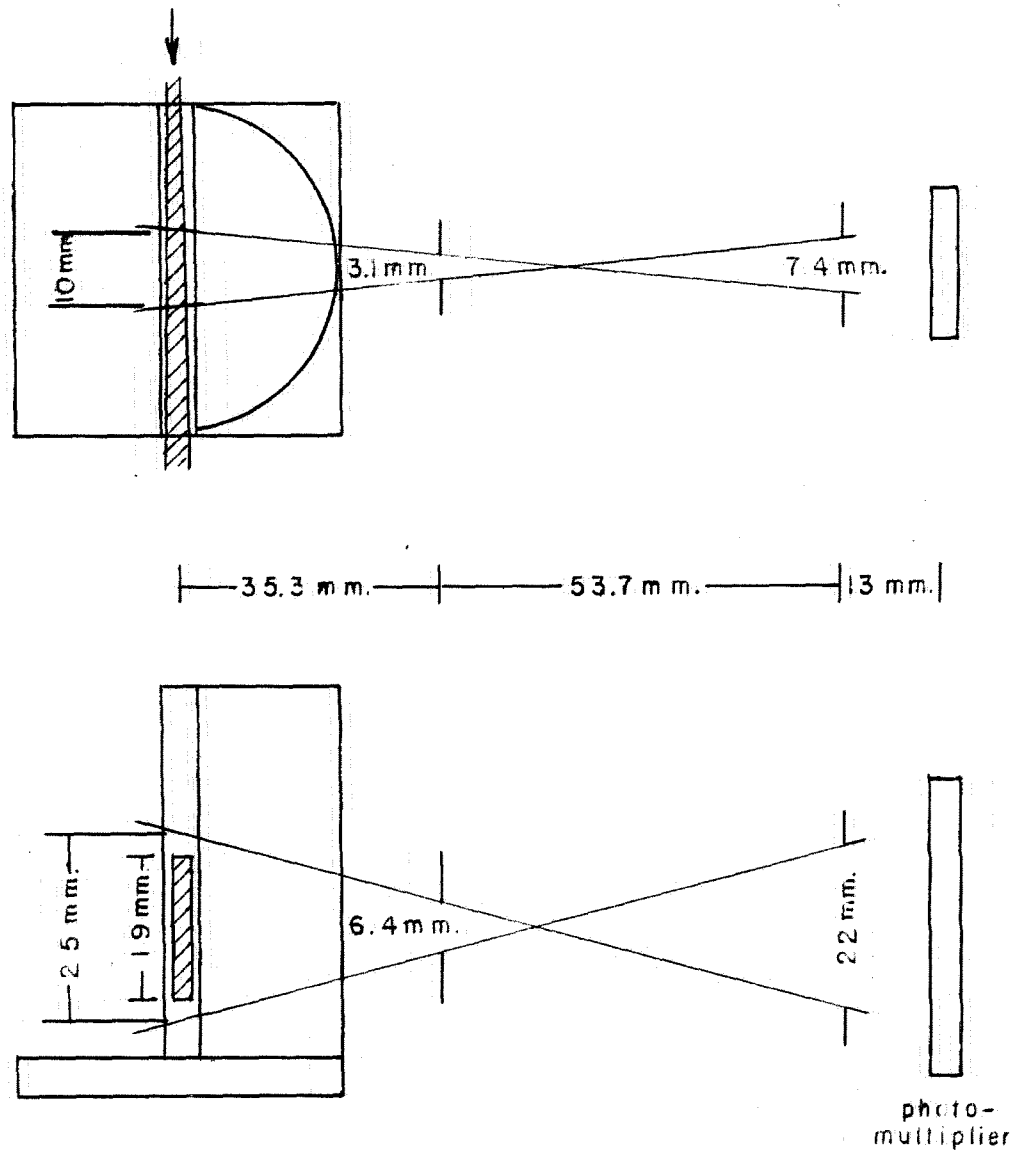

FIGURE 3

PATH OF INCIDENT LIGHT BEAM
AND PHOTOMULTIPLIER FIELD OF VIEW

C) Standardization of the apparatus.

Before making scattering measurements on unknown systems, it is necessary to eliminate spurious optical effects which may introduce errors. This Section describes the search for such effects and their elimination.

1) The sensitivity of the photomultiplier to vertically and horizontally polarized light.

The following test was performed to determine whether the photomultiplier shows a difference in sensitivity toward vertically and horizontally polarized light. The incident beam was reduced in intensity by interposing an opal glass diffuser and a neutral filter. The 546 mμ. (green) line of the mercury arc was isolated by means of the filter described below. The photomultiplier was set at zero degrees, directly intercepting the incident beam. The polaroid filter was placed before the photomultiplier and rotated so that the vertical and the horizontal components were alternately passed, while galvanometer deflections were recorded for each. This procedure was repeated at various incident intensities. The instrument showed 1.1% higher sensitivity to the horizontal component. This effect should be compensated when extremely accurate depolarization measurements are required, though in these investigations such was not the case.

2) Transmission of the light filters.

Since the intensity of Rayleigh scattering is proportional to λ^{-4}, it is important that the incident light be as nearly monochromatic as possible and of precisely known wavelength, λ. Two sets of glass filters are furnished with the instrument, one for isolating the 546 mμ. line, and the other for isolating the 436 mμ. (blue) line of the mercury arc spectrum. The curves of optical density versus wavelength were determined for these filters using a Beckmann model DU spectrophotometer. They showed no secondary maxima, and widths of 25 mμ. and 37 mμ. at optical densities corresponding to transmission of one-half of their maximum transmitted intensities, for the 546 mμ. and 436 mμ. filters respectively.

3) Reflections from cell walls.

Serious errors may be introduced into light-scattering measurements if care is not taken to eliminate reflection of the scattered light at the walls of the cell. This is particularly true of measurements at small angles to the incident beam. Most serious reflections can be expected to occur at the glass-air interface of the back wall of the solution compartment due to the relatively large refractive index change occurring there and to the large portion of this interface which is viewed by the photomultiplier (see figure 3). That such reflections do indeed

appear, and that they have been successfully eliminated is clearly seen from the data of table 1. These data were obtained as follows: the solution compartment of a cell was filled with a dilute solution of fluorescein in water. The 436 mμ. filter was placed in the incident beam and a yellow filter (Corning #3484) was placed over the aperture of the photomultiplier nosepiece. The latter filter eliminated the scattered blue light and permitted the passage only of the yellow light due to fluorescence. In the absence of reflections the intensity read by the photomultiplier should be proportional to $1/\sin \theta$ at any angle, θ, to the incident beam, since the volume of illuminated solution seen by the photomultiplier is proportional to $1/\sin \theta$ and since the intensity of fluorescent radiation is the same in all directions. In table 1, the function $1/\sin \theta$ is listed in line 1, and the ratio of the photomultiplier reading at angle θ to that at ninety degrees is indicated in line 2. The agreement is poor at angles far from ninety degrees.

The same cell was then painted, as indicated in figure 1 by heavy black lines and cross-hatching, with Melanoid Bituminous Paint manufactured by I. C. I. Paints, Ltd., Slough, England and kindly supplied by Professor R. M. Badger. Lines 3, 4, 5, and 6 of table 1 show the relative readings obtained with the painted cell for four different dilutions of the fluorescein solution. Evidently the source of reflections causing deviations from

Table 1

angle, θ	31°	40°	45°	50°	60°	70°	80°	90°	100°	120°	130°	135°
1. 1/sin θ	1.94	1.55	1.41	1.30	1.15	1.06	1.01	1.00	1.01	1.15	1.30	1.41
2. unpainted	3.72	2.94	1.67	1.38	1.18	1.06	1.00	1.00	1.03	1.21	-	1.53
3. painted	1.94	1.55	1.44	1.32	1.17	1.07	1.01	1.00	1.01	1.14	1.31	1.40
4. painted	1.85	1.53	1.41	1.29	1.14	1.06	1.01	1.00	1.01	1.14	1.28	1.36
5. painted	1.79	1.47	1.39	1.31	1.14	1.06	1.01	1.00	1.02	1.17	1.30	1.39
6. painted	1.83	1.48	1.39	1.32	1.16	1.09	1.04	1.00	1.04	1.18	1.33	1.44

Relative photomultiplier readings with illuminated fluorescein solutions in unpainted and in painted light-scattering cells. All readings have been adjusted to unity at ninety degrees.

$1/\sin\theta$ has been effectively eliminated. The somewhat low readings at 31° and at 40° may be due to decreased transmission of the light scattered at these angles through the wall between the solution and solvent compartments.

Melanoid Bituminous Paint is to be recommended not only for its ability to eliminate reflections, but also because of its durability. These cells were used for several months before it became necessary to repaint them. The paint can be removed easily when desired by rinsing the cells in warm benzene. The procedure recommended for painting is to mask those areas of the cell which are to be left unpainted and apply the paint, thinned somewhat with benzene, by means of a spray-gun. The paint dries rapidly in air and the cells can be used within twenty-four hours.

D) Obtaining data.

The quantity of interest in light-scattering measurements is the Rayleigh ratio, $R(\theta)$, which is defined as

$$R(\theta) = \frac{J(\theta)}{I_o} = \frac{i(\theta,r)\, r^2}{I_o} \qquad \text{I}$$

where θ is the angle between the incident beam and the scattered ray, $J(\theta)$ is the radiant intensity (erg $\sec^{-1}\omega^{-1}$) emitted in the direction θ by unit volume of scattering fluid, I_o is the irradiance (erg $\sec^{-1}$ cm^{-2}) of the incident

unpolarized beam, and $i(\theta,r)$ is the irradiance per unit volume of scattering fluid due to the scattered light at the distance r from the scattering volume element, and at the angle θ.

The importance of $R(\theta)$ lies in the fact that it is related to the molecular weight, shape, size, and solvent-solute interaction of the solute molecules. The molecular weight is a function of the limiting value of $R(0)/c$, where c is the solute concentration, as c becomes zero. The shape and size of the solute molecules are obtained from the dependence of $\lim_{c \to 0} R(\theta)/c$ on θ. The solvent-solute interaction is given by the dependence of $R(0)/c$ on the concentration of the solute*. The theory and explicit form of these relations has been adequately reviewed (4), (5), (6), (7). However, since the details of experimental procedures are frequently sketchy or lacking in the literature, vary somewhat from one laboratory to another, and are still undergoing development, they may profitably be examined here.

1) Methods of measurement.

There exist essentially three distinct experimental methods of obtaining the required data; the absolute method in which the absolute value of $R(\theta)$ is determined without reference to the scattering power of some previously deter-

---

* These relationships are usually stated in terms of R(90) or τ, the solution turbidity. The above are equivalent, though simpler and more general.

mined standard; the relative method in which the scattering from the solution under investigation is compared directly to the known intensity of scattering from some standard; and the turbidity method in which the total scattered light flux is determined.

a) The absolute method.

Here one measures directly the ratio of $i(\theta,r)$ to I_o. Since the latter is of the order of 10^6 times as great as the former, it is necessary to attenuate the incident beam by a known factor of this magnitude before measuring its intensity with the photomultiplier. This is normally accomplished by placing the proper neutral filters in the beam. However, filters of optical density as great as this (optical density equal to six) are extremely difficult to calibrate. Occasionally, a combination of neutral filters of lower density and a diffuse reflector of known reflectance are employed to obtain attenuation by a known factor, but the advantage gained by use of a filter of low density is lost in the increased complexity introduced with the reflector. For a discussion of recent efforts to determine the absolute scattering powers of several pure liquids and solutions, see references (8) and (9).

As originally designed, the instrument used in this laboratory was supposed to be capable of absolute measurements. However, in view of the difficulties inherent in

obtaining absolute measurements, it was deemed preferable to employ the relative method.

b) The relative method.

Any substance of reproducible and accurately known light-scattering power can be employed as a standard against which the scattering power of unknowns can be compared. Benzene seems to be the standard of choice since it can be readily purified, has a rather high scattering power compared to most pure liquids, and has a value of R(90) which is known for two convenient wavelengths of light. These are given by Carr and Zimm (9) as 48.5×10^{-6} for 436 mμ. and 16.3×10^{-6} for 546 mμ. These values are used throughout the light-scattering determinations subsequently to be described.

The advantage of the relative method as compared with absolute measurements is the greater likelihood of balancing small errors inherent in the geometry of the apparatus, since the standard scattering is measured under conditions identical with those under which the unknown is measured.

Benzene is not the ideal standard liquid, however. It has a refractive index of 1.52 for light of wavelength 4358 A. (9), whereas most of the aqueous solutions to be investigated have refractive indexes near 1.34 at that wavelength. The effect due to this difference must be allowed for. The necessary correction will be discussed in subsection 2 of this Section. Furthermore, though the scattering power of benzene is high relative to most pure

liquids, it is still only in the neighborhood of 1/20 th as great as that of most of the solutions examined in this investigation. This frequently necessitates a change of scale on the galvanometer when comparing the two, which may introduce a small error. The ideal standard would be an aqueous solution of some highly scattering substance which could be reproducibly prepared and stable. Such a standard is not yet available.

c) The turbidity method.

A measure of the total flux scattered by unit volume of a fluid is given by its "turbidity". It is related to the optical density of ordinary spectrophotometry, for colorless solutions, by the equation

$$\tau = \frac{2.303\, d}{l} \qquad \text{II}$$

where τ is the turbidity, d is the optical density, and l is the length of the column of liquid through which the beam of light is passed. In general the relation between τ and $R(\theta)$ is a complicated one (10), (11) which depends upon the size and shape of the scattering particles in the solution. However, for sufficiently small and optically isotropic particles, it assumes the simple form (for $\tau l \ll 1$)

$$\tau = \frac{16\pi}{3} R(90) \qquad \text{III}$$

$$R(\theta) = (1 + \cos^2 \theta) \cdot R(90) \qquad \text{IV}$$

Hence for such particles, a measurement of the optical density of their solution by the well standardized methods of spectrophotometry is equivalent to a light-scattering determination of $R(\theta)$. It is only necessary that the solution have a sufficiently high optical density to be easily measurable without resorting to the use of excessively long cuvettes.

2) Correction of experimental measurements.

Before the measurements can be used to compute the properties of the solute molecules under investigation, it is necessary to correct for several optical effects which cannot be eliminated in the experimental procedure. Some of these can be safely ignored except in extreme situations. Since a summary of all the corrections which may be necessary is not available in the literature, it seems desirable to review them briefly here. Throughout the light-scattering investigations to be described, those corrections which were believed to be of significance will be indicated.

a) Solvent scattering.

The light scattered from a solvent which has been purified by the same procedure as applied to the solution must be measured and subtracted from the solution scattering to obtain the scattering due to the solute particles. Solvent scattering usually amounts to about 2% of that from the most dilute solution when water is the solvent,

but it may be as high as 22% in extreme cases, such as when 5M urea is used as a solvent. This correction also includes a correction for the scattering from traces of dust and for possible residual reflections.

b) Optical density correction.

From figure 3 it is evident that the incident beam must traverse about 2.2 cm. of the solution before reaching the center of the cell where the scattering is viewed by the photomultiplier. Hence the incident intensity to be used in calculating $R(\theta)$ will depend itself upon the turbidity of the solution. Fortunately, the attenuation of the incident beam in this manner is extremely slight for most solutions at low concentrations (usually less than one percent) and is eliminated by an extrapolation to zero concentration. However, when it is desired to obtain accurate values of $R(\theta)$ for a solution of high turbidity, or when an accurate value of the concentration-dependence constant, B, is required, the correction for this effect should be applied. This can be done to a sufficient approximation by determining the turbidity of the solution in the spectrophotometer and using the relation

$$\frac{I_o'}{I_o} = e^{-\tau l} \qquad V$$

where I_o is the original incident intensity, I_o' is the intensity incident upon the scattering volume at the center

of the cell, and ℓ is the length of the path traversed by the incident beam in the solution before reaching the scattering volume element which is seen by the photomultiplier, in this case 2.2 cm.

c) Reflection of the incident beam.

It is interesting that attention was first directed toward the necessity of making this correction as late as 1952 (12). When a beam of light is normally incident upon the plane interface between two transparent phases of different refractive indexes, the fraction of incident intensity which is reflected is

$$R = \left(\frac{n_2 - n_1}{n_2 \quad n_1}\right)^2 \qquad \text{VI}$$

where R is the fraction of the incident intensity which is reflected, and n_1 and n_2 are the refractive indexes of phases 1 and 2 respectively. The light-scattering cells used here are constructed of pyrex glass with $n_d = 1.4727$. Thus at the interface between the cell wall and the surrounding air $R = 0.036$ and the scattered light is due not only to the incident beam, but also contains contributions from the scattering of the reflected beam. This effect may be neglected if the angular distribution of scattered intensity is symmetrical about 90 degrees, as it is for small particles, since it is cancelled by an identical effect in the benzene standard. However, for largerparticles, where there is deviation from such symmetry and where the

angular dependence of the scattering is of interest, this effect must be compensated. This is done by using

$$J(\theta) = J_a(\theta) - R \cdot J_a(180 - \theta) \qquad \text{VII}$$

where $J(\theta)$ is the true radiant intensity scattered in the direction θ, $J_a(\theta)$ is the apparent (uncorrected) radiant intensity scattered in the direction θ, and R is given by equation VI. The same correction must also be applied to the reading given by the standard. As an illustration of the magnitude of this effect, it may be pointed out that an apparent dissymmetry* of 1.50 would become 1.55 upon applying the correction above.

The value of R for the water-glass interface is only 7% of that for the glass-air interface, and thus its effect may be neglected.

d) The volume effect.

As pointed out in Section C, subsection 3, the volume of illuminated solution viewed by the photomultiplier is proportional to $1/\sin\theta$. To allow for this fact the apparent $R(\theta)$ must be multiplied by $\sin\theta$.

e) The refractive index effect.

Since the photomultiplier must have a finite aperture, some of the scattered rays that are seen by it have not

---

* The dissymmetry, z, is defined as $J(45)/J(135)$ and is a convenient measure of the size of the scattering particles. For particles with a maximum dimension less than about 1/20 th of the wavelength of light, the dissymmetry will be equal to unity. For larger particles z will be greater than unity.

passed normally through the face of the light-scattering cell and so have suffered refraction. With a standard of the same refractive index as the solution being examined, the effect would be identical for both and would cancel. However, it must be considered when absolute determinations are to be made or when a standard having a different refractive index than that of the solution is to be used. Unfortunately, there is some dispute as to how the correction for this effect is to be made. According to Brice, Halwer and Speiser (8) and Carr and Zimm (9), the factor by which an apparent $J(\theta)$ must be multiplied in order to obtain the true scattering intensity when a cylindrical cell is used, Q_n, is given by

$$Q_n = n \left[1 - \frac{\Delta r}{x}\left(\frac{n-1}{n}\right)\right] \qquad \text{VIII}$$

where n is the refractive index of the scattering liquid, r is the distance from the center of the cell to the face at which the scattered ray emerges, and x is the distance from the center of the cell to the photomultiplier sensing element. The square of this quantity is the correction factor to be applied when using a cell with a plane viewing window.

For the light-scattering instrument used in this laboratory, $r = 2.2$ cm. and $x = 10.2$ cm. Consequently, for $\lambda = 436$ mμ., benzene should have a value of $Q_n = 1.42$, water should have $Q_n = 1.27$, and the ratio $Q_n(\text{water})/Q_n(\text{bz.})$ is equal to 0.894. This ratio is the factor by which

apparent scattering intensities measured relative to benzene must be multiplied. When $\lambda = 546$ mμ. this factor is 0.906. For solvents other than water or dilute buffer correspondingly different correction factors must be employed.

Hermans and Levinson (13), however, have criticised the derivation of equation VIII and have given a derivation which indicates that the correct expression for Q_n, in the case that the photomultiplier does not see beyond the edge of the incident beam, is simply n^2 for both a cylindrical and a plane-faced cell. They state that only in the case that the scattering volume viewed can be considered as a point source does the above equation apply. Furthermore, these authors indicate that when the photomultiplier view extends beyond the edge of the beam, as it does in the instrument used here, the correct factor to be used is neither n^2 nor that given by equation VIII, but is rather some more complicated expression which they do not give.

On the other hand, Mommaerts (14) seems to have confirmed the correction factor as given by Brice for the plane-faced cell. He does not state whether the photomultiplier in his apparatus sees beyond the edge of the beam, but since it is of a design similar to that used in this laboratory such is probably the case.

The experimental verification of the applicability of equation VIII to the methods used in this study will be discussed in Section E.

f) Depolarization of the scattered light.

According to the Rayleigh law for small, isotropic molecules, the scattered light should be completely polarized at ninety degrees to the incident beam, with the electric vector perpendicular to the plane formed by the incident beam and the direction of the scattered ray. If, however, the molecules of solute are anisotropic, the scattered light at ninety degrees will also include a contribution from a small horizontally polarized component. The contribution of this component to the scattered intensity must be eliminated before calculating the molecular weight, since the calculation has its ultimate theoretical basis in the Rayleigh law. Cabannes (15) has shown that the factor by which the transverse scattering intensity must be multiplied to eliminate the depolarization effect is $\frac{6 - 7\rho}{6 + 6\rho}$, where ρ is the ratio of the horizontally polarized component intensity to the vertically polarized component intensity. The incident beam is unpolarized.

For almost all macromolecules in solution, ρ is equal to 0.01 or less, giving a correction factor of 0.98 or more. Throughout the investigations described here the depolarization was consistently found to be entirely negligible. The depolarization correction factor will hence be ignored.

3) Preparation of liquids for scattering measurements.

Since the intensity of light scattering from a solution depends upon the weight-average molecular weight of the solute, the method is highly sensitive to the presence of large particles. It is therefore imperative that all liquids on which measurements are to be made be as free as possible of extraneous material such as dust or aggregated proteins. The best method of achieving this end depends greatly upon the liquid being examined. During the course of these investigations, the procedures employed underwent a gradual evolution. The resulting conclusions are summarized briefly here.

For non-aqueous liquids, such as benzene, almost any clarification procedure is adequate. Filtration through sintered glass, centrifugation, and distillation have all been successfully employed.

For aqueous solutions, on the contrary, no clarification procedure is completely adequate. The best that can be achieved is the reduction of the solvent scattering to a value sufficiently low that the fact that this value is unreproducible is unimportant. For protein solutions, this is best accomplished by ultracentrifugation in the Spinco Preparative Ultracentrifuge and withdrawal of the solution through the hole in the tube cap without removing the plastic tube from the rotor. A pipet with a fine stem is useful for this purpose. An ordinary syringe is unsatisfactory, possibly because of minute particles of glass which are

washed off the ground glass surfaces. Protein solutions should be centrifuged repeatedly, transferring the solution to a clean plastic tube each time, until a constant dissymmetry is obtained.

Filtration of protein solutions introduces the possibility of losing protein by retention on the filter. For other solutions, or when the possible loss of solute is immaterial, filtration by pressure through sintered glass is also recommended. Suction filtration is liable to cause the formation of minute bubbles in the solution which would invalidate light-scattering measurements.

The cleanliness of pipets and light-scattering cells is critical. The procedure finally arrived at, and one which appears to be completely satisfactory, is to treat all glass surfaces with a warm nitric and sulfuric acid mixture, rinse thoroughly with distilled water, and finally rinse by allowing hot acetone vapor to reflux on the surface.

In all cases, solutions should be inspected for visible motes in the incident beam immediately before measuring scattering intensities.

E) Calibration.

In view of the uncertain nature of the refractive index correction (Section D, subsection 2e) and of the many other possible sources of error in making light-scattering measurements, it is highly desirable to have some independent means of checking their accuracy.

From the discussion of the turbidity method (Section D, subsection 1c) it is evident that such a possibility exists in the special case of a solution of small, isotropic, yet highly scattering particles. There has been recently made commercially available an aqueous suspension of silica which has just these properties, and which is in addition stable over long periods of time. A sample of this material, called "Ludox" (E. I. DuPont de Nemours and Co.) was kindly supplied to the author by Dr. Gerald Oster. Measurements of R(90) made with the light-scattering apparatus were compared with values of R(90) computed from spectrophotometric data on the same solutions. The two were found to be in excellent agreement.

1) Procedure.

The sample of "Ludox", which is supplied as a 30% aqueous solution, was diluted with distilled water to make both 3% and 0.3% solutions. Each solution was clarified by pressure filtration through a medium sintered-glass disc and transferred, with a dustless pipet, to a 10 cm. spectrophotometric silica cuvette which had first been carefully cleaned. Distilled water was similarly treated and transferred to another clean 10 cm. cuvette which had been calibrated against the first. The optical density of each solution was determined at the wavelengths 436 mμ. and 546 mμ.

A portion of each solution was then transferred,

again with a dustless pipet, to a clean light-scattering cell and R(90) measured for the two wavelengths in the usual way, by comparison with a benzene standard. The dissymmetry was also measured at the same time.

2) Treatment of data.

The optical density correction and the refractive index correction according to equation VIII were applied in obtaining R(90) by light scattering. Since the dissymmetry was not exactly unity (i.e., since the particles were not quite "small"), a slight refinement of equation III was used to compute the value of R(90) from the optical density. This relation may be derived as follows: by analogy to equations II and III, one may write

$$\tau_i = \frac{2.303\ d}{\ell}\frac{1}{Q} = \frac{16\pi}{3} R(90)\frac{1}{P(90)} \qquad \text{IX}$$

where d is the optical density measured in the spectrophotometer, ℓ is the length of the spectrophotometric cuvette, Q^{-1} is a factor which, when multiplied by the measured turbidity, $\tau = 2.303d/\ell$, gives the turbidity which would be observed if the same solution consisted of small particles; this ideal turbidity is designated τ_i ; and $P^{-1}(90)$ is a factor, which when multiplied by R(90) gives the value of R(90) which would be observed if the same solution consisted of small particles. Both $P^{-1}(90)$ and Q-1 are fixed by the size and shape of the particles,

which can be computed from the dissymmetry. For values of the dissymmetry not much greater than unity, the ratio of Q^{-1} to $P^{-1}(90)$ is practically independent of assumptions concerning the particle shape. For further details, see reference (10).

Equation IX gives, with τ defined above,

$$R(90) = \frac{3\tau}{16\pi} \frac{P(90)}{Q} \qquad X$$

P(90) and Q were obtained from tables given by Doty and Steiner (10). P(90)/Q was found to be 1.01 in each case. R(90) was calculated according to equation X from the spectrophotometric data and compared to R(90) obtained from light-scattering measurements.

3) Results.

The values of R(90) obtained by the two methods, together with the dissymmetries, z, for the "Ludox" solutions are given in table 2.

4) Discussion.

The agreement between these two methods indicates that the light-scattering measurements obtained with the instrument in this laboratory are satisfactorily accurate. It is interesting that the refractive index correction given by equation VIII appears to be applicable in this instance. It is possible, however, that the apparent agreement is fortuitous, in which case the refractive

index correction factors may be considered to be empirically determined in the above calibration.

Table 2

"Ludox" conc.	λ mμ.	z	R(90) light scattering	R(90) spectro-photometry	percent difference
3%	436	1.08	10.2×10^{-3}	10.2×10^{-3}	0.0
3%	546	1.08	4.30×10^{-3}	4.08×10^{-3}	-5.1
0.3%	436	1.10	1.50×10^{-3}	1.55×10^{-3}	+3.0
0.3%	546	1.14	0.637×10^{-3}	0.638×10^{-3}	+0.2

Comparison of R(90) measured by light scattering and by spectrophotometry

PART II - THE MOLECULAR PROPERTIES OF RAT-TAIL TENDON COLLAGEN

A) Introduction.

A thorough review of the present state of knowledge concerning the structure of collagen has been given by Bear (16). It would appear that although a great deal of work has been done on this protein from the point of view of x-ray diffraction, electron microscopy and chemical analysis, little information about the physical chemistry of collagen solutions is available. It was the purpose of these investigations to make some start toward filling this gap.

As for x-ray diffraction evidence, suffice it to say here that there is support for the existence of an amino acid residue length of 2.9 A. along the fiber axis, a repeating unit of seven such residues every 20 A. or of ten every 29 A., and a long period of about 640 A. There is also some support for the alternative possibility of a residue length of 0.95 A. and repeating groups of three every 2.9 A. Perpendicular to the fiber axis, the x-ray data are compatible with hexagonal packing of cylinders with a center-to-center distance of from 12 A. to 20 A., depending upon the degree of hydration, (16), (17), (18). However, there is a great deal of disagreement on even such sketchy interpretations of the data, a completely different sort of structure having been suggested, for example, by

Randall and coworkers (19).

Connective tissues, skin, or fish swim bladder tunic may be extracted with various acid or alkaline media to obtain solutions of collagen. Such solutions give precipitates upon neutralization, addition of salts, or addition of various biological substances, and considerable attention has been directed toward the electron microscopic examination of such precipitates (20). Addition of sodium chloride or of other salts of monovalent cations to final concentrations of 0.1 to 0.2 M causes the formation of fibrils showing the 640 A. axial repeat characteristic of native collagen. At somewhat higher concentrations the precipitated fibrils show axial periods about one-third as long, and no visible structure at still higher concentrations of salt. Skin, extracted with citrate buffer and dialysed against water, gives another type of fibril with spacings of 1800 to 3000 A., possibly as a result of the presence of glycoprotein in the extract. Alkaline phosphate buffer extracts of skin produce a third kind of structure when dialysed against citrate buffer. These show segments of length similar to the long spacing above, about 2200 A., but the segments are separated into unconnected units rather than aggregated end-to-end to form a fibril. These segments seem to be connected with the presence of adenosine triphosphoric acid in the extracts. All three forms may be interconverted. All display high angle x-ray patterns

characteristic of native collagen.

The meaning of these results is still unclear, though Schmitt, Gross and Highberger (20) state that they believe the presence of thin fibrous protein particles of length about 2200 A. in various extracts is indicated.

Little is known about the particles present in these "soluble" collagens. Thaureaux (21) has shown that acid extracts of rat-tail tendon and fish swim bladder tunic show strong streaming birefringence and optical activity compared to the same solutions after heating. Bresler and coworkers (22) have investigated the sedimentation and diffusion of the particles present in citrate extracts of mammalian hide and report that these appear to be cylinders with the dimensions of 380 A. in length and 16.7 A. in diameter, and with a molecular weight of 70,000. Salo (23) has carried out viscosity studies on extracts of the tunic of carp swim bladder and reports the presence of molecules with an axial ratio of 47.5. None of these investigations appears to be as careful or reliable as could be desired.

B) Rat-tail tendon collagen in dilute acetic acid.

Tendons from the tail of the white rat swell rapidly in even extremely dilute acetic acid solutions (1/250,000 acetic acid or greater). Within twenty-four hours the supernatant may be decanted as an extremely viscous, clear solution of soluble collagen. Such dilute acetic acid

solutions of rat-tail tendon collagen will be designated as RTC throughout the remainder of this discussion. Since RTC is easily prepared and is initially in a relatively high state of purity, and since tendons from the tails of freshly sacrificed rats are readily available, this material was chosen as the subject of this investigation.

1) Preparation of RTC.

Tendons may be removed from rat tails as clean white threads of diameter about one millimeter. After rinsing with distilled water, swelling and dissolution was carried out in acetic acid solutions of concentrations ranging from 1/250,000 to 1/2500 by volume and no apparent difference in the product with changing concentration of acetic acid was noted. Acetic acid solutions of 1/10,000 were arbitrarily chosen as the solvent to be used in subsequent studies.

After swelling for twenty-four to forty-eight hours, the supernatant was passed through a Buchner funnel without filter paper to remove undissolved tendon, and the solution centrifuged for twenty minutes at 9000 g. under refrigeration in the Spinco Model L preparative ultracentrifuge (head #30 at 10,000 r.p.m.). The undissolved tendon continued to swell and dissolve when additional dilute acetic acid was added.

2) Characterization of RTC.

RTC is a clear, colorless, extremely viscous solution. Prepared as above, it contains approximately 0.1% of dissolved protein. Refractive index measurements, drying to constant weight and nitrogen analysis are in agreement on the protein concentration, indicating that there can be little dissolved matter other than protein.

Examination of air-dried RTC by the methods of electron microscopy* shows only a matted background. There is no evidence for the presence of fibrils of native collagen, as may be verified by reference to figure 4a, a typical electron micrograph obtained from RTC.

The addition of NaCl to final concentrations of 0.1 M causes a precipitate to be formed, which appears under the electron microscope to consist of fibrils similar to those found in native collagen. The 640 A. spacing is clearly evident in figures 4b and 4c. An excellent collection of electron micrographs of precipitated collagen has been published by Noda and Wyckoff (24).

Loofbourow and coworkers (25) have published the ultraviolet absorption spectrum of highly purified RTC. The ultraviolet spectrum of a sample of RTC prepared as indicated above without further attempts at purification

---

* Thanks are due to Mr. Howard Hill for his skillful operation of the electron microscope and for preparing the electron micrographs reproduced in this dissertation.

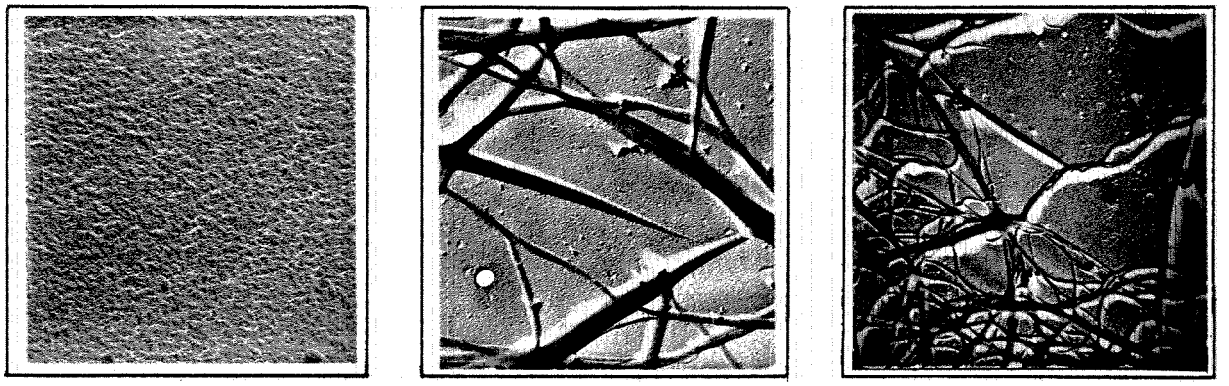

A B C

A) RTC, Pd shadow, 12,000 x

B) Salt-precipitated RTC, OsO_4 fixative, Pd shadow, 12,000 x

C) Salt-precipitated RTC, OsO_4 fixative, Pd shadow, 6950 x

FIGURE 4

ELECTRON MICROGRAPHS

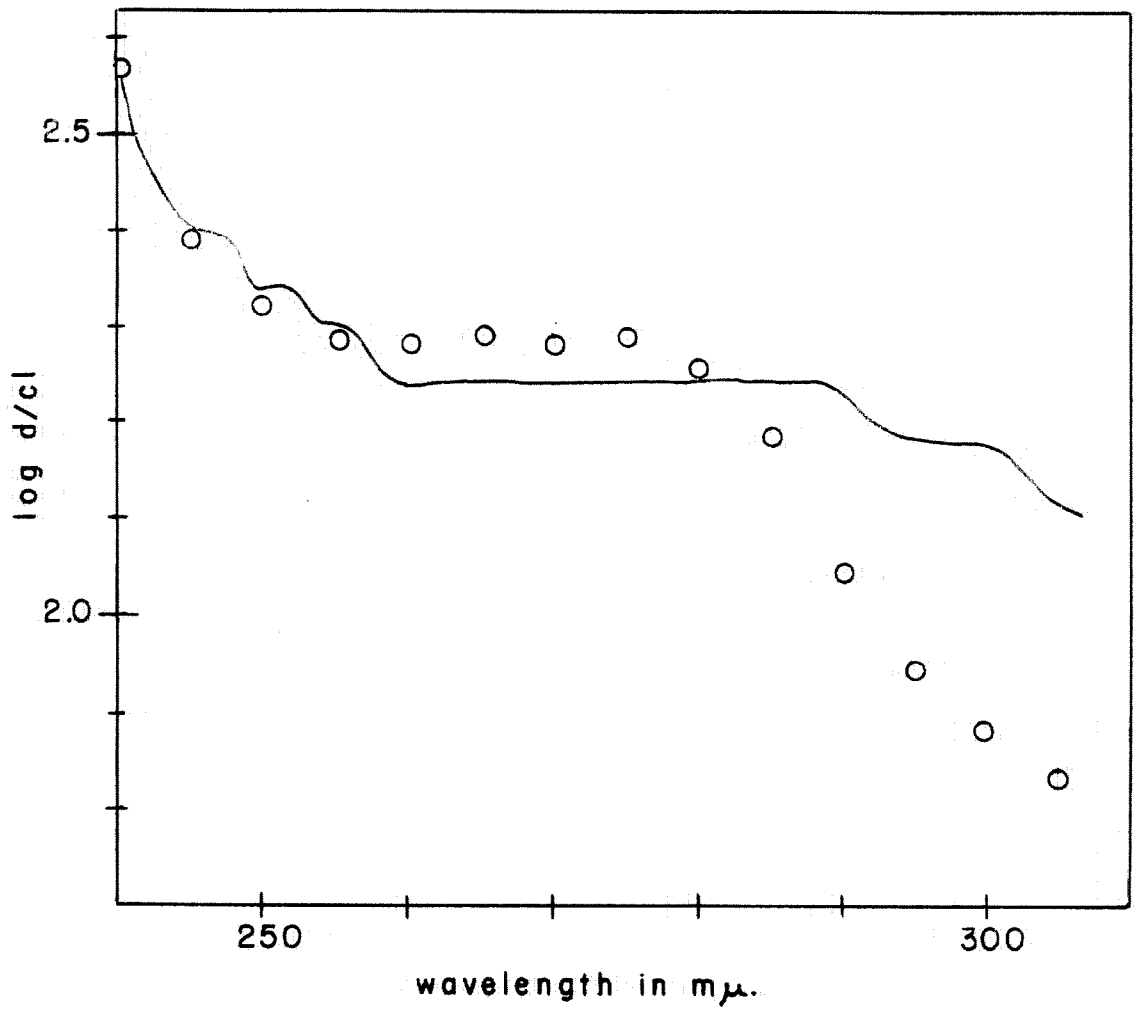

o observed for this preparation of RTC
— observed by Loofbourow for purified RTC

d optical density
c concentration, gms/ml.
l length of path, cm.

FIGURE 5

U.V. ABSORPTION OF RTC

was determined with a Beckman Model DU spectrophotometer. Figure 5 shows that the spectrum of this preparation was essentially the same as that obtained by Loofbourow, indicating that further purification was unnecessary. The protein concentration in this preparation was 9×10^{-4} gms./ml. and the length of the light path through the cuvette was 1.0 cm. Of particular significance is the absence of peaks in the region from 250 mμ. to 280 mμ., corresponding to the absence of phenyl groups in the side chains, a characteristic property of collagen.

3) Light-scattering studies.

Preliminary attempts at obtaining reproducible light-scattering data on RTC indicated that the preparation consisted of a continuous distribution of particle sizes. Pressure filtration through an ultrafine glass sinter removed most of the dissolved collagen, as indicated by a drop in the light scattering to almost that of water. At the other extreme, filtration through a medium-fine glass sinter gave a solution with an apparent dissymmetry of 6.3 for $\lambda = 436$ mμ., a value which in excess of the upper theoretical limit for both rods (2.2) and random coils (5.8). For particles of very large dimensions this result is not entirely unexpected, since the assumptions implicit in the derivation of these limits are no longer valid.

Dissymmetries of intermediate values, ranging from 2.1

to 6.3, could be obtained by varying the filtration or centrifugation procedure used to clarify the solution. The data in table 3 are quoted to demonstrate that continued centrifugation is capable of producing a fractionating effect by removing the larger particles in a distribution, and that this effect may be followed by means of light scattering. Column 1 indicates the length of time for which the sample of RTC was centrifuged at 60,000 g. The same sample was used for successive centrifugations. Column 2 lists galvanometer deflections which are proportional to the ninety degree scattering, and hence is a monotonic function of the protein concentration and very roughly proportional to it. Column 3 shows the observed dissymmetry, uncorrected for the reflection of the incident beam. The decrease in the dissymmetry observed in table 3 is too great and in the wrong direction to be attributed to ordinary concentration dependence. It appears

Table 3

time, min.	90^{o} scattering	dissymmetry
15	89	3.93
60	71	2.66
120	55	2.28
120	51	2.19

decrease in average particle size with continued centrifugation.

rather that the larger particles are being removed by the repeated centrifugation.

In view of the heterogeneity of RTC, it is clear that unambiguous quantitative results cannot be obtained concerning the distribution of sizes and shapes of the particles without resorting to elaborate fractionation procedures. This does not imply, however, that interesting qualitative indications cannot be obtained by the methods of light scattering. Hence data were collected for the preparation of a Zimm plot (9) for RTC, as will now be described.

A solution of RTC was prepared as above and dilutions of this solution to 1/2, 1/4 and 1/8 the original concentration were made with 1/10,000 acetic acid. Before measuring the scattered light intensities, each solution was centrifuged at 60,000 g. for 90 minutes and the sample inspected visually for clarity. Measurements of the scattered light intensity relative to that at ninety degrees for benzene were made at 90, 70, 55, 45 and 35 degrees to the direction of the incident beam. This was done for two wavelengths, $\lambda = 436$ mμ. and 546 mμ. Solvent scattering at the same angles and wavelengths was determined for a sample of the solvent which had undergone the same purification treatment as the RTC solutions. The nitrogen content of each solution was determined colorimetrically by Nessler's method.

The data obtained in this manner are presented in table 4, where scattering intensities relative to that of benzene at ninety degrees are given for each angle and

protein concentration for the two wavelengths.

Table 4

λ, mμ.	conc. gms./cm^3	90°	70°	55°	45°	35°
436	7.83×10^{-4}	6.70	11.7	25.3	50.6	124
436	3.53×10^{-4}	1.44	2.29	4.55	8.43	18.2
436	1.78×10^{-4}	0.84	1.38	2.91	5.72	13.8
436	0.98×10^{-4}	0.42	0.66	1.28	2.44	5.74
436	solvent	0.09	0.12	0.21	0.34	0.93
546	7.83×10^{-4}	13.8	25.2	57.5	115	288
546	3.53×10^{-4}	2.48	4.32	8.68	16.5	35.0
546	1.78×10^{-4}	1.59	2.76	6.11	12.6	31.2
546	0.98×10^{-4}	0.69	1.17	2.50	4.87	12.2
546	solvent	0.14	0.22	0.36	0.72	2.7

Angular and concentration dependence of light scattering from RTC solution for two wavelengths.

Plots of the function $Kc/R(\theta)$ versus $\sin^2 \theta/2 + 600\ c$ were prepared from these data. The constant K is given by

$$K = \frac{2\pi^2 n^2 (dn/dc)^2}{N \lambda^4} \qquad \text{XI}$$

where n is the refractive index of the solvent (water in this case), dn/dc is the refractive increment of the solute, N is Avogadro's number, λ is the wavelength of light in vacuum, and c is the protein concentration in gms./cm^3. The concentration was obtained from the nitrogen analysis by assuming rat-tail tendon collagen to have the same

nitrogen content as kangaroo-tail tendon collagen, given as 17.5% by Salo (26).

The values of K were 5.86×10^{-7} and 2.18×10^{-7} for $\lambda = 436$ mμ. and 546 mμ. respectively. These were computed using values of dn/dc obtained for gelatin (see Part III, Section B) since at the low concentrations of protein characteristic of solutions of RTC an accurate estimate of dn/dc would not be possible.

The factor 600 by which c is multiplied was arbitrarily chosen to spread the data over a convenient range on the abscissa of the Zimm plots.

In calculating $R(\theta)$ corrections were made for solvent scattering, the refractive index effect and the volume effect; other corrections were considered negligible. $R(\theta)$ was divided by the polarization factor, $1+\cos^2\theta$, so that the extrapolated curve for $c = 0$ would represent the shape of $P^{-1}(\theta)$ directly, as is customary.

The resulting angular and concentration dependence curves and their extrapolations to $c = 0$ and $\theta = 0$ are shown in figures 6 and 7. The extrapolated curve for $c = 0$ is equivalent to a plot of $P^{-1}(\theta)$ versus $\sin^2 \theta/2$ and gives information on the size and shape of the particles. The extrapolated curve for $\theta = 0$ is equivalent to a plot of $Kc/R(0)$ versus concentration and displays the concentration dependence of the scattered light intensity uninfluenced by the particle size. The intercept of these two curves on

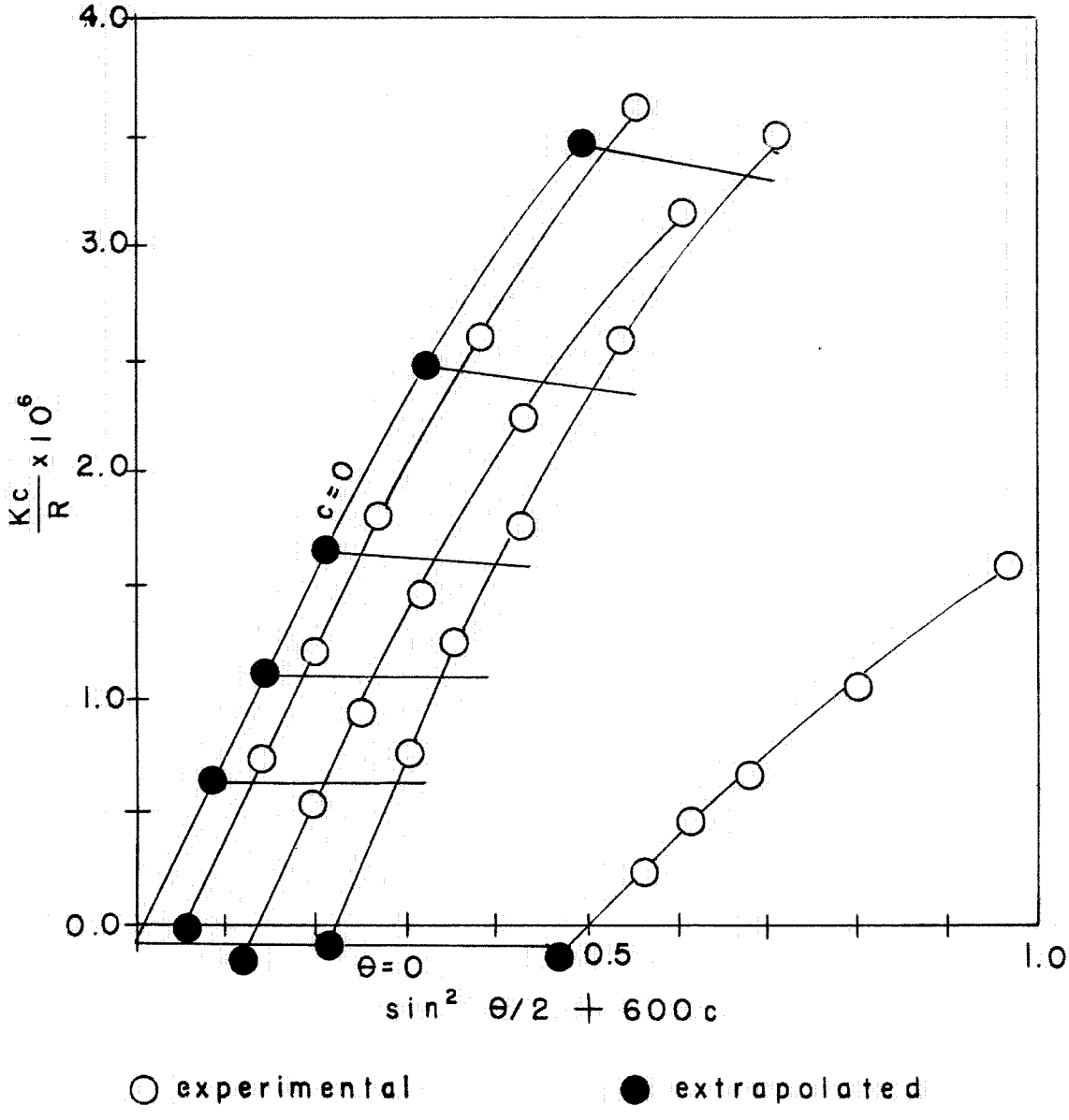

FIGURE 6

Zimm Plot for RTC

$\lambda = 436$ mμ.

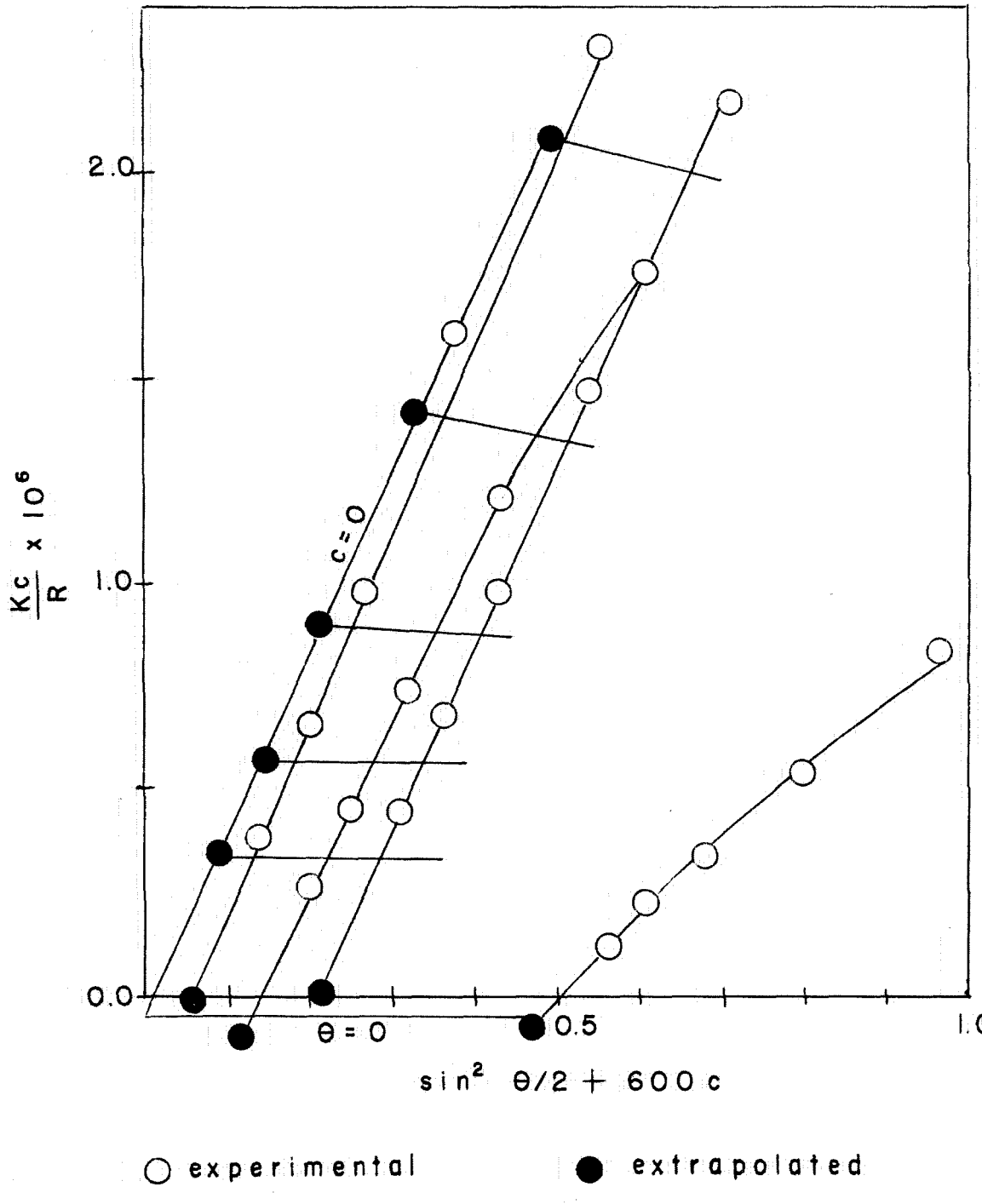

FIGURE 7

Zimm Plot for RTC

$\lambda = 546\ m\mu$

the ordinate is equal to the reciprocal of the weight-average molecular weight of the particles in solution.

From figures 6 and 7 it is evident that the intercept on the ordinate is zero to within the error of the measurements. A possible interpretation of this result is that the RTC in these solutions is organized into extremely large aggregates, perhaps extending continuously throughout the entire volume of the solution.

Another unusual feature of these plots is the sudden change in the shape of the angular distribution curves on going from the highest concentration to the three lower concentrations, though at the same time the $\theta = 0$ curve is flat, indicating that $Kc/R(0)$ is independent of concentration. In terms of the "excluded volume" interpretation (27) of the angular and concentration dependence of scattering,

$$\frac{Kc}{R(\theta)} = \frac{1}{MP(\theta)} \left\{ 1 + \frac{4\pi D^3 N}{3M} \cdot \Phi(x) \cdot c \right\} \qquad \text{XII}$$

where $\Phi(x) = \frac{3}{x^3} (\sin x - x \cos x)$ and $x = \frac{4\pi D}{\lambda'} \sin \theta/2$.

D is the radius of the spherical volume surrounding each particle center from which other particle centers are excluded. λ' is the wavelength of light in the medium. The other symbols have their usual meaning. It is interesting that the quantity $\frac{4\pi D^3 N}{3M}$ is simply the total excluded volume per gram of particles, which quantity may be denoted by the symbol v. In the region of importance, Φ is a

decreasing function of x. Hence, for a given value of v greater than zero, $Kc/R(\theta)$ will increase more slowly with $\sin \theta/2$ for large c than for small c. This is the observed behavior in figures 6 and 7. However, at $\theta = 0$ we have $P(0) = 1$, $x = 0$, and $\Phi(x) = 1$ so that

$$\frac{Kc}{R(0)} = \frac{1}{M}\left\{1 + vc\right\} \qquad \text{XIII}$$

and the non-zero value of v should cause the $\theta = 0$ curve to have a non-zero slope. However, the slope of this curve in figures 6 and 7 is evidently zero and an explanation of this behavior must be sought elsewhere. A possibility is that between the first and second concentrations an expansion of the dimensions of some of the particles takes place without altering the average molecular weight. This would leave the scattering at $\theta = 0$ unaltered, but increase the slope of the angular distribution curves, corresponding to the effects observed.

It should be mentioned here that dissymmetry data alone, without reference to the entire set of Zimm curves, are probably unreliable for RTC. For example, dissymmetries on the solutions for which the above data are reported are erratic, showing values (uncorrected for reflection of the incident beam) of 5.2, 3.8, 5.0 and 4.4 for the four solutions in order of decreasing concentration and at $\lambda = 436$ mμ., while for $\lambda = 546$ mμ. they were 5.9, 4.4, 5.9 and 5.2.

Dissymmetry and ninety-degree scattering data for another preparation of RTC were also obtained. The viscosity and sedimentation velocity studies reported in subsections 4 and 5 were performed on the same samples as those used in this investigation.

In this instance, the dissymmetries were still higher than those for the previous preparation but not so variable. They are plotted versus concentration in figure 8. These values were obtained by diluting the original solution directly in the light-scattering cell; only the highest concentration was clarified by centrifugation in the usual manner. This fact may account for the decreased scatter of the experimental points from a smooth curve.

It is to be noted, however, that in this case the dissymmetries <u>decrease</u> with decreasing concentration; this is the opposite of the behavior to be expected on the basis of the Zimm curves of figures 6 and 7. That is, such behavior would be compatible with a negative value of the parameter v in equation XIII, or with a decrease in the average extension of the particles as they are diluted. In any event, the difficulties in the way of drawing unambiguous conclusions about the detailed molecular properties of RTC are clear.

The extrapolated dissymmetries of figure 8 are compatible with a random coil with r.m.s. end-to-end distance of at least 5000 A. The molecular weight computed from the ninety-degree scattering by the dissymmetry method (4) was

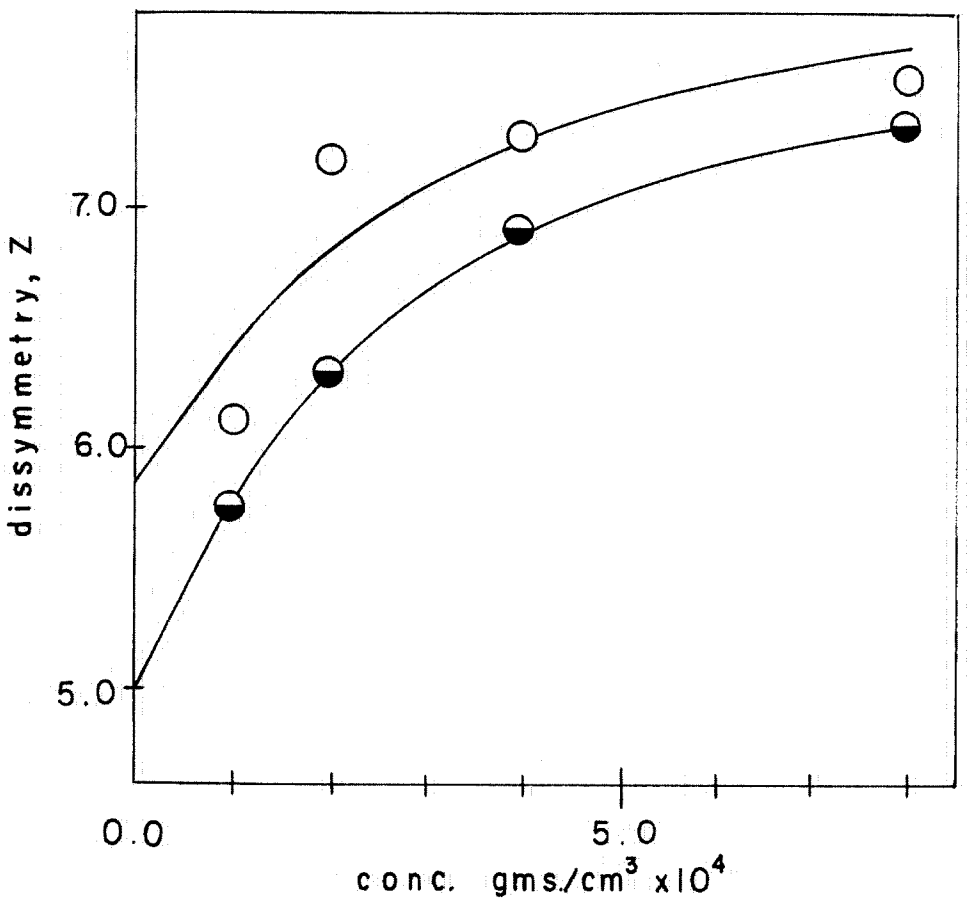

FIGURE 8

DISSYMMETRIES FOR RTC

20 million, though this value is of doubtful significance except as a possible lower limit.

4) Intrinsic viscosity.

The interpretation of viscosity measurements on RTC is complicated by both the electroviscous effect and by orientation of the particles in the velocity gradient. The former is of uncertain magnitude (28) and is probably important for RTC since the solution contains no salts to swamp out charge effects. The orientation of the RTC particles in a shear gradient is evident from the fact that RTC shows streaming birefringence (21). The electroviscous effect tends to increase the apparent viscosity, while the orientation effect does the reverse. Correction for these two factors would be uncertain, and therefore viscosity data for RTC are here reported without attempt at interpretation in terms of molecular properties other than in the most qualitative sense.

A sample of RTC was prepared as previously (the same preparation as that for which the light-scattering data have been reported on page 47) and efflux times for a series of concentrations of the protein were determined using an Ostwald viscometer. All measurements were made in a thermostated bath at 25.0° C. The initial stock solution was centrifuged at 60,000 g. for twenty minutes before being introduced into the viscometer in order to remove particles which could interfere with free flow

through the capillary. The concentration of the centrifuged stock solution was determined by Nessler's method. Dilutions were made directly in the viscometer, all added solvent being first passed through a medium-fine glass sinter. The data are presented in table 5.

Table 5 - Viscosity data for RTC

C_w	t, sec.	$\frac{\ln t/t_o}{C_w}$	$\bar{G}$, sec^{-1}
8.13×10^{-2}	1052.5	24.2	346
5.41×10^{-2}	559.0	24.8	653
3.60×10^{-2}	366.5	25.4	995
2.40×10^{-2}	274.0	26.0	1330
1.59×10^{-2}	223.6	26.4	1630
1.06×10^{-2}	196.0	27.4	1860
solvent	146.7	-	2490

Column one of this table gives the protein concentrations in units of grams per 100 cm^3, C_w, the customary unit of concentration in viscosity studies. The second column gives efflux times, t, in seconds for each solution and for the solvent. The solvent efflux time is represented by t_o in column three. $\bar{G}$ in column four represents the average velocity gradient in the liquid flowing through the viscometer capillary during each run. It can be shown that

$$\bar{G} = \frac{8v}{3\pi r^3 t} \qquad \text{XIV}$$

where V is the volume of fluid which flows through the capillary in time t, and r is the radius of the capillary. In the viscometer used here, r is equal to 2.1×10^{-2} cm. and V is equal to 3.98 cm^3.

Figure 9 shows the plot of $\frac{\ln t/t_o}{C_w}$ versus C_w. It is seen that the intercept on the ordinate is 28. This quantity is known as the intrinsic viscosity, $[\eta]$. It should be remarked that this is an exceptionally large value of $[\eta]$ and that correction for the effect of orientation in the velocity gradient by extrapolating additional data to $\bar{G} = 0$ would result in an even higher value for this parameter. For purposes of comparison it is pointed out that Doty and Bunce (29) have found for the highly extended molecule of desoxypentose nucleic acid in the minimally degraded state a value of $[\eta]$ equal to 19.9 dl./gm. for $\bar{G} = 1000$ sec^{-1}. In agreement with the results of the light-scattering studies of subsection 3, it must be concluded that RTC contains a system of highly extended structures.

5) Sedimentation velocity.

Interpretation of sedimentation velocities for RTC is likewise complicated by several factors. In a low ionic strength system such as RTC the "primary charge effect" becomes important (30). It may cause a reduction in the observed sedimentation velocity by one-half in the limit of a high concentration of colloidal electrolyte and a low

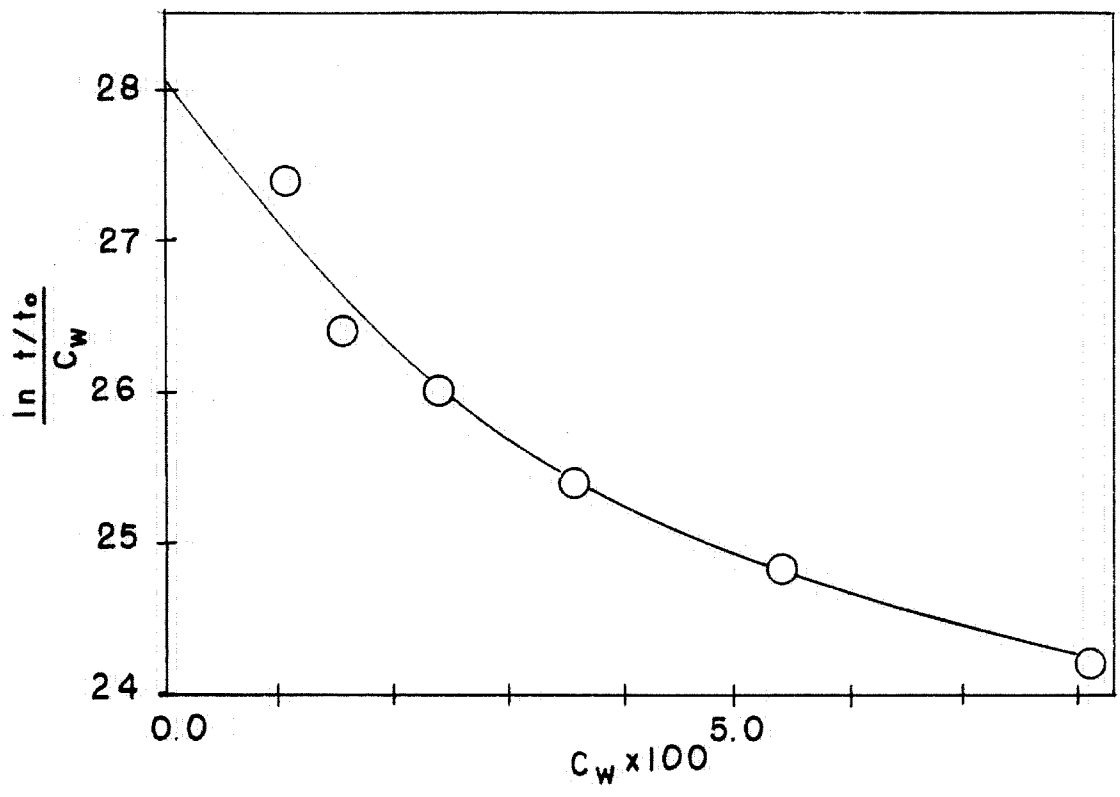

FIGURE 9

VISCOSITIES FOR RTC

neutral salt concentration. A further complication involving the shape of the sedimenting boundaries is encountered in systems of high viscosity; the dependence of the sedimentation velocity of the particle upon the particle concentration may lead to artificial sharpening of the boundary (in the usual case of a higher concentration causing a lower sedimentation velocity) and hence false conclusions concerning monodispersity. These effects must be kept in mind when considering the sedimentation behavior of RTC.

A preparation of RTC was centrifuged for 20 minutes at 60,000 g. and an aliquot transferred to a light-scattering cell. After each set of light-scattering measurements a portion of the solution in the cell was removed and subjected to ultracentrifugal analysis without further treatment. The remaining solution in the cell was diluted further by adding dilute acetic acid and stirring cautiously without removing it from the cell. The results of the light-scattering measurements have already been noted on page 47.

The ultracentrifuge in use at this laboratory has been described earlier by Singer and Campbell (31). All runs were performed at a rotor temperature of 24 ± 1 degree C. and at a rotor speed of 850 cps. Some of the sedimentation diagrams obtained are reproduced in figure 10. The times indicated are computed from the beginning of the rotor acceleration.

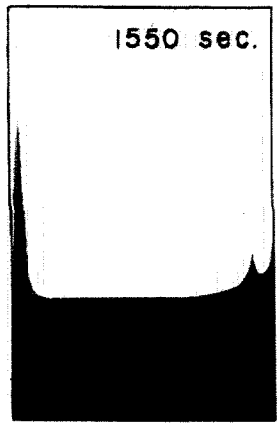

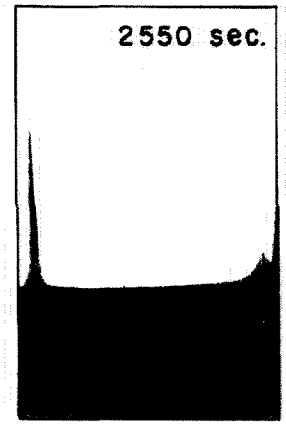

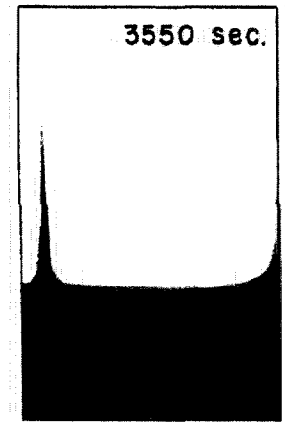

$c = 8 \times 10^{-4}$ gms./cm.^{3}

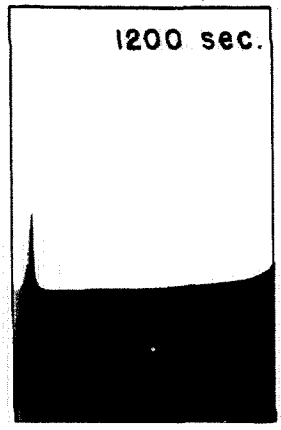

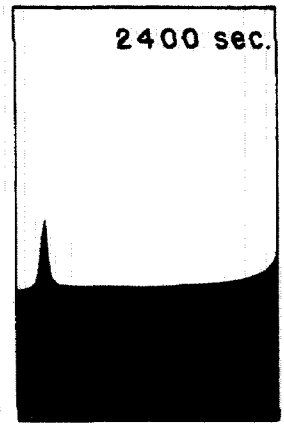

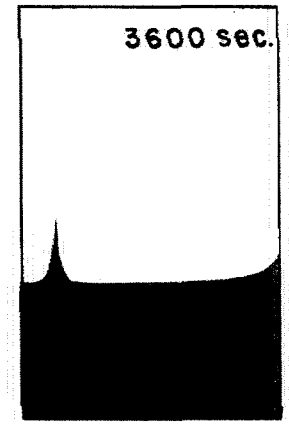

$c = 4 \times 10^{-4}$ gms./cm.^{3}

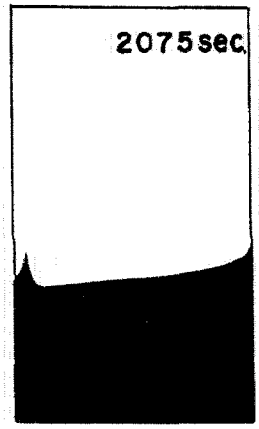

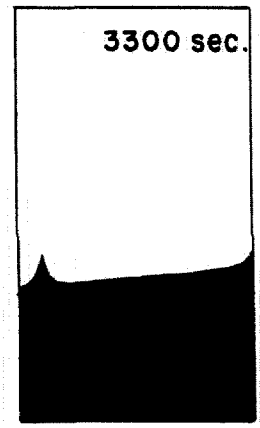

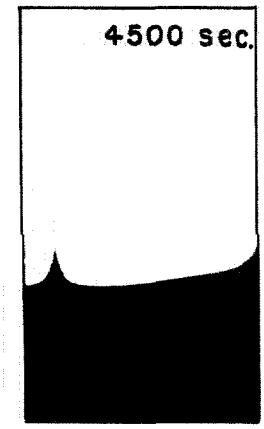

$c = 2 \times 10^{-4}$ gms./cm.^{3}

FIGURE 10

SEDIMENTATION DIAGRAMS OF RTC

An interesting feature of the sedimentation diagram of the solution containing 8×10^{-4} gms./cm^3 of protein is the appearance of a second small peak at the bottom of the cell. This peak must represent material of very high sedimentation constant since it is already at the bottom of the cell within the 1550 seconds necessary to accelerate the rotor to full speed and obtain the first photograph of the schlieren pattern. Furthermore, it appears to be in equilibrium with the material of the main boundary as it does not appear in the sedimentation diagrams of the solution containing 4×10^{-4} gms./cm^3 of protein. As pointed out in the discussion of the dissymmetries of these solutions, there also seems to be some evidence for a decrease in the average size of the particles upon dilution in the consequent decrease of the dissymmetry.

The extrapolation to zero concentration of the sedimentation constants for these solutions is shown in figure 11. The value 3.2×10^{-13} sec. was obtained for s^{w}_{20} at zero concentration of the protein.

6) Discussion.

In view of the many uncertainties already pointed out it would be fruitless to attempt a detailed interpretation of the viscosity and sedimentation behavior of RTC. It should, however, be noted that the sedimentation constant observed above is far too small to represent the behavior of

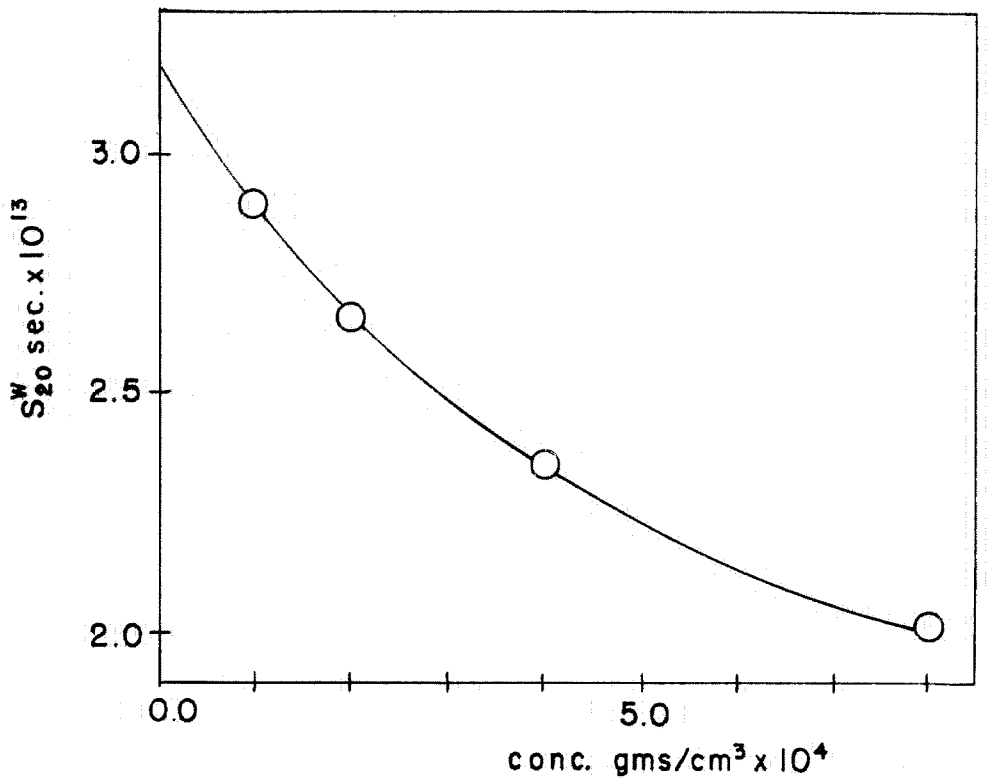

FIGURE II

SEDIMENTATION CONSTANTS FOR RTC

particles of molecular weight greater than 20 million (from light scattering) even though their large frictional coefficients (from viscosity) are considered. This is not an unexpected result since, as has been mentioned, the sedimentation constants will be reduced by the primary charge effect and the viscosity will be decreased as a result of the orientation of the molecules in the velocity gradient. It is also possible that the observed sedimenting boundaries do not represent the behavior of individual independent structures in the solution, but rather the collapse of a network structure, or gel, extending throughout the entire volume of the solution, due to the application of the centrifugal field (30). Indeed, for a solution of particles as extended as those of RTC appear to be, one would expect such network formation down to extremely low concentrations. This hypothesis could be tested by determining whether the observed sedimentation rates were dependent upon the strength of the applied centrifugal field.

Mention should also be made of the fact that although heterogeneity with respect to sedimentation has been demonstrated for RTC by means of light scattering, the sedimenting boundaries in figure 10 appear to be quite sharp. This may be explained as due to either the high concentration dependence of the sedimentation constants or else as characteristic of the collapse of a gel in the centrifugal field (30).

It is evident that these investigations of RTC have raised more questions than they have answered and have done little more than to point out some of the features of the system which warrant more careful study. This study, however, will probably have to await the development of a more complete theory of the physical properties of large charged networks in low ionic-strength solutions.

To recapitulate, it appears probable that RTC contains large networks of individual strands which are themselves too thin to be resolved by the electron microscope. The solution appears to contain a wide spread of network sizes and its properties probably depend cricically on many factors in the preparation of the solutions. A few suggestions for some possible factors are time of swelling, solvent conductivity, method of clarification, temperature of storage and, in general, any variable which could influence the final distribution of shapes and sizes of the fragments.

C) Rat-tail tendon collagen in concentrated urea solutions.

It has been mentioned that when salts are added to dilute acetic acid solutions of rat-tail tendon collagen, the collagen is precipitated in a form which has the appearance of native collagen fibrils under the electron microscope. This precipitate can now be dissolved in 5 M aqueous urea containing 2% NaCl to give a collagen solution with quite different physical properties from those of RTC. Such urea solutions of rat-tail tendon collagen will be

designated as URTC in the following discussion. A summary of some of the conspicuous physical properties of URTC follows.

URTC does not give a precipitate with salt; the solvent, as has been mentioned, itself contains 2% NaCl, well above the salt concentration necessary to completely precipitate RTC.

These solutions have a markedly lower viscosity than RTC solutions at the same concentrations of protein.

Preliminary measurements by Dr. A. Rich show that URTC displays only weak streaming birefringence at shear gradients which are sufficient to cause RTC to be markedly birefringent.

Light-scattering dissymmetries are within the normal range, about 2.0, indicating a molecular size for which the theory of light scattering is probably valid.

These differences between the properties of URTC and those of RTC cannot be attributed to a fractionation or other alteration of the collagen upon precipitating and redissolving, since if the precipitate is again redissolved in 1/10,000 acetic acid instead of in concentrated urea, a solution is obtained which again has the general properties characteristic of RTC.

A series of physical investigations was carried out on URTC with the intention of attempting to characterize as completely as possible the collagen molecules in the solution. These studies will now be discussed.

1) Preparation of URTC.

About 100 ml. of RTC solution, prepared as described in the previous Section, was completely precipitated by addition of saturated aqueous NaCl dropwise, with stirring, until further precipitation was not observed. The solution was stored under refrigeration for about one hour to permit coagulation of the precipitate. The precipitate was then sedimented and the supernatant decanted. The sediment was resuspended in about 50 ml. of solvent, consisting of 5 M urea and 2% NaCl, with 0.01% merthiolate as a preservative, and stored under refrigeration for three days. The preparation was then allowed to stand at room temperature for one day. At this time, all of the original precipitate had dissolved. The solution was centrifuged for 30 minutes at 60,000 g. The resulting stock solution of URTC was used for the light-scattering, viscosity and sedimentation velocity studies to be described.

2) Determination of protein concentration.

Exactly 25.0 ml. of the above URTC solution was placed in a dialysis sack and dialysed in the cold for eleven days against 1/10,000 acetic acid. The contents of the sack were then removed and the sack rinsed with a little excess dilute acetic acid which was added to the rest of the solution. The final volume of solution was 46 ml. This was analysed for nitrogen by Nessler's method, and the protein

concentration of the original URTC stock solution estimated assuming the protein to contain 18% nitrogen. A result of 36×10^{-4} gms./cm^3 was arrived at for the collagen concentration.

3) Light-scattering studies.

Preliminary investigation indicated little variability in the dissymmetry of URTC and that centrifugation for 20 minutes at 60,000 g. was sufficient to bring the dissymmetry of the stock solution down to its constant minimum. In obtaining the data reported here, half of each sample was removed from the light-scattering cell after reading the scattering intensity and replaced with clarified solvent. The diluted solution was then stirred cautiously before the next series of measurements was taken. The withdrawn portion of each sample was saved for ultracentrifugal analysis. In this way, four solutions, each one-half as concentrated as the previous one, were studied. Solvent scattering measurements were obtained by treating a sample of solvent in exactly the same manner as the solution.

There are several difficulties inherent in attempting to accurately measure the solute scattering of URTC. First, the mixed solvent itself scatters a good deal more than water alone. Solvent scattering, in this case, can be minimized by using recrystallized urea and pressure filtration of the solvent mixture through an ultrafine

glass sinter. In this way solvent scattering was reduced to 20% of the total scattering intensity for the most dilute URTC solution studied.

Determination of the protein concentration in URTC also presents some difficulties. The dialysis method described above is probably satisfactory if care is taken to allow sufficient time for complete removal of the urea, though the loss of protein through small pinholes in the membrane would be difficult to detect.

Similarly, the estimation of dn/dc for a protein in such a mixed solvent involves the necessity of ensuring that the composition with respect to the solvent components is identical for both the protein solution and for the solvent mixture against which it is compared. However, there is little reason to expect the refractive increment of the protein to differ appreciably from that for the protein in water.

Finally, there is a complication in the light-scattering properties due to the presence of more than two components in the solution. According to the theory of Ewart, Roe, Debye and Mc Cartney (32), the preferential absorption of one of the solvent components by the solute can cause an alteration in the apparent extrapolated molecular weight of the solute, depending on whether the refractive index of the absorbed component is higher or lower than the refractive index of the solvent mixture. In the case of the system bovine serum albumin- urea-water, Doty and Katz (33) have found that no

preferential absorption occurs at the protein isoelectric point, but that urea is absorbed above the isoelectric point while water is absorbed below it. The effect was considerable at urea concentrations of about 8 M.

Because of its dependence on deviations from the isoelectric point, the selective absorption phenomenon seems to be due to electrostatic forces. The system being studied here contains a high salt concentration which is, presumably, capable of swamping out such forces. Furthermore, the urea concentration is only 5 M in contrast to the 8 M urea concentrations used by Doty and Katz. Finally, the pH of the solvent mixture was found to be 6.9 to 7.1, while the isoelectric point of native collagen is given by Gustavson (34) as 7 to 8. Therefore the collagen in URTC is probably close to its isoelectric point, where Doty and Katz found no effect at any urea concentration for the protein bovine serum albumin.

In view of these considerations it was felt that only slight selective absorption effects could occur and that these could be safely ignored. Nevertheless, it must be pointed out that some possibility of error due to this phenomenon does exist.

Light-scattering data were obtained for both the 546 mμ. and 436 mμ. wavelengths. The size and molecular weight (by the dissymmetry method) computed from the data for 436 mμ. were, however, found to be lower than those computed for 546 mμ. by more than could be accounted for as

experimental error. The molecular weight from the former was, indeed, 70% of that from the latter. The cause of this discrepancy was sought both in the possible presence of fluorescence (35) and in deviations from the normal type of angular scattering pattern.

Though no evidence of fluorescence was found, the complete angular scattering curve for 436 mμ. revealed a small peak in the region of 65 degrees to the incident beam. No such peak was found with the 546 mμ. wavelength, nor was there such a peak in the angular scattering curves of "Ludox" with either wavelength.

The angular scattering curves of URTC and of "Ludox" are illustrated in figures 12 and 13. These curves were obtained as follows: angular scattering intensities, relative to the scattering intensity for benzene at ninety degrees, were corrected by subtracting solvent scattering and multiplying the result by $\sin \theta / 1 + \cos^2 \theta$. The resulting data were then plotted so that the curves for the two wavelengths coincided at 60 degrees on the arbitrary relative scattering intensity scale (ordinate). Thus, were "Ludox" a solution of small, isotropic particles, the angular scattering curves for that liquid would be two coincident horizontal lines, one for each wavelength.

Figure 12 shows a peak at 65 degrees for URTC with $\lambda = 436$ mμ., which just rises above the general level of experimental fluctuations. It was therefore concluded that the size and refractive index of the URTC molecules are

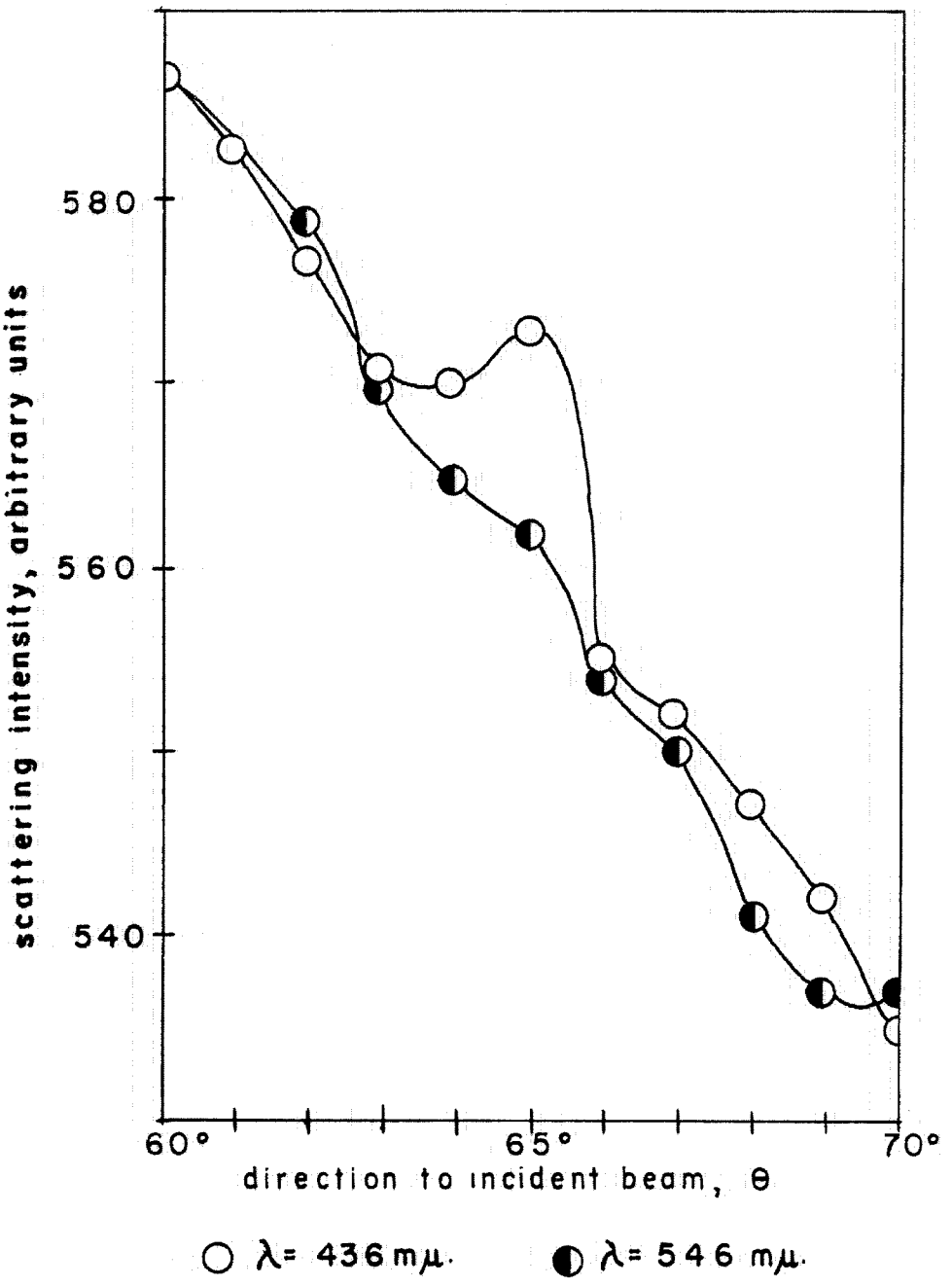

FIGURE 12

ANGULAR SCATTERING
OF URTC NEAR 65°

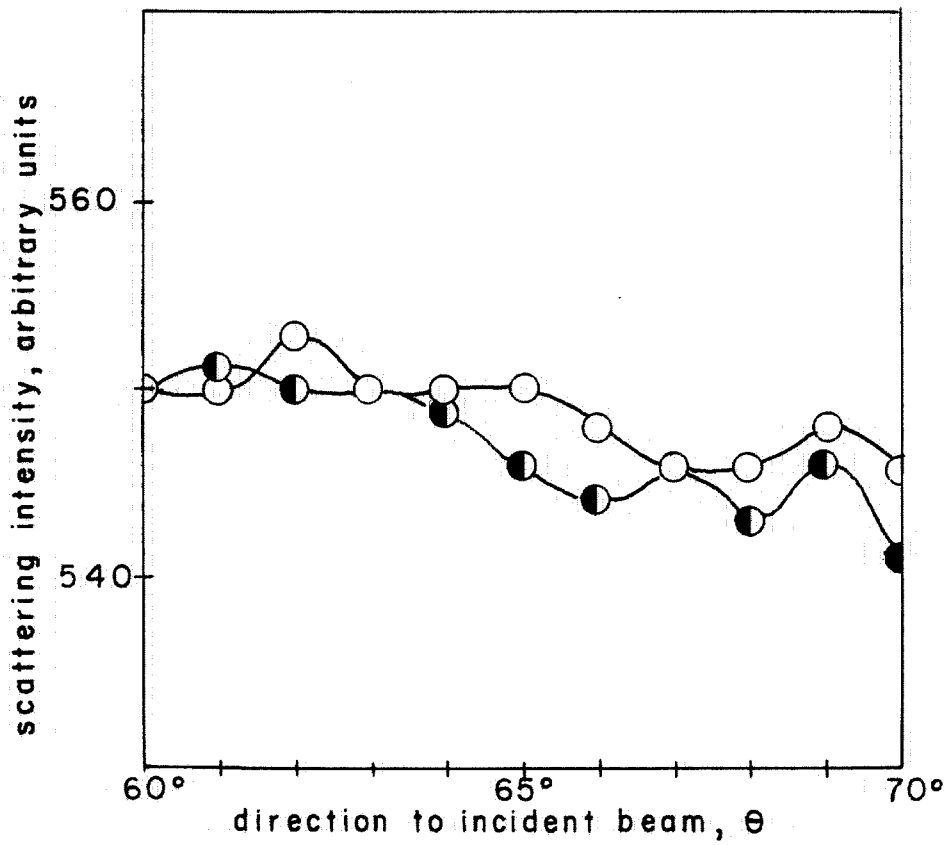

FIGURE 13

ANGULAR SCATTERING
OF "LUDOX" NEAR 65°

sufficiently large so that interpretation of the scattering on the basis of the Debye theory (5) for the shorter wavelength would have been unreliable. For the longer wavelength, no similar effect was apparent. The data for $\lambda = 546$ mμ., therefore, were considered to be of use. The results of scattering measurements performed at this wavelength are interpreted below.

Table 6 shows the concentrations of protein and the scattering intensities, relative to that for benzene at ninety degrees, for URTC with light of wavelength 546 mμ.

Table 6

conc. gms./cm^{3}x10^4	45°	90°	135°
36	27.4	8.44	15.2
18	16.5	5.05	9.13
9.0	9.57	2.89	5.25
4.5	6.19	1.73	3.14
solvent	1.07	0.34	0.61

Ninety-degree scattering and dissymmetry data for URTC at $\lambda = 546$ mμ.

These data, corrected for solvent scattering and for the refractive index effect, were used in preparing the plot of Kc/R(90) versus c shown in figure 14. The refractive index of the solvent mixture was found to be 1.38 at the appropriate wavelength. K was calculated using a value of 0.183 for dn/dc. This value was obtained from measurements

of the refractive increment of gelatin in the same solvent, since such solutions could be prepared containing a high and accurately known protein concentration (see Part III, Section B). A value of 2.34×10^{-7} was computed for K.

From figure 14 it is seen that the limiting value of Kc/R(90) at c = 0 is 4.8×10^{-6}. According to the theory of the dissymmetry method (4), the reciprocal of this quantity multiplied by $P^{-1}(90)$ gives the molecular weight of the solute. The latter function may be obtained from the dissymmetry. A plot of the dissymmetry versus concentration is shown in figure 15, from which the limiting value at c = 0 is found to be 1.82. Correction for the reflection of the incident beam results in a dissymmetry of 1.91.

Doty and Steiner (10) have tabulated values of $P^{-1}(90)$ as a function of the size and shape of the molecule; these may in turn be deduced from the dissymmetry. Table 7 shows the characteristic dimension, D, the function $P^{-1}(90)$ and the molecular weight, M, obtained from the tables of Doty and Steiner for the two molecular models considered possible for URTC.

Table 7

model	D in A.	$P^{-1}(90)$	M
thin rod	2.2×10^3	1.77	3.7×10^5
random coil	1.5×10^3	1.71	3.6×10^5

For the thin rod D represents the length; for the random coil D represents the root-mean-square average

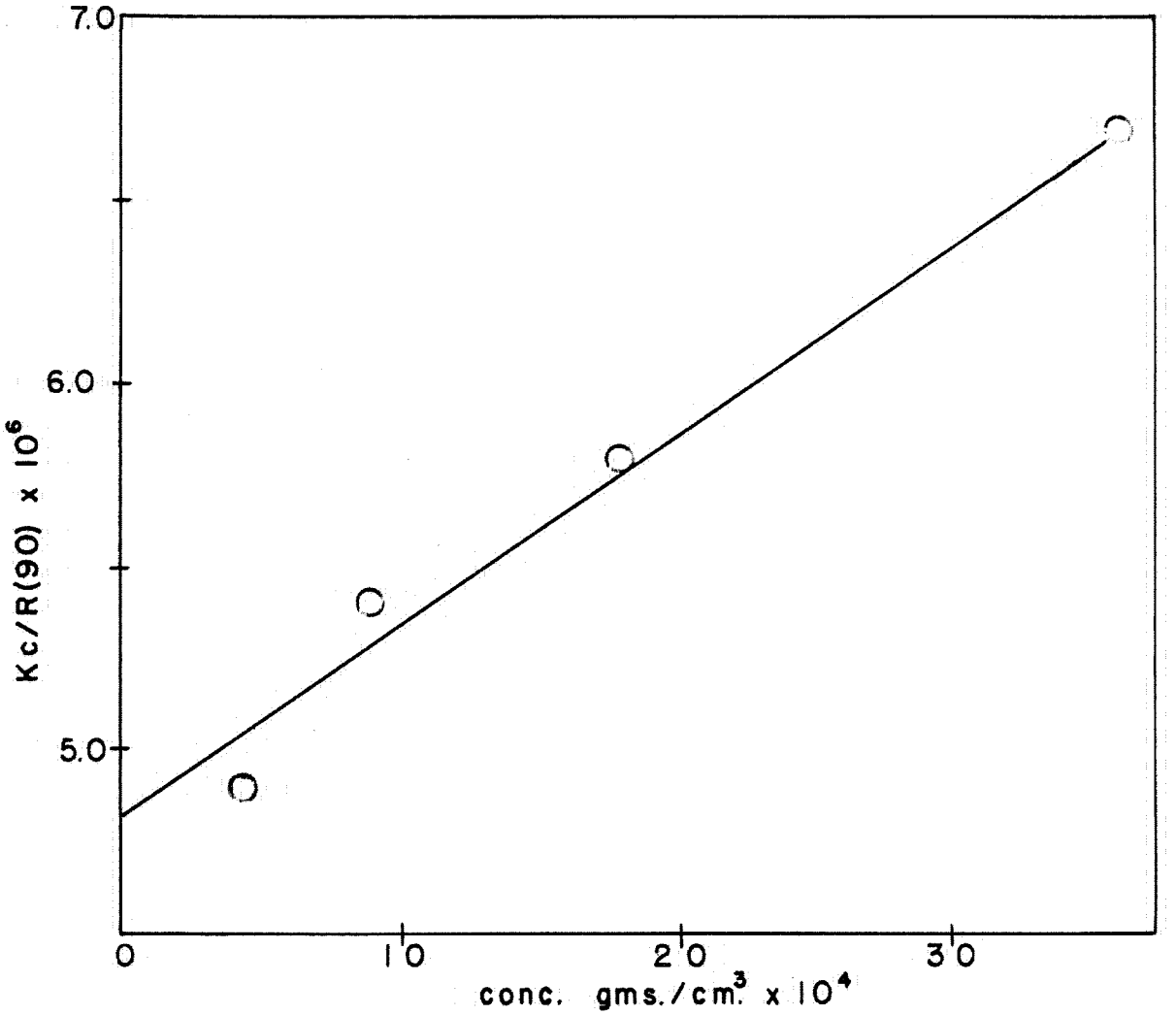

FIGURE 14

90° SCATTERING OF URTC

FOR $\lambda = 546$ mμ.

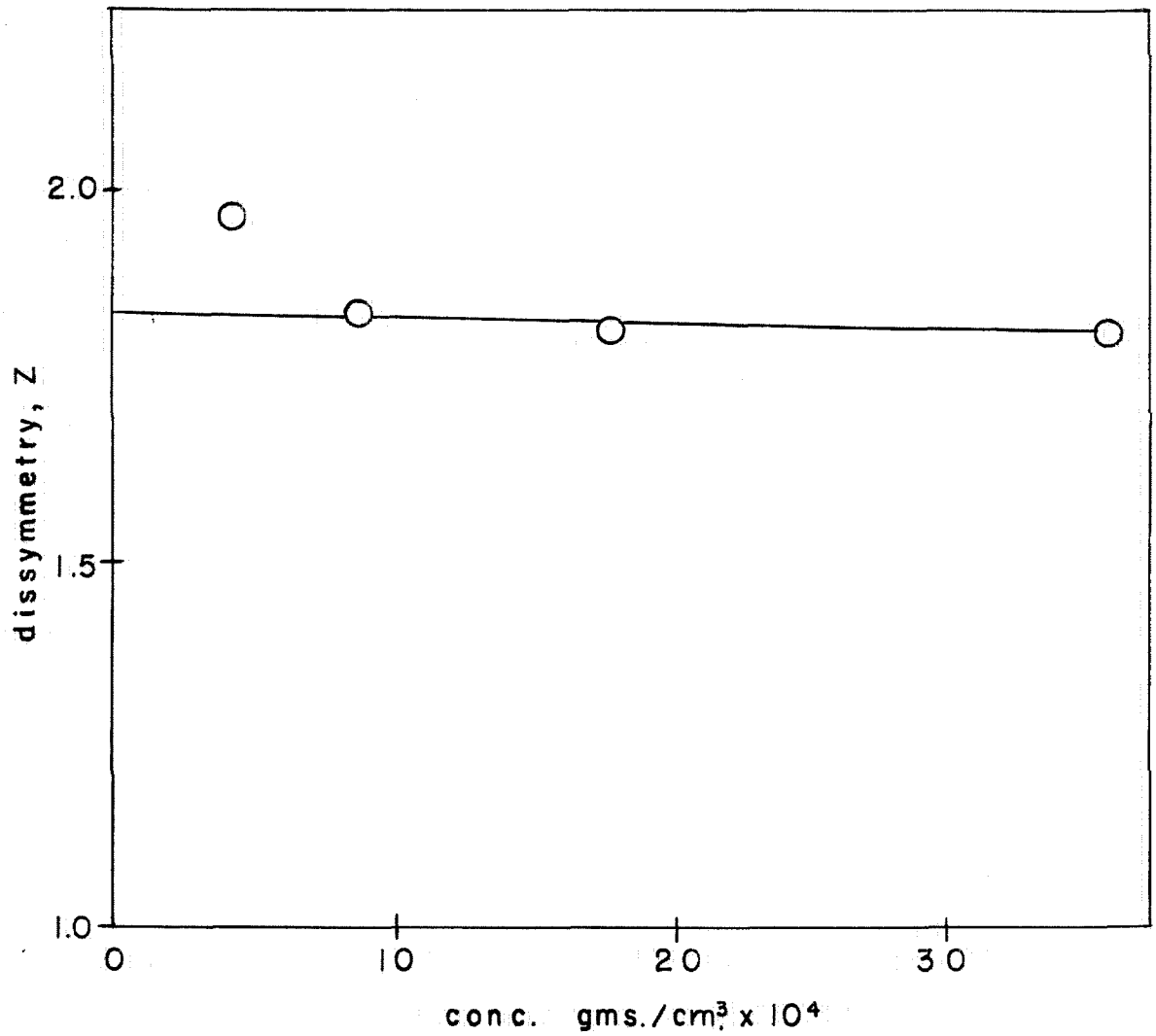

FIGURE 15

DISSYMMETRIES FOR URTC

$\lambda = 546$ mμ.

distance between the ends of the chain. It is now possible to determine which of these models best fits the data by means of simple geometrical considerations.

The r.m.s. end-to-end distance of the random coil is given by (5)

$$R^2 = n \left(\frac{1 - \cos\varphi}{1 + \cos\varphi}\right) \ell^2 \qquad \text{XV}$$

where R is the r.m.s. end-to-end distance, n is the number of elements in the chain, φ is the angle between successive elements and ℓ is the length of each element. Taking $R = 1.5 \times 10^3$ A., $\ell = 4$ A., about the length of the rigid unit in the polypeptide chain, and $\varphi = 110^\circ$, one obtains 6.8×10^4 as the number of elements in the chain, n; this is the number of amino acid residues required to construct a random coil of polypeptide chain with the given value of R. Using 93 as the average residue weight for collagen (16), the molecular weight of this polypeptide chain would be 63×10^5, or almost twenty times that observed. It must therefore be concluded that the actual URTC molecule is a good deal more rigid than the random coil model permits.

Turning now to the thin-rod model, it is evident that the radius of the rod is given by

$$r^2 = \frac{Mv}{\pi LN} \qquad \text{XVI}$$

where r is the radius of the rod, M is the molecular

weight, v is the specific volume of the rod-like molecules, L is the length of the rod, and N is Avogadro's number. From the experimental values of $M = 3.7 \times 10^5$ and $L = 2.2 \times 10^3$ A., and assuming that the volume occupied by one gram of collagen molecules in the solution is at least equal to the normal dry specific volume for proteins, 0.74 cm^3/gm, one obtains for the radius of the rod a value of 8 A. This figure is actually a minimum radius since the volume occupied by the molecule plus possible enclosed solvent may be somewhat greater than the dry partial specific volume of the protein.

It is interesting to note that the diameter of the rod, 16 A., compares well with the x-ray diffraction evidence for cylinders of diameter 12 - 20 A. depending on the hydration of the collagen. Furthermore, the length of the rod, 2200 A., is exactly the hypothetical length given by Schmitt, Gross and Highberger (20) for the elementary fiber on the basis of electron microscopic evidence.

A final computation of interest is based on the assumption that the rod is constructed of a single coiled polypeptide chain in the form of a helix. In this case the length per residue along the axis of the helix is found to be 0.55 A. If the rod consists of several intertwining helixes, the length per residue will be the appropriate multiple of this figure.

In general, however, the above conclusions must be considered as tentative in view of the several possible

sources of complications mentioned in the course of this discussion.

4) Intrinsic viscosity.

Viscosity measurements were made on a sample of the same URTC stock solution as was used for the light-scattering studies reported above. The sample was centrifuged for twenty minutes at 60,000 g. The same Ostwald viscometer was employed as that used for studying the viscosity of RTC. All measurements were made in a thermostated water bath at 25.0° C.

The flow time for the solvent mixture (5 M urea, 2% NaCl and 0.01% merthiolate) was 181.1 seconds. The flow time for water was 144.3 seconds. The density of the solvent mixture at 25.0° C. was found to be 1.086 gm./cm^3. Hence the solvent viscosity was computed as 1.22×10^{-2} Poises, using the I. C. T. value for the viscosity of water at that temperature, 8.95×10^{-3} Poises. Dilutions of the original stock solution were made directly in the viscometer by adding the necessary volume of solvent which had first been passed through a medium-fine glass sinter.

Table 8 gives the protein concentrations in grams per 100 cm^3 and the corresponding efflux times for several dilutions of the URTC stock solution.

Table 8 - Viscosity data for URTC

C_w	t, sec.	$\frac{\ln t/t_o}{C_w}$	G, sec^{-1}
36×10^{-2}	260.8	1.01	1400
24×10^{-2}	230.2	1.00	1590
16×10^{-2}	212.6	0.98	1720
11×10^{-2}	201.8	1.01	1810
7.1×10^{-2}	195.0	1.04	1870
solvent	181.1	-	2020

The meaning of the symbols in table 8 is the same as in table 5. It is evident that an extrapolation of $\frac{\ln t/t_o}{C_w}$ to $C_w = 0$ would give an intrinsic viscosity of about 1.0 dl./gm. It is noteworthy that the intrinsic viscosity of URTC is about 1/28 th that of RTC. This value, however, is probably somewhat low due to the fact that it was not extrapolated to zero flow gradient, but the error cannot be very large since URTC does not exhibit extreme orientation.

5) Sedimentation velocity.

After each light-scattering measurement, half of the solution in the light-scattering cell was withdrawn and subjected to ultracentrifugal analysis. The first three concentrations contained sufficient protein to provide useful sedimentation diagrams, the fourth being too dilute to give a clearly visible sedimenting boundary. All runs were made at rotor speeds between 987 and 1000 cps., and at temperatures

of 22 ± 1° C. Some of the sedimentation diagrams obtained are shown in figure 16. An unusual feature of these diagrams is the extreme curvature of the baseline upon which the protein boundary moves. That this is probably due to the high urea concentration in the solvent mixture may be seen from the following discussion.

Application of the theory of sedimentation equilibrium (36) shows that, at equilibrium, the ratio of the concentration of the solute at position 2 in the cell to that at position 1 is given by

$$\frac{c_2}{c_1} = \exp\left\{\frac{M\,(1 - \bar{v}\rho)\,\omega^2\,(x_2^2 - x_1^2)}{2RT}\right\} \qquad \text{XVII}$$

where M is the solute molecular weight, $\bar{v}$ is its partial specific volume, ρ is the solution density, ω is the angular velocity of the rotor, x_1 and x_2 are the distances of positions 1 and 2 from the center of rotation, R is the gas constant and T is the absolute temperature. To compute the relative concentrations of urea, in this case, at the top and bottom of the cell upon attaining equilibrium, substitute the values $M = 60$, $\bar{v} = 0.71$, $\rho = 1.086$, $\omega = 2 \times 10^3$, $x_2 = 7.08$ cm., $x_1 = 5.95$ cm., $R = 8.314$ ergs deg^{-1} mol^{-1} and $T = 298°$ K., and obtain

$$\frac{c_2}{c_1} = e^{0.22} = 1.25$$

Since this ratio is not too far from unity, it follows that both c_2 and c_1 are close to the average urea concentration, $\bar{c}$,

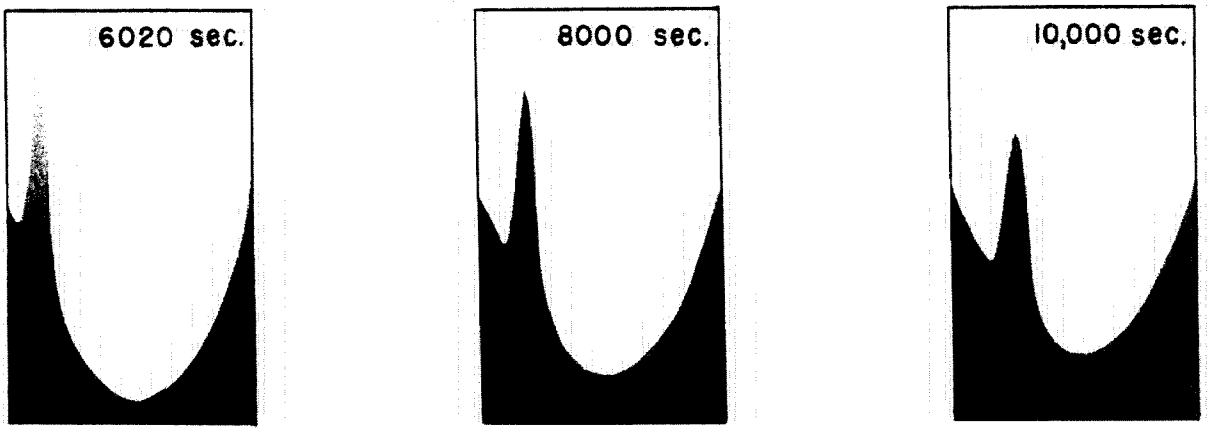

$c = 36 \times 10^{-4}$ gms./cm.^{3}

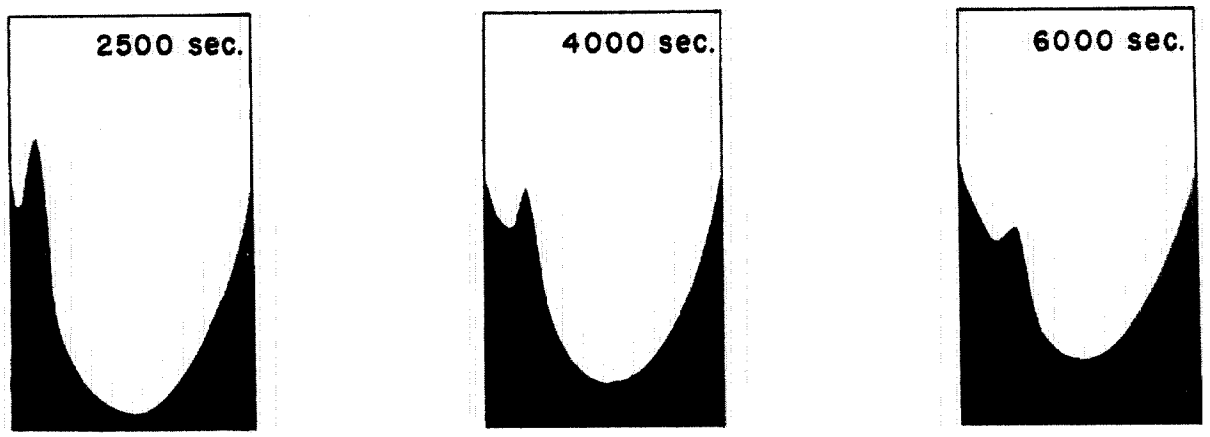

$c = 18 \times 10^{-4}$ gms./cm.^{3}

FIGURE 16

SEDIMENTATION DIAGRAMS OF URTC

for the 5 M solution, about 0.3 gms./cm^3 , so that one may write

$$\frac{c_2 - c_1}{c_1} = \frac{\Delta c}{\bar{c}} = 0.25$$

or $\Delta c = 0.075$ gms./cm^3. Apparently the equilibrium difference in the urea concentration between the top and bottom of the cell is sufficient to cause a considerable refractive index gradient. As is evident from figure 16, even though the urea has probably not yet reached its equilibrium distribution, it has progress far enough in this direction to cause a refractive index gradient in the cell which is evident as a marked curvature of the baseline. That this curvature is characteristic of the solvent and not a result of the behavior of the dissolved protein was established by running pure solvent in the ultracentrifuge. As expected, the same curvature of the baseline was obtained.

The peak representing the sedimenting protein boundary is superimposed upon this distorted baseline, thus becoming flattened and skewed. This effect makes it difficult to measure sedimentation velocities in solutions of protein concentration less than 1 x 10^{-3} gms./cm^3 and thus only the sedimentation velocities of the three most concentrated solutions are given here. A plot of the reciprocals of the sedimentation constants at 25.0° C. and in the 5 M urea solvent (s^u_{25}) versus concentration of protein is shown in figure 17. Plotting the reciprocals instead of the constants themselves tends to result in a more nearly linear

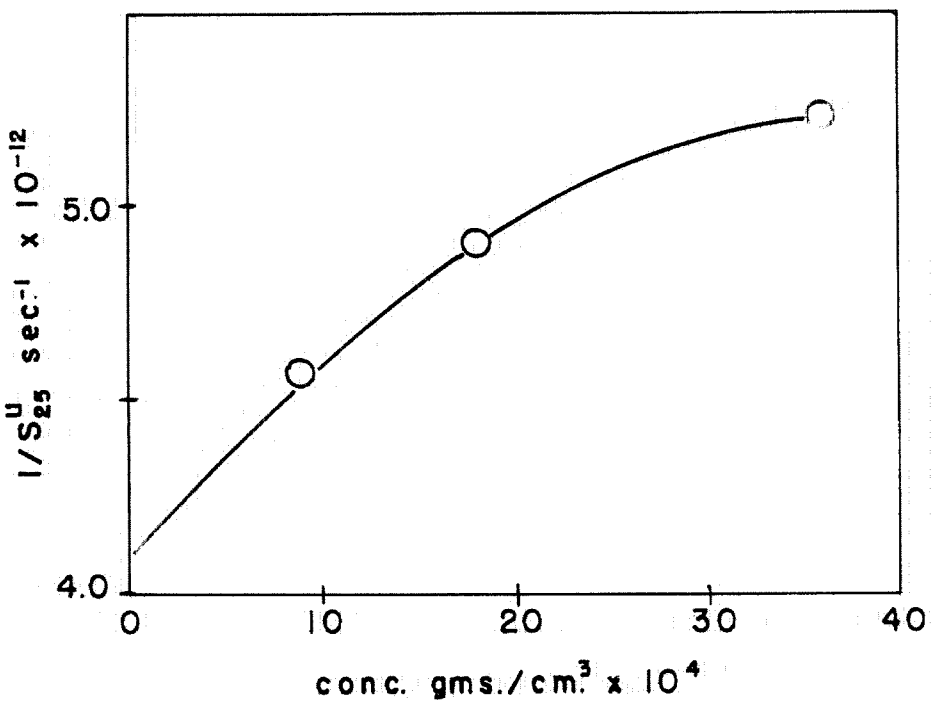

FIGURE 17

RECIPROCALS OF SEDIMENTATION CONSTANTS FOR URTC

extrapolation. It appears, however, that the curve begins to turn downward in the low concentration region, making the extrapolation to zero concentration somewhat uncertain. An approximate value of the extrapolated sedimentation constant may be taken as 2.4×10^{-13} sec., though the correct value may be considerably greater if the curve actually continues its descent near zero concentration.

6) Interpretation of viscosity and sedimentation velocity of URTC.

It has been common practice to interpret hydrodynamic measurements such as viscosity and sedimentation velocity by assuming that the hydrodynamic ellipsoid of revolution equivalent to the molecule of solute has the same volume as that calculated for the solute molecule from its partial specific volume. The well known Simha equation (28) may be used to compute the axial ratio of the ellipsoid from the viscosity number, and in turn the Perrin equation (28) gives the parameter f/f_o as a function of this axial ratio. If f/f_o is substituted in the sedimentation rate equation, one obtains for the molecular weight of the sedimenting molecule

$$M^{2/3} = \frac{N^{2/3} \cdot 6\pi\eta \left(\frac{3\bar{v}}{4\pi}\right)^{1/3} \cdot s}{(1 - \rho\bar{v})} \left(\frac{f}{f_o}\right) \qquad \text{XVIII}$$

where M is the molecular weight of the solute, N is Avogadro's

number, η is the solution viscosity, $\bar{v}$ is the partial specific volume of the solute, ρ is the solution density, s is the sedimentation constant of the solute, f is the frictional coefficient of the solute molecule and f_o is the frictional coefficient of a sphere of the same volume as the actual solute molecule.

Applying this procedure to the data for URTC, one obtains for the viscosity number a value of 137, an axial ratio of 45, $f/f_o = 2.8$ and, from equation XVIII, $M = 1.8 \times 10^5$. These parameters are compatible with a rod of diameter 18 A. and length 830 A. Though the diameter is in rough agreement with the diameter computed from light scattering, 16 A., the molecular weight and length are in serious disagreement with the light-scattering values of 3.7×10^5 and 2200 A.

Recently, Scheraga and Mandelkern (37) have criticised the assumption that the equivalent hydrodynamic ellipsoid has the same volume as the partial specific volume of the protein molecule and have pointed out instances where serious interpretive errors have occurred as a result. They recommend, instead, that the molecular weight be independently determined and that the volume and axial ratio of the ellipsoid be treated as the unknowns to be determined by two separate hydrodynamic measurements. These authors have given tables of the experimental hydrodynamic quantity, β, as a function of the axial ratio of the ellipsoid. They have also pointed out that this ellipsoid

does not necessarily bear a simple relation to the molecule represented by it. The equation for β in terms of the hydrodynamic measurements reported here for URTC is

$$\beta = \frac{Ns[\eta]^{1/3}\,\eta}{M^{2/3}\,(1 - \bar{\nu}\rho)} \qquad \text{XX}$$

where the symbols have their previous meanings. Computation of β by substitution of the value for M determined by light scattering results in $\beta = 1.75 \times 10^6$. But the lowest physically possible value for β is 2.12×10^6, for the case in which the axial ratio of the ellipsoid is unity. For a rod-like molecule of the dimensions indicated by the light scattering of URTC, a value of 3.00×10^6 would seem more appropriate. The cause of this discrepancy is most likely to be found in the low extrapolated sedimentation constant, due to the complications already indicated, and a somewhat low intrinsic viscosity due to neglect of the orientation of the molecules of URTC in a velocity gradient. It may also be a result of a somewhat high molecular weight from light scattering, especially if URTC is not strictly monodisperse but has a distribution containing a tail of high molecular weight material.

7) Dialysis of URTC.

When URTC is exhaustively dialysed against very dilute aqueous acetic acid, the viscosity of the solution increases sharply and in general it displays the properties typical of

RTC solutions. However, it has been found that the light-scattering properties of these preparations depend on the length of time during which the collagen has been subjected to the action of 5 M urea. In general, the longer the URTC was allowed to incubate before dialysis, the smaller the particles in the dialysed solution appear to be. Furthermore, the ease of precipitation of the collagen from the dialysed solution also follows a similar course, the solutions of shorter incubation period precipitating most readily upon the addition of NaCl, while URTC which has been allowed to stand for one month before dialysis will then give no precipitate at all.

Examination of the precipitate obtained from dialysed URTC by means of electron microscopy shows that it consists of intertwining fibrous networks, but that the structure characteristic of both native collagen fibrils and of precipitated RTC fibrils is not present. Typical electron micrographs of such precipitates are shown in figure 18.

Table 9 summarizes the results of light-scattering measurements of a preliminary nature which were performed on three samples of dialysed URTC. Unfortunately, these were all different original URTC preparations, but all displayed about the same dissymmetry before dialysis. Each preparation was allowed to incubate for a different period of time, as indicated in table 9, then exhaustively dialysed against 1/10,000 acetic acid in the cold for approximately the same period of time. Each dialysed solution was clarified

Table 9

duration of incubation in 5M urea		1 day	3 days	30 days
duration of dialysis		7 days	11 days	10 days
light-scattering dissymmetry, z	436 mμ.	4.3	3.0	1.9
	546 mμ.	4.5	2.9	1.6
R for random coil, from z	436 mμ.	2900 A.	1900 A.	1100 A.
	546 mμ.	3900 A.	2300 A.	1100 A.
molecular weight	436 mμ.	6×10^6	1.8×10^6	1.0×10^6
	546 mμ.	12×10^6	2.2×10^6	1.2×10^6
precipitability with NaCl		ppts. readily	ppts. slowly	no ppt.

Effect of incubation period on results obtained from light-scattering measurements on dialysed URTC solutions.

by centrifuging for 20 minutes at 60,000 g. A sample of each clarified solution was transferred to a light-scattering cell and a series of concentrations examined by the procedure already outlined previously. As usual, the portions of the solutions removed after each set of light-scattering determinations were retained for nitrogen analysis by Nessler's method.

Measurements were made with both the 436 mμ. and 546 mμ. wavelengths. Appropriate correction factors were applied in computing the results shown in table 9, and all have been extrapolated to zero concentration. Molecular weights were computed by the dissymmetry method.

For purposes of comparison, it is recalled that the molecular weight obtained by the dissymmetry method on a solution of RTC was about 20×10^6, and for URTC it was 0.37×10^6.

Attention is called to the fact that the discrepancy between the molecular weights and sizes calculated from the data for the two wavelengths decreases as the average size of the particles in solution becomes smaller, supporting the hypothesis that such discrepancies are due to the failure of the simple scattering theory when confronted by particles of sufficient size to give dissymmetries near 2.0 (recall light-scattering results for URTC).

It is hardly necessary to point out the great number of possible spurious effects which could have influenced the

results indicated in table 9. A great deal of work has been left undone in this preliminary study, but if a tentative conclusion may be drawn at this point, it appears to be that the dissociation of RTC by urea takes place in two distinct steps. The first, rapid step is the splitting of the particles in RTC into smaller entities which may be the molecules of collagen. The second, slower process consists of a gradual removal of the ability of these "molecules" to reaggregate upon removal of the urea.

In any event, these results indicate that a subject for further investigation exists.

D) The transformation of RTC to gelatin.

Gelatin is prepared by heat treatment of animal matter containing collagen. Thaureaux (21) has studied the change in the streaming birefringence and optical rotation of soluble collagens brought about by heating. It was found that the optical rotation of solutions of rat-tail tendon collagen in dilute formic acid remained practically unchanged upon warming from 10° C. to 40° C., then dropped suddenly upon reaching 40° C. Likewise, the strong streaming birefringence of these solutions also disappeared when they were warmed to 40° C. These changes were interpreted by Thaureaux as a transformation of the collagen to "parent" gelatin.

The light-scattering experiments to be described here were performed in order to determine the nature of the change

occurring in the particles of RTC when they are heated to 40° C. or above, and to try to obtain information about the structure of the parent gelatin molecules which result.

1) Qualitative observations.

If a freshly prepared solution of RTC is clarified by centrifugation for 20 minutes at 60,000 g. and a portion thereof placed in a light-scattering cell which is then warmed at 50° C. for about 1/2 hour, a change in the light scattering is observed which indicates a slight contraction in the average extension of the particles in solution. Specifically, there occurs a decrease in the dissymmetry accompanied by an increase in the ninety-degree scattering. Evaporation of the solvent is ruled out as a cause for this phenomenon by covering the cell during the warming period. Further warming at this temperature produces no further effect.

Without disturbing the cell contents, about four drops of saturated NaCl solution, which has been first clarified of motes by centrifugation, may now be added and the cell contents gently stirred. The solution now contains about 1% NaCl. A light-scattering measurement on this solution now indicates a very marked average contraction of the particles, which is completed by an additional 10 minutes of warming at 50° C. No significant change in the light scattering is observable if the solution is allowed to cool to room temperature. Such heated RTC solutions containing 1%

NaCl will be designated as HRTC in the following discussion.

The HRTC solution may now be centrifuged to a constant dissymmetry, which was not possible for the RTC solution. Since this involves a sharp drop in the dissymmetry accompanied by a moderate decrease in the ninety-degree scattering, it may be concluded that the process consists of the removal of a small quantity of rather highly aggregated protein. The molecules in these solutions are probably to be identified with parent gelatin, and as such, their size and shape are of some considerable interest.

Table 10 shows the results of light-scattering measurements in an experiment such as described in the above paragraphs. The dissymmetries are uncorrected for reflection. The figures for the ninety-degree scattering in table 10 are simply galvanometer deflections on an arbitrary scale, and serve merely to provide a basis for comparison. The data shown are those for the wavelength 546 mμ.

Sedimentation diagrams of such a parent gelatin preparation containing 7.4×10^{-4} gms./cm^3 of protein and at a temperature of 22° C. are shown in figure 19. They show a single sedimenting boundary which diffuses in the normal manner. The sedimentation constant computed from these diagrams and corrected to water at 20° C. is 3.24×10^{-13} sec. A concentration series was not run at this time, the object of the sedimentation experiment being only

Table 10

sample and treatment	z	90° scattering	interpretation
RTC centrifuged 20 min. at 60,000 g.	6.0	205	extended, electrically charged networks
heated at 50° C. for 1/2 hour	5.3	214	probably slight decrease in average extension
1% NaCl added	3.5	423	marked decrease in average extension due to weakened electrical repulsions
heat again at 50° C. for ten minutes	3.2	540	completion of above process
centrifuge to constant dissymmetry	1.9	430	removal of aggregated protein debris

The transformation of RTC to parent gelatin as followed by ninety-degree scattering intensity and dissymmetry, z.

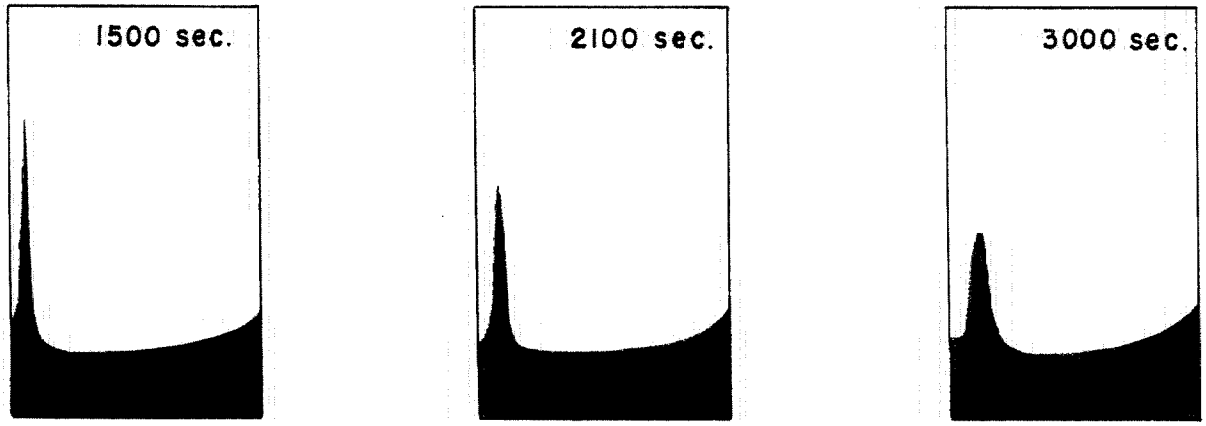

$c = 7.4 \times 10^{-4}$ gms./cm.^{3}

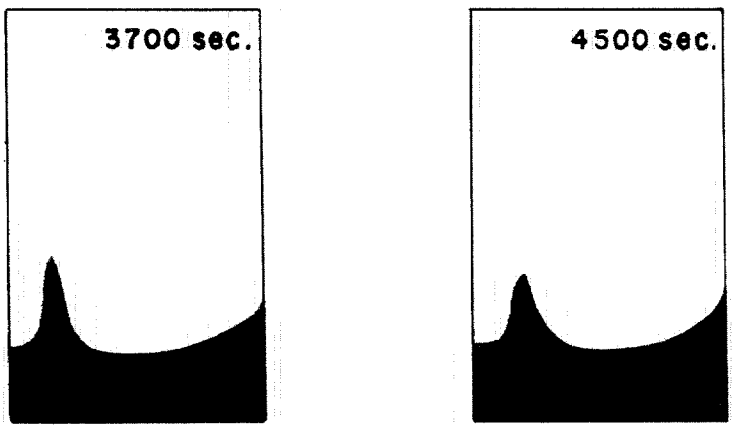

FIGURE 19

SEDIMENTATION DIAGRAMS OF HRTC

to determine whether the preparation was obviously heterogeneous with respect to sedimentation velocity. The evidence offered by both the sedimentation diagrams and by the fact that HRTC may be centrifuged to constant dissymmetry are in agreement in indicating the probable homogeneity of the parent gelatin preparation.

2) Angular and concentration dependence of light scattering by HRTC.

In view of the fact that the parent gelatin solution appears to be homogeneous, contains sufficient salt to neutralize possible interfering charge effects (27), shows a dissymmetry less than 2.0, and has a solvent scattering background essentially that of water, it was thought profitable to try to obtain data sufficiently complete and accurate to permit the unambiguous characterization of the solute molecules.

The necessary data were obtained in the manner described previously. Each concentration was diluted by a factor of 1/2 directly in the light-scattering cell and a portion of each solution was saved for nitrogen analysis. Table 11 shows the scattering intensities as a function of angle for several concentrations of a preparation of parent gelatin. The scattering intensities were measured relative to that of benzene at 90 degrees. The protein concentrations were estimated from nitrogen analyses assuming 17.5% nitrogen in the dry protein.

Table II

λ, mμ.	conc. gms./cm^3 x 10^4	45°	50°	60°	70°	80°	90°	100°	110°	120°	130°	135°
436	14.7	24.0	19.0	13.1	9.73	7.76	7.00	6.89	7.58	8.70	10.8	12.4
436	7.37	13.7	10.8	7.40	5.29	4.24	3.75	3.75	4.10	4.63	5.76	6.54
436	3.68	7.00	5.60	3.75	3.83	2.18	1.93	1.89	2.12	2.41	2.93	3.35
436	1.84	3.84	3.08	2.08	1.48	1.20	1.03	1.03	1.20	1.32	1.63	1.94
436	solvent	0.53	0.36	0.17	0.14	0.11	0.10	0.11	0.15	0.16	0.19	0.22
546	14.7	31.9	25.6	17.8	13.5	10.9	9.73	9.57	10.7	12.1	14.9	17.2
546	7.37	17.1	13.5	9.24	6.75	5.35	4.81	4.61	5.35	6.01	7.22	8.61
546	3.68	9.50	7.51	5.15	3.70	2.83	2.50	2.45	2.97	3.24	3.92	4.69
546	1.84	5.20	4.29	2.64	1.92	1.51	1.39	1.32	1.78	1.78	2.18	2.57
546	solvent	1.06	0.55	0.35	0.20	0.14	0.14	0.14	0.35	0.35	0.35	0.35

Angular and concentration dependence of light scattering from parent gelatin solution for two wavelengths.

The data in table 11 were corrected for solvent scattering, reflection of the incident beam at the exit face of the cell, the refractive index effect, the change in illuminated volume viewed by the photomultiplier, and the corrected intensities were divided by $1 + \cos^2 \theta$. Figures 20 and 21 represent the set of angular and concentration dependence curves at the wavelengths 436 mμ. and 546 mμ. respectively. K was computed using the refractive index of water for n (equation XI) and the refractive increment, dn/dc, for gelatin giving 5.86×10^{-7} and 2.18×10^{-7} at the two wavelengths. The factor 600 by which c is multiplied was chosen arbitrarily to provide a convenient range on the abscissa for plotting the curves.

According to the theory of the Zimm plot (9), the reciprocal of the intercept on the ordinate is equal to the weight-average molecular weight of the solute. Reference to figures 20 and 21 shows that the intercept is identical for the two plots, giving M 1.1 x 10^6.

Information on the shape and size of the molecules may be obtained from the extrapolated curves designated c = 0, the equation of which may be written

$$\lim_{c=0} \frac{Kc}{R(\theta)} = \frac{P^{-1}(\theta)}{M} \qquad \text{XXI}$$

Multiplication by M of the ordinates of points on these extrapolated curves gives the curves $P^{-1}(\theta)$ versus $\sin^2 \theta/2$.

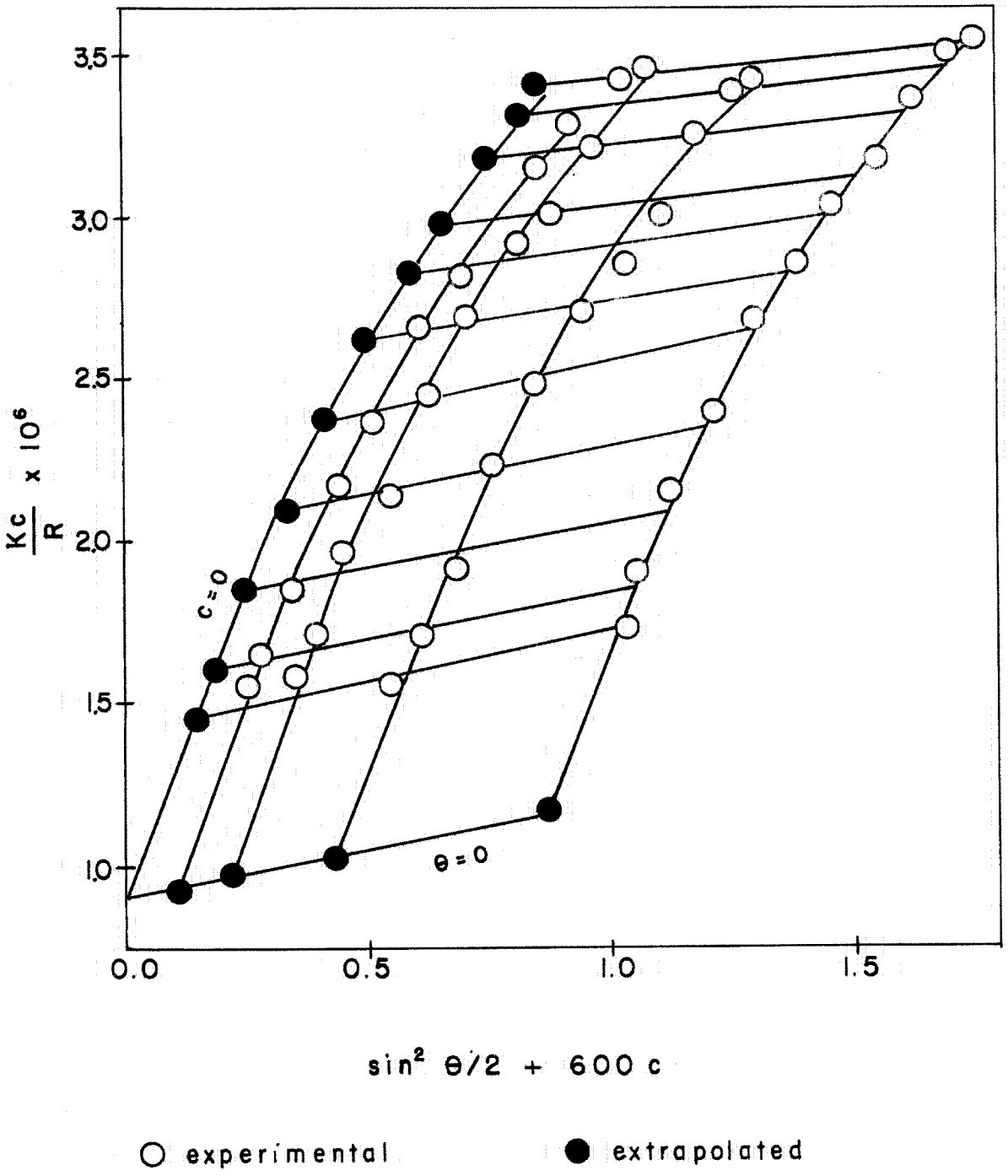

FIGURE 20

ZIMM PLOT FOR HRTC

λ = 436 mμ.

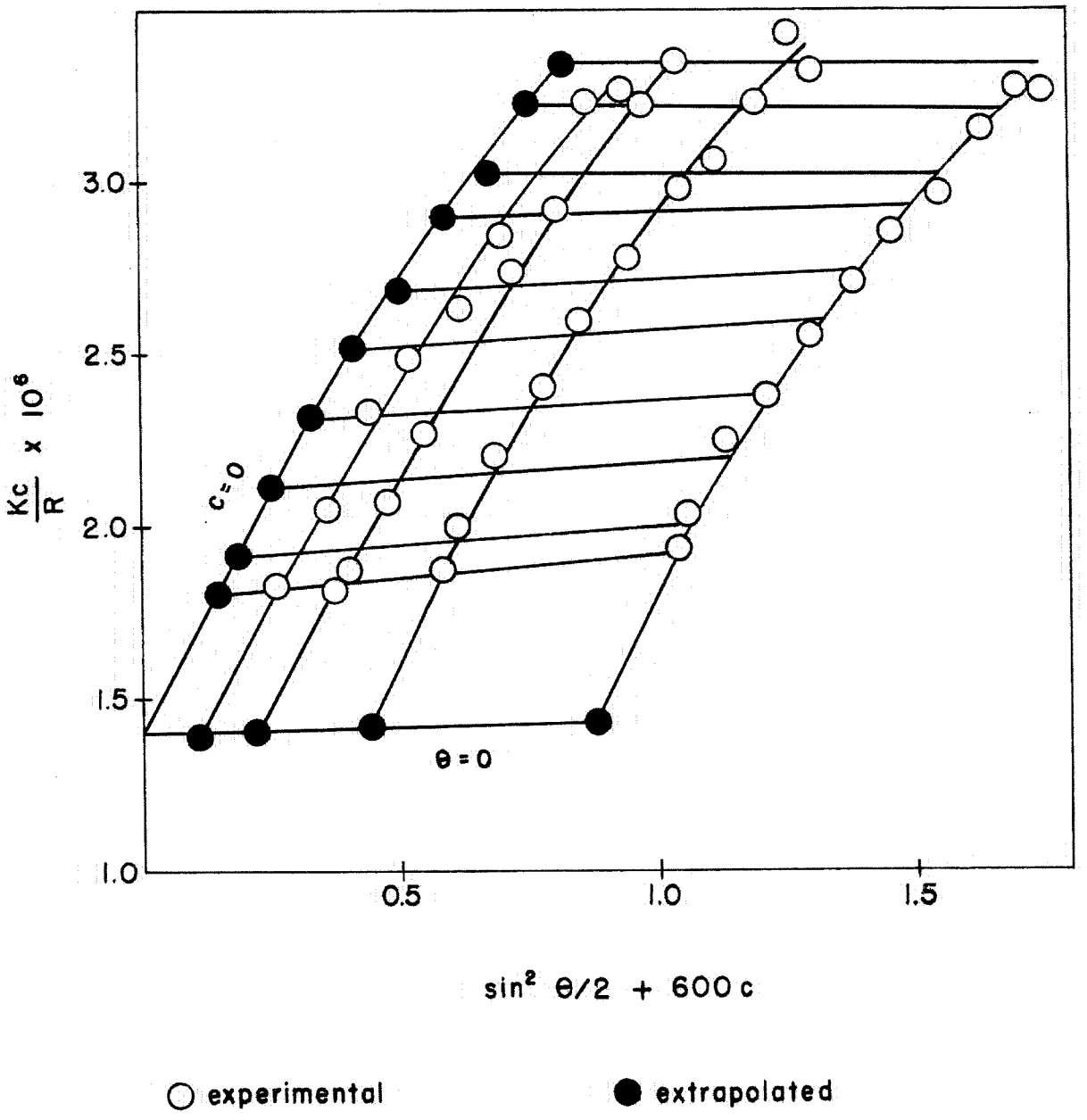

FIGURE 21

ZIMM PLOT FOR HRTC

$\lambda = 546$ mμ

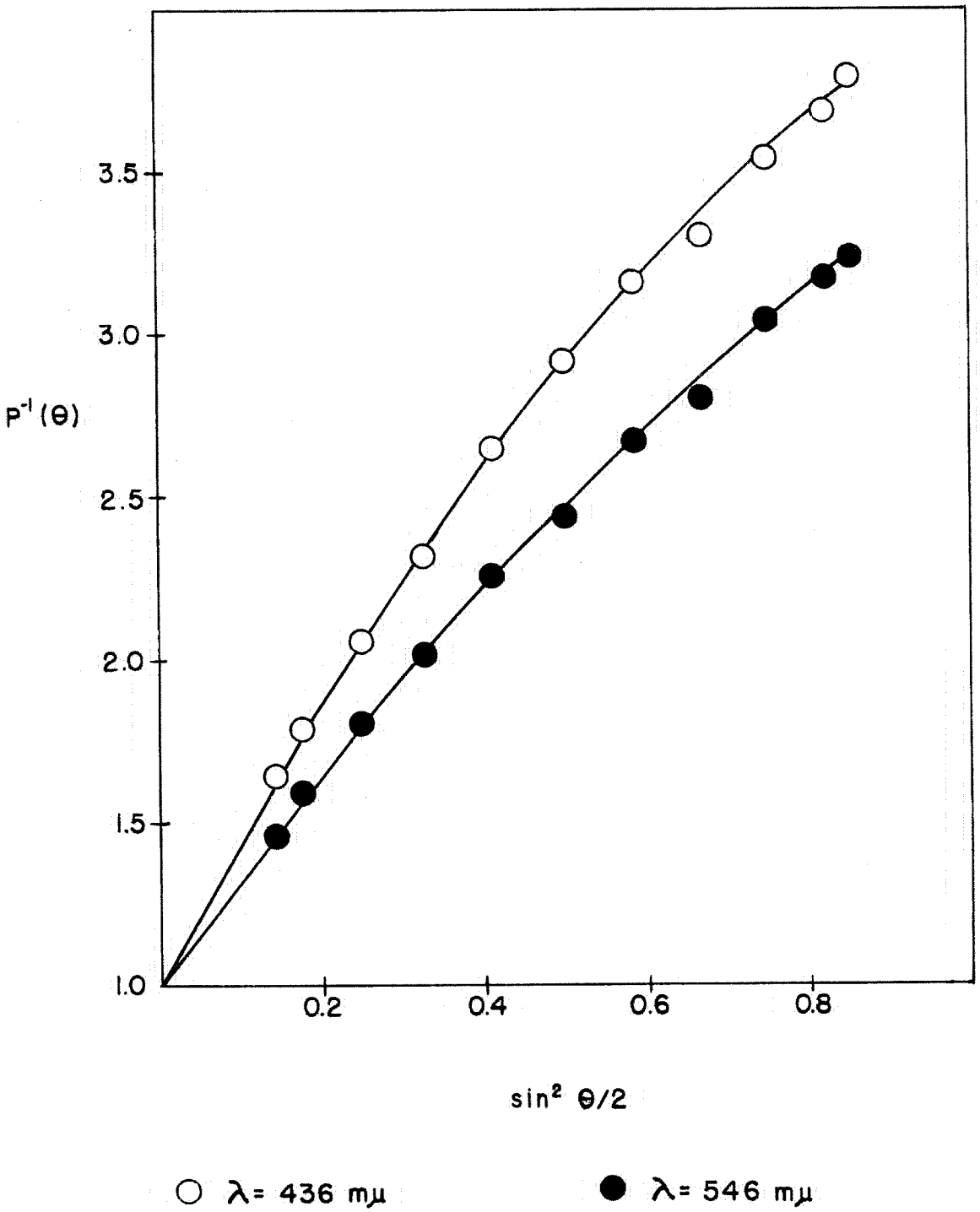

FIGURE 22

$P^{-1}(\theta)$ FOR HRTC

These are shown in figure 22.

If the theoretically derived $P^{-1}(\theta)$ function for a particular model of the molecule is expanded for small values of θ, one obtains (9)

$$P^{-1}(\theta) = 1 + \frac{8\pi^2}{9\lambda'^2} R^2 \sin^2 \theta/2 \qquad \text{XXII}$$

for the random coil with r.m.s. end-to-end distance of R, or

$$P^{-1}(\theta) = 1 + \frac{4\pi^2}{9\lambda'^2} L^2 \sin^2 \theta/2 \qquad \text{XXIII}$$

for thin rods with length L, where λ' is the wavelength of light in the solution. Thus R or L can be computed from the initial slope of the $P^{-1}(\theta)$ versus $\sin^2 \theta/2$ curves obtained experimentally.

The initial slopes obtained from figure 22 are 4.25 and 3.25 for 436 mμ. and 546 mμ. respectively, giving R = 2300 and 2500 for the random coil model and L = 3200 and 3500 for the rod model. The discrepancy between the results for the two wavelengths may again be attributed to the large size of the solute particles, with preference probably going to the figures for λ=546 mμ. as being more accurate.

A choice between the two models can now be made by means of two distinct criteria. First, the geometrical considerations outlined on page 71 may be applied. Using equation XV with R = 2500 A., ℓ = 4 A., Φ = 110°, the number of residues, n, is estimated as 1.9×10^5. Multiplying

by the average residue weight, 93, the molecular weight compatible with a random coil of this size is found to be 18×10^6, or almost eighteen times that observed. Thus the rod is probably the correct model.

The second and more reliable method of determining the actual shape of the molecule is to plot the theoretical $P^{-1}(\theta)$ functions for each model using the characteristic dimensions experimentally determined in the independent variable* and compare with the experimental points plotted on the same coordinates. This is just equivalent to selection from the entire family of $P^{-1}(\theta)$ curves for a given shape that one which has the same initial slope as the experimental curve. This has been done in figure 23. The theoretical curves were plotted with the aid of tables given by Doty and Steiner (10). The superiority of the rod model is again clear. It may be concluded, therefore, that the parent gelatin molecule is a rod of molecular weight 1.1×10^6 and with a length of approximately 3500 A.

The minimum diameter of the rod is given by equation XVI as 22 A. The length per residue computed on the assumption that the rod is constructed of a single-chain helix is 0.3 A. or the appropriate multiple of this for a multiple-helix structure.

---

* $\frac{4\pi^2}{\lambda'^2} L^2 \sin^2 \theta/2$ for rods and $\frac{8\pi^2}{3\lambda'^2} R^2 \sin^2 \theta/2$ for random coils.

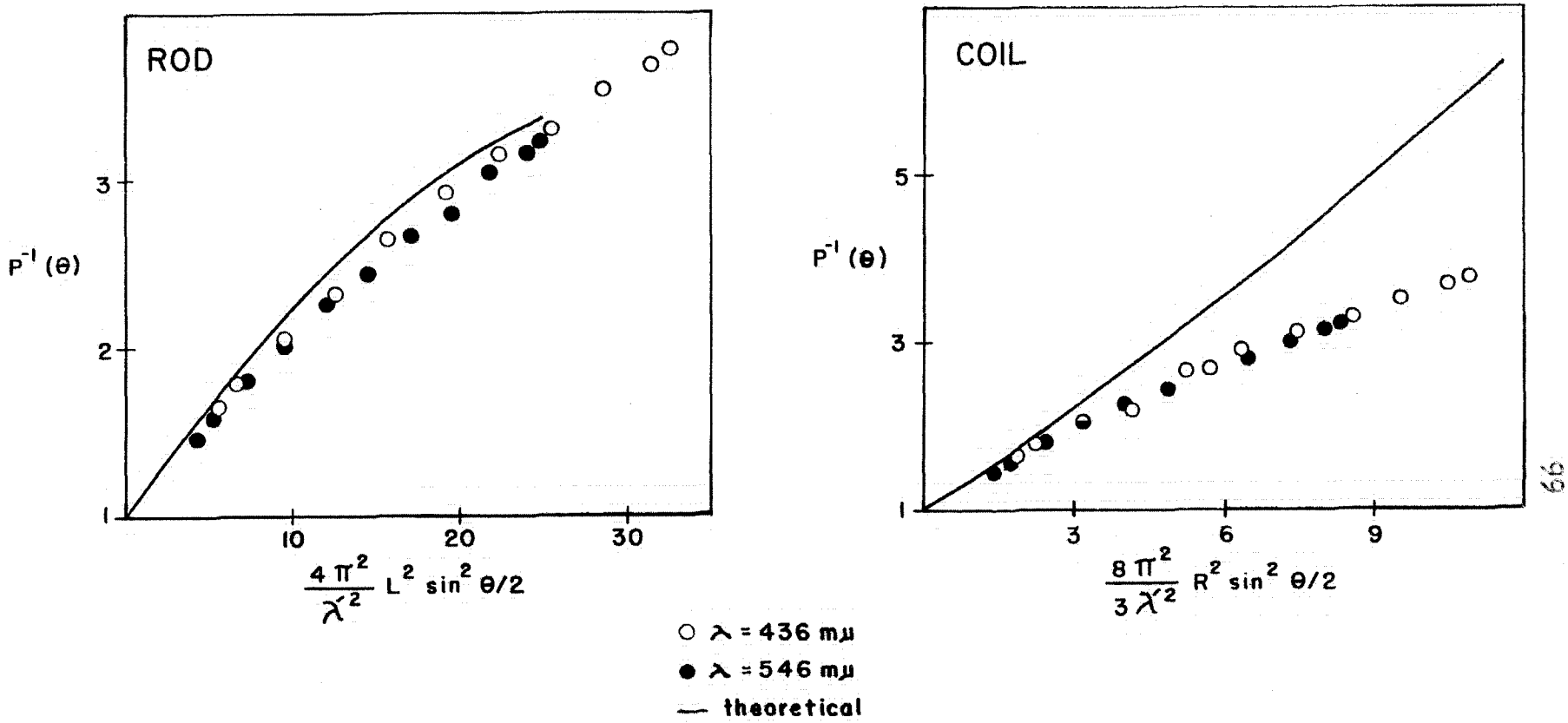

FIGURE 23

THEORETICAL $P^{-1}(\theta)$ FOR RODS AND COILS

E) A theory of the molecular properties of rat-tail tendon collagen.

A relatively simple picture of some of the structural features of rat-tail tendon collagen is capable of accounting for all of the observations reported in this Part. Figure 24 is a schematic representation of this structure for a typical region within a collagen fibril. The symbol ~O~

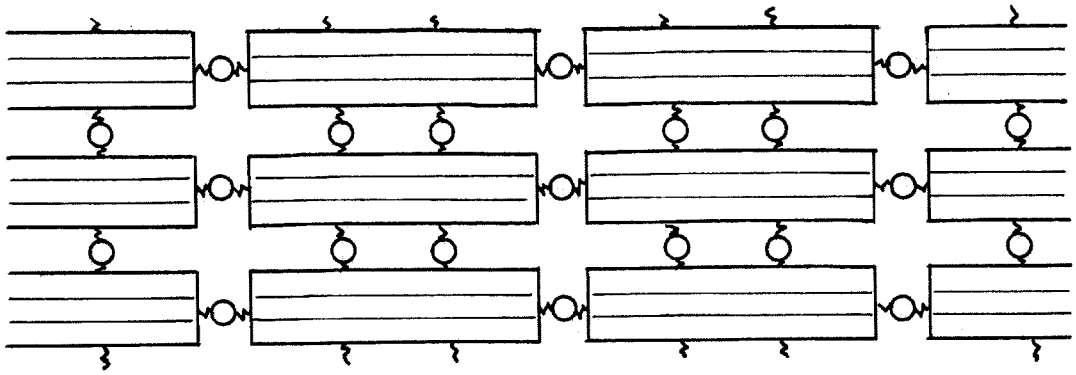

Figure 24

represents a bond having the following properties: the bond is permanently broken by heating to about 40° C.; the bond is temporarily broken by 5 M urea; after a sufficient length of time in the presence of urea, however, the bond loses its ability to reform when the urea is removed; the bond is easily stretched. A hydrogen bond between the ends of coiled, thermally labile chains may possibly have such properties. At sufficiently high temperatures thermal motion of the chains would cause the rupture of the relatively weak hydrogen bond and the resultant distortion of the chain, perhaps sufficient to cover the bond-forming site,

would prevent the reformation of the hydrogen bond when the temperature is again lowered.

The ability to break hydrogen bonds is a well known property of urea solutions. After a sufficient length of time the probability of a chain assuming a distorted configuration may be high enough to cause a large proportion of the bonds to lose their ability to reform. The extensibility of the bond may be attributed to the extension of the coiled chains to which the hydrogen-bond forming sites are attached.

It is noteworthy that the bonds responsible for the gelation of gelatin are similarly ruptured by concentrated urea as well as by heat, though they do not lose their ability to reform. That this is so has been confirmed by the author in an experiment in which gelatin was dissolved in 5 M urea and stored for over a month. Upon removal of the urea by dialysis against saline, the gelatin was found to be still capable of gel formation. The explanation for this difference may be, for example, that the bond-forming chains are shorter or stiffer and less likely to be distorted in gelatin.

The symbol 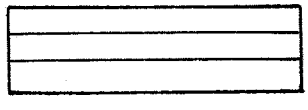 represents what may be considered to be the collagen molecule. Each such molecule consists of a group of three submolecules of the same length as the combined molecule held together by ordinary hydrogen bonds which may be broken by the action of

concentrated urea, but are not to be considered as especially thermally labile or extensible. It is quite possible that each submolecule represents a single polypeptide chain. The molecular weight of the single chain deduced from the light-scattering studies on URTC is 0.37×10^6, and that of the whole molecule is 1.1×10^6, or about three times as great, as found in the investigation of HRTC.

The manner in which the observations of the properties of collagen reported here may be explained on the basis of figure 24 will now be elucidated.

When a fibril is placed in a dilute acid solution the molecules become charged electrically due to the fact that their isoelectric point of 7 - 8 (34) is near neutrality. In the absence of salts these charges exert a strong repulsion on each other; consequently the structure swells and disintegrates into gel-like fragments to give the solution which has been designated RTC. These fragments are responsible for the very large molecular weight and the high dissymmetry observed. It is also likely that a solution containing such networks would show very high viscosity and a low sedimentation constant. The small diameters of the individual strands within each fragment prevent them from being visible in electron micrographs.

Only a few of the gel-bonds, ~O~ , within the fragments are broken, however, allowing the structure to retain its internal relationships intact over large areas.

If salt is now added to neutralize the electrical repulsions, or if the solution is made neutral by the addition of ammonium hydroxide, some of the gel-fragments will collapse into their original configurations. Thus electron micrographs of the resulting precipitate will show the characteristic native collagen structure in many places.

If the RTC solution is heated to 40° C. or higher for a few minutes most of the gel-bonds will be broken though the repulsions are not removed. Each molecule is still effectively surrounded by a large volume from which the others are excluded, but the molecules are now free to move relative to one another under shearing stress. This may be the explanation of the suddenly lowered viscosity with only a slight corresponding change in the light scattering.

Addition of salt to this heated solution permits the repulsions to be neutralized and leaves essentially an ordinary solution of collagen molecules or parent gelatin. Centrifugation removes the few undepolymerized aggregates and brings the dissymmetry down to its constant low value.

The average length of the molecules in solution is observed to be 3500 A. This is not necessarily equal to the length of the molecule in the tendon fibril or in the dried electron microscopic preparations. There is evidence from low-angle x-ray scattering studies on protein solutions that proteins undergo swelling to as much as twice their initial volume upon dissolving (38), (39). For the collagen

molecule this effect could take the form of an increase in the diameter and a shortening of the length of the rod. Bear (16) quotes G. C. Nutting and R. Borasky as having reported finding evidence for exactly this phenomenon in wetted collagen. If each residue occupies a length of 2.9 A. along the axis of the dry fibril, an overall length of 11,500 A. is calculated for the molecule in the dry state.

If the collagen is dissolved in 5 M urea and 2% NaCl, all the hydrogen bonds, both between the molecules and between the submolecular chains, are broken. Electrical repulsions are neutralized by the presence of the salt so that the solution consists simply of separate submolecules. These are probably in a "super contracted" state, accounting for a length of only 2200 A. which was found for these submolecules in URTC. The ability of urea to cause marked shrinkage of collagen fibers has been observed previously (34).

If the urea solution is dialysed against dilute acetic acid before the gel-bonds have been permanently destroyed, large networks will be formed by the reformation of these bonds. However the original order among the molecules will have been lost so that upon addition of salts, or upon neutralization, a precipitate will be formed but none of the native collagen structure will be discernible in the electron micrographs of the precipitate. If, on the other hand, the gel-bonds have been largely destroyed by distortions of the

chains to which they are attached, dialysis against dilute acetic acid will only permit the short hydrogen bonds between submolecules to reform, producing a distribution of aggregates of molecular size comparable to the original collagen molecules, about M 1 x 10^6 (see table 9). But the absence of long gel-bonds, capable of causing extensive cross linkage, will prevent reformation of large gel-networks.

The above picture of the structure of collagen is by no means presented as anything more than a schematic framework into which all the observations herein reported may be fitted without undue strain. Many further experiments immediately suggest themselves and a great deal of refinement is required before those described here can be considered as completely unambiguous and accurate. However, if nothing else, a rather detailed hypothesis has been presented which may serve as something of a basis for future exploration.

PART III - A LIGHT-SCATTERING STUDY OF A FRACTIONATED GELATIN

A) Objectives.

The object of the following brief study was to determine whether the shape of the gelatin molecule could be inferred from a study of the angular and concentration dependence of light scattering in a solution of a relatively homogeneous gelatin fraction. Though it was found impossible to distinguish between hypothetical molecular shapes on the basis of results for this fraction alone, a weight-average molecular weight for the fraction was computed, a method of obtaining the desired information about the structure of the molecule was suggested, and a familiarity was gained with the pitfalls which must be avoided in completing the investigation.

B) Procedures.

The gelatin used in this study was identified as shipment number 47033 of Wilson Co. Ucopoco Special nonpyrogenic gelatin. Fractionation was carried out by Dr. J. Vinograd employing an alcohol-precipitation method similar to that described by Pouradier and Venet (40). The first precipitate upon addition of alcohol, containing about one percent by weight of the total quantity of gelatin in solution, was discarded.

Light-scattering measurements were performed on Fraction IIa (the first subfraction of the second fraction) in an acetate buffer of pH 5.0 containing 0.15 M NaCl. The isoelectric point of the gelatin was determined to be 9.21.

Values of the refractive increment were determined on solutions of the unfractionated crude gelatin. Accurately known concentrations, in the neighborhood of 1%, were prepared by dissolving carefully weighed amounts of the crude gelatin. A moisture content of 11.5% was estimated for this material by drying one-gram samples to constant weight in an evacuated oven at 90° C. Thus the true protein concentration of each solution could be computed from the known proportion of anhydrous protein in the weighed sample.

The refractive increments at wavelengths 436 mμ. and 546 mμ. were measured in a differential refractometer constructed by R. H. Blaker (41). Their values were found to be 0.190 and 0.183 $cm^3/gm.$ respectively. These values were also used for the refractive increments of rat-tail tendon collagen in Part II*.

Protein concentrations in the solutions used for light-scattering studies were determined subsequent to centrifugation to constant dissymmetry to allow for the loss of protein by

---

* The refractive increment of gelatin in a solvent consisting of 5 M urea, 2% NaCl, and 0.01% merthiolate was determined in the same manner and found to be 0.183 $cm^3/gm.$ at $\lambda = 546$ mμ. This value was used in computing the molecular weight of URTC by light scattering (pp. 67-68).

sedimentation. A micro-Kjeldahl method was employed and the nitrogen content of the dry protein was assumed to be 18%.

C) Light-scattering study.

There are four possible sources of error in light-scattering studies on gelatin solutions which deserve careful consideration. The first is the possibility that the solution will actually be in an early (non-rigid) stage of gel formation when light-scattering measurements are being made. If a gelatin solution is warmed at 40° C. for a sufficient length of time to allow its dissymmetry and ninety-degree scattering to reach a constant low value and then stored at room temperature for several hours, both the scattering intensity and the dissymmetry will rise sharply, even though a rigid gel has not yet formed. This seems to indicate that the formation of large aggregates of molecules takes place preliminary to the formation of a rigid gel. Hence, if the light scattering is to be interpreted in terms of the unpolymerized gelatin molecules, care must be exercised that such aggregation does not occur in the course of the measurements.

The second source of possible error is in the degradation of the gelatin molecules upon heating. Viscosity studies by Vinograd indicate that no significant decrease in the viscosity of gelatin solutions occurs after several hours of incubation at 40° C., but that raising the tempera-

ture to 50° C. seems to cause a definite viscosity decrease in the same time interval. He has also found, however, that degelling is accelerated at the higher temperature. Accordingly, when preparing a gelatin solution for light-scattering measurements, it is necessary to strike a balance between the temperature and the time of incubation in order to allow complete degelling but only negligible degradation.

A third complication is the possibility that microbubbles may be formed and stabilized upon heating a gelatin solution. Their presence would, of course, cause anomalous light-scattering results. These can probably be removed by centrifugation.

Finally, there seems to be somewhat more difficulty associated with attempting to centrifuge solutions of fractionated gelatin to constant dissymmetry than is ordinarily encountered with most proteins. An increased time or speed of centrifugation is less efficacious in this respect than a series of short, high-speed centrifugations accompanied by transference of the solution to a clean plastic centrifuge cup after each run.

In view of the above considerations, the following procedure was adopted: a solution of fraction IIa containing approximately 1% protein was warmed to 40° C. and centrifuged for 15 minutes at 9000 g. in an unrefrigerated centrifuge in order to remove undissolved matter. Solutions of protein concentration of approximately 1/2%, 1/4% and 1/8% were then prepared from this stock solution. A sample

of each solution was subjected to three centrifugations at 90,000 g. with transference of the sample to a clean plastic centrifuge cup after each run. During this procedure the centrifuge rotor and its contents were kept near 40° C. by warming the rotor in a water bath before each run. The temperature of the solutions was found to have dropped to 36° C. by the end of each run.

After each group of three such centrifugations, the solution was run into a light-scattering cell and the ninety-degree scattering and dissymmetry measured. It was found that warming the cell and contents to 45° C. for five minutes then reduced the ninety-degree scattering slightly, but that at the same time no decrease in the dissymmetry was observed*. Further warming at 45° C. did not affect the scattering. Hence all subsequent light-scattering measurements were made after warming the cell and contents for five minutes at 45° C., which is apparently sufficient to complete the degelling process.

The group of three centrifugations was then repeated and the light scattering again examined in the same manner. This procedure was continued until the dissymmetry of a solution did not change by more than 2% upon recentrifuging. A total of six to nine such centrifugations with transference proved adequate for all solutions.

---

* This effect is probably due to the "melting" of a few small gel-aggregates. It may indicate that the first aggregates formed are of the same extension as the monomeric molecules, as would be the case for side-by-side aggregation of rods. Similar indications have also been found by P. Doty (42).

It was thought likely that any micro-bubbles formed during the initial warming of the solutions to 40° C. would have been removed by the centrifugation procedure and that subsequent warming to 45° C. would have little further effect. The entire procedure required not more than three hours. Viscosity measurements performed by Vinograd on solutions which had undergone the above treatment showed that no degradation had occurred.

Scattering intensities were measured in the usual manner for the four concentrations of gelatin at angles from 45 degrees to 135 degrees and at wavelengths of 436 mμ. and 546 mμ. The data obtained are given in table 12, where the scattering intensities are, as usual, relative to that of the benzene standard at ninety degrees.

Correction of these data was made for solvent scattering, reflection of the incident beam at the exit face of the cell, the refractive index effect, and the change in the volume of illuminated solution viewed by the photomultiplier with angle. The results were divided by the factor $1+\cos^2\theta$. Figures 25 and 26 represent the set of angular and concentration dependence curves of the Zimm plot derived from the data for wavelengths 436 mμ. and 546 mμ. respectively. The values of K are 5.86×10^{-7} and 2.18×10^{-7}. The factor 50 by which c is multiplied was arbitrarily chosen to provide a convenient range on the abscissa.

Table 12

λ, mμ.	conc. gms./cm^3 x 10^3	45°	50°	60°	70°	80°	90°	100°	110°	120°	130°	135°
436	8.83	73.5	63.4	48.6	39.3	34.1	32.1	32.6	36.2	42.7	53.6	60.6
436	4.41	57.1	48.6	37.6	30.0	25.8	24.0	24.6	27.1	31.7	39.8	44.9
436	2.20	31.1	27.2	20.6	16.5	14.0	13.2	13.2	14.6	17.1	21.2	24.1
436	1.10	17.4	14.8	11.8	9.01	7.67	7.06	7.20	8.19	9.45	11.8	13.2
436	solvent	0.5	0.3	0.2	0.13	0.10	0.10	0.10	0.25	0.19	0.2	0.2
546	8.83	82.6	70.1	53.6	43.0	37.4	35.4	36.6	41.5	49.1	61.5	69.6
546	4.41	66.1	58.4	45.0	36.0	31.0	28.7	29.6	33.4	39.5	49.1	56.4
546	2.20	38.8	33.0	25.4	20.1	17.6	16.5	17.0	19.2	22.6	28.2	31.4
546	1.10	20.8	17.9	13.5	11.0	9.36	8.70	9.13	10.4	12.0	15.2	17.1
546	solvent	0.7	0.5	0.2	0.2	0.15	0.11	0.15	0.6	0.3	0.3	0.3

Angular and concentration dependence of light scattering from gelatin Fraction IIa for two wavelengths.

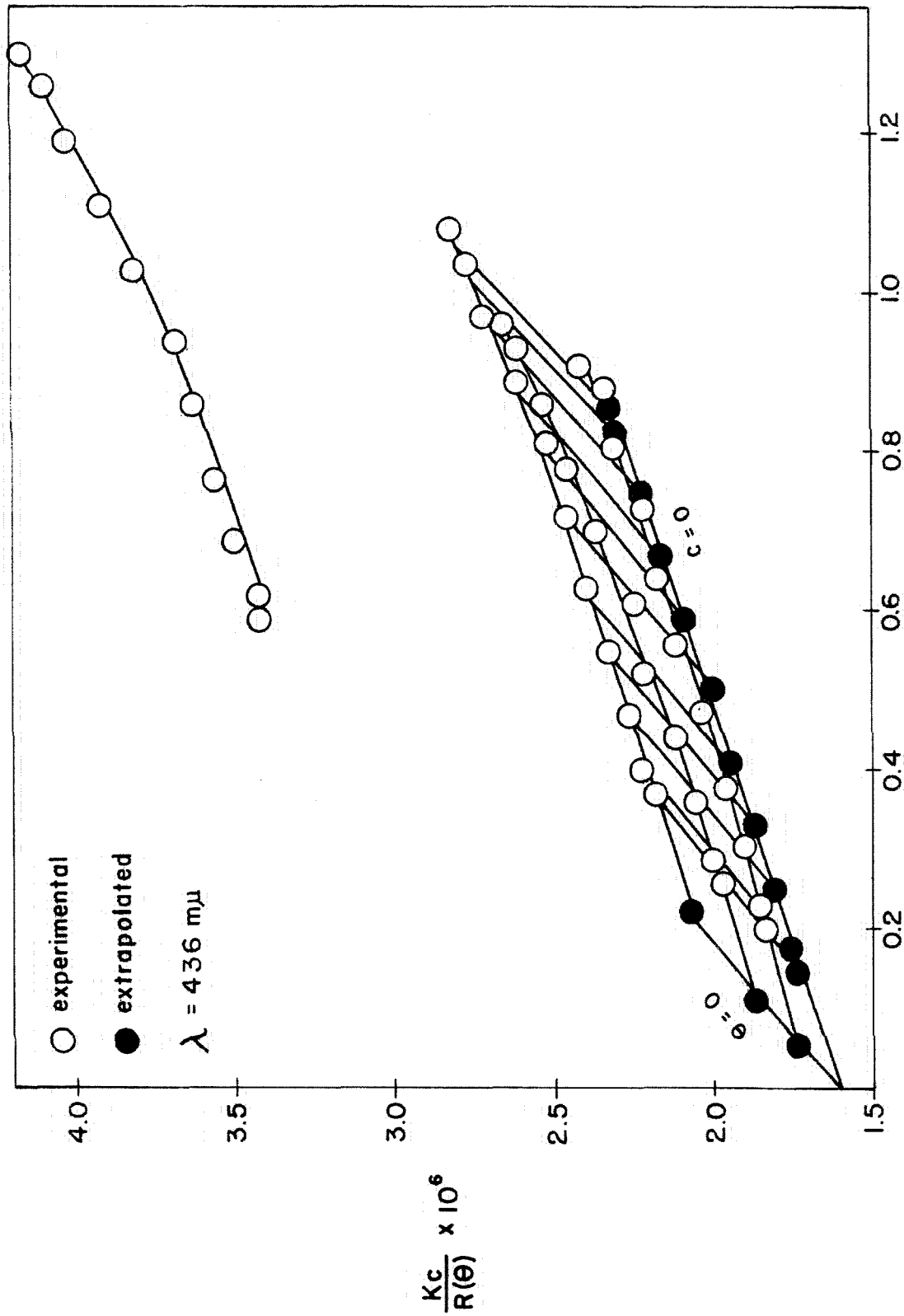

FIGURE 25 ZIMM PLOT FOR GELATIN FR. IIa

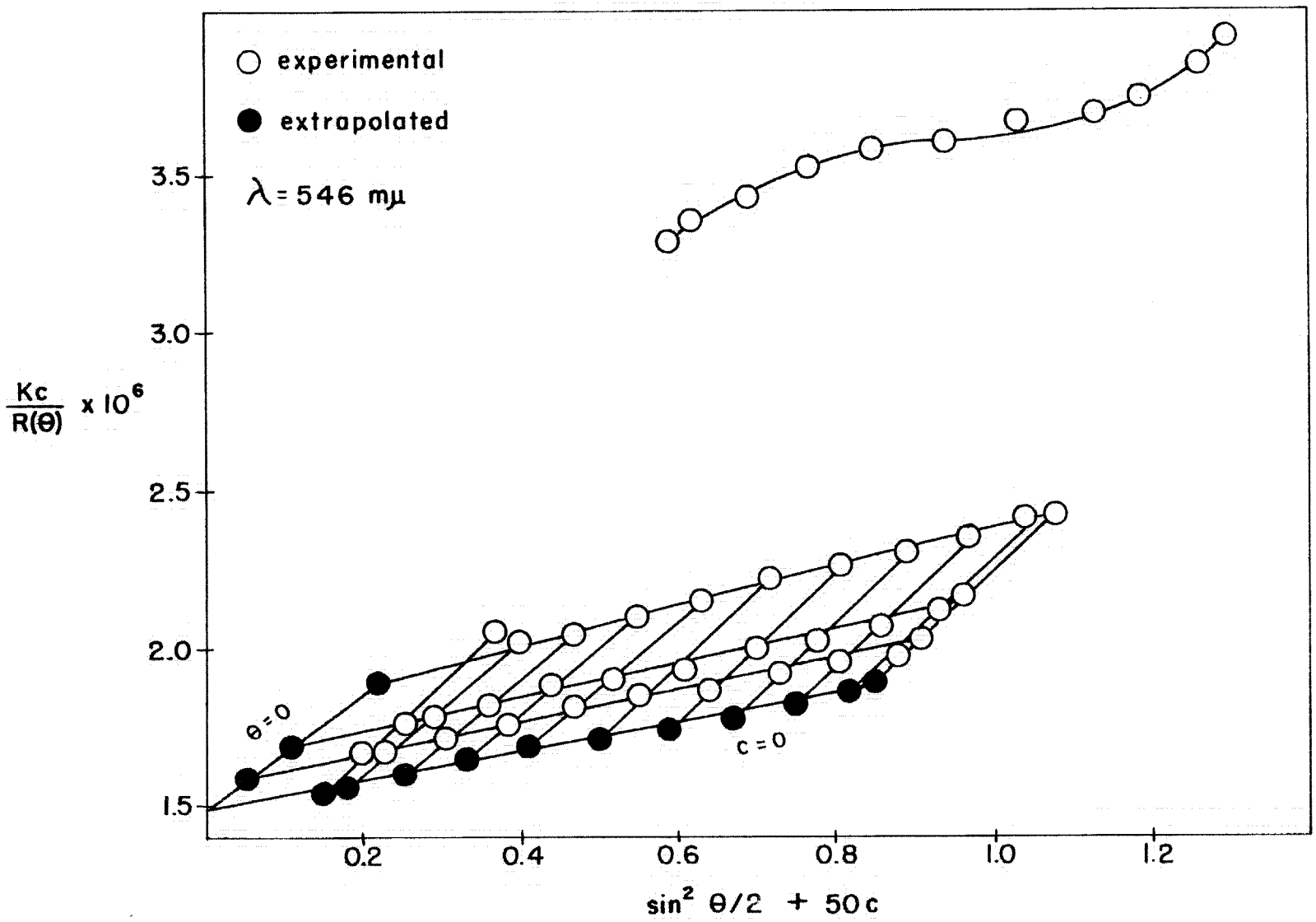

FIGURE 26 ZIMM PLOT FOR GELATIN FR. IIa

The information obtained by applying the methods of analysis discussed on page 93 to figures 25 and 26 is summarized in table 13.

Table 13

λ, mμ.	M_w	R random coil	L thin rod
436	6.3×10^5	790 A.	1200 A.
546	6.7×10^5	740 A.	1100 A.

The geometrical considerations outlined on page 71 do not permit the elimination of either of these hypothetical models. The rod would have a minimum diameter of about 30 A., while a truly random coil with R equal to the experimental value would have a molecular weight of about 18×10^5.

Furthermore, following the procedure discussed on page 98, a plot of the experimental $F^{-1}(\theta)$ curve was compared with those theoretically predicted for the two models. Due to the short range of the independent variable experimentally available (i.e.-the small value of the ratio between the characteristic dimension and λ') it was found that the experimental points fitted both theoretical curves equally well.

D) Discussion.

The significant feature of the results summarized in table 13 is the unexpectedly large size of the molecules in Fraction IIa. Scatchard and coworkers (43), on the basis of

sedimentation and viscosity studies of a series of successively more highly degraded gelatins, concluded that the parent gelatin molecule had a length of 800 A., a diameter of 17 A., and contained about 1170 residues, implying a molecular weight of about 1.1×10^5.

Pouradier and Venet (40), who determined the number-average molecular weights of a series of gelatin fractions, reported their highest value to be 2.5×10^5. This figure, too, is somewhat low compared to those of table 13, though it should be recalled that the number-average will always be less than or equal to the weight-average given by light scattering. It may be concluded, tentatively, that the gelatin used in the studies reported by Pouradier and Venet had suffered a greater degradation in preparation than that used to prepare Fraction IIa.

Before concluding this Section, it may be in order to suggest a possible method by which the shape of the gelatin molecule could be determined. From equation XV it is evident that the ratio of M to R^2 would be constant for a series of fractions if the molecules were indeed random coils, while equation XVI shows that, for a series of fractions of molecules which were actually rods of constant radius, the ratio of M to L would be constant. Thus by determining M, R and L as in table 13 for several gelatin fractions it may be possible to decide which of these models best fits the gelatin molecule.

PART IV - X-RAY DIFFRACTION STUDIES ON FEATHER KERATIN

A) Objectives.

The purpose of the studies reported in Part IV was to collect more complete x-ray diffraction data on feather keratin than have been reported in the literature and to utilize these data in an attempt to evaluate a structure for feather keratin which has been recently proposed by Pauling and Corey (44).

B) Review of present knowledge of the structure of feather keratin.

The x-ray diffraction pattern of feather keratin is the most complex that has been yet obtained from a non-crystalline protein. This pattern was first discussed by Astbury in 1931 (45) when a photograph obtained from a specimen of goose quill was reproduced. Astbury pointed out that the positions and intensities of the diffraction maxima differed markedly from those observed on photographs of other keratinous proteins. In 1932 Astbury and Marwick (46) reported that the spacing of an important meridional reflection was altered from 3.1 A. to 3.3 A. when feather keratin was stretched by 6% in the direction of the fiber axis. Further stretching caused the fiber to break.

Corey and Wyckoff (47) later reported interplanar

spacings measured on diffraction patterns of chicken feather quill and found prominent equatorial reflections at 11.0 A. and 4.68 A.

These observations by Astbury and Marwick and by Corey and Wyckoff seem to have provided the basis for the usual classification of feather keratin with the β proteins, since the latter show a characteristic prominent meridional reflection at 3.32 A. and important equatorial reflections at 9.8 A. and 4.65 A. (48). Feather keratin is pictured as being composed of polypeptide chains which are somewhat more folded than those of other β proteins. It must be pointed out, however, that all efforts at causing feather keratin to contract to the alpha form or to the super-contracted form have so far failed. In general, support for the classification of feather keratin as a β protein appears to be weak. Indeed, evidence for assigning it to the α-protein class will be presented in Section F, subsection 3.

An alternative hypothesis which has received some support is that feather keratin may contain linear combinations of globular protein units. Evidence for this hypothesis lies in some supposed similarities between interplanar spacings observed in feather keratin and in crystalline pepsin (49) and it is strengthened by the reported similarity of the feather keratin diffraction diagram to that of F-actin (50). Both crystalline pepsin and F-actin are presumed to contain globular units.

There have been only two detailed proposals for the

structure of feather keratin, both of which were based on the alpha rather than the beta types of structure. In 1951 Pauling and Corey (51) suggested that the unit of structure of feather keratin may contain two layers of α helixes in combination with one layer of polar pleated sheet. The existence of the polar pleated sheet is now considered unlikely, however due to fact that " a polar pleated sheet constructed of L-amino acid residues is unsymmetrical and would have a tendency to curve." (52). Recently Pauling and Corey (44) have suggested that the unit cell of feather keratin may contain a seven-strand cable of α helixes and two three-strand ropes. An investigation of the intensities of the near-equatorial reflections to be expected from such a structure is the subject of Section E, subsection 3.

A few observations on the biological occurrence of the feather keratin type of structure may be appropriate here. Rudall has made a rather extensive exploration of this topic (53) and has found evidence for the existence of feather keratin in all parts of the feather produced from the "intermediate cells"; that is, in the barbs, barbules, rachis, quill, and medulla. However he has found α keratin to be present in the quill sheath, generated by the "stratum cylindricum". Diffraction patterns of the feather keratin type are also obtained from tortoise shell, snake scales, and lizard claw, providing evidence for the common

ancestry of birds and reptiles and supporting the notion that feathers have descended from modified reptilian scales.

Further discussions of the detailed background of the Pauling-Corey structure, of the interplanar spacings found in feather keratin by other investigators, and of the evidence for the existence of a 1.5 A. meridional reflection in the feather keratin diffraction pattern will be deferred until their appropriate Sections.

C) Obtaining a suitable diffraction photograph.

Meridional and equatorial spacings for feather keratin have been reported by Corey and Wyckoff (47), Astbury and Bell (54), Bear (55), and Rudall (53). Corey and Wyckoff included a reproduction of the diffraction diagram which indicated that their specimen was not very well oriented. The other authors did not include reproductions of the photographs from which their data were obtained, so it is difficult to assess the accuracy with which the spacings of the diffraction maxima may have been measured. An excellent feather keratin diffraction diagram was published in a later review by Rudall (56), but spacings were not given. In view of this apparent shortage of complete x-ray diffraction data in the literature, it was decided that the best possible feather keratin diffraction pattern should be obtained before undertaking a comparison of the results predicted for the Pauling-Corey model with the experimental evidence.

Bear (55) and Astbury and Bell (54) have reported that sea-gull feather keratin yielded x-ray diffraction photographs showing maximum orientation. It was therefore felt wise to concentrate attention on this material. In the subsequent portions of this dissertation, all feather keratin referred to will be that obtained from sea-gull feathers. The search for the specimen with optimum orientation took two separate directions. The first consisted of trying various treatments on samples of sea-gull feather keratin; the second was to investigate the degree of orientation in different parts of the feather. Preliminary diffraction photographs of each sample were taken with nickel-filtered copper K_α radiation in an evacuated cylindrical camera of radius 3.0 cm. The fibers were mounted vertically and with their broad faces parallel to the x-ray beam.

Optimum results were obtained with any particular sample when it was microtomed to give a section about 20 micra thick and then dried over P_2O_5 for two weeks or more in an evacuated desiccator. The drying procedure produced a marked improvement in the definition of the diffraction photographs obtained with a microtomed section, but had no evident effect on samples of approximately 0.5 mm. thickness. The microtoming procedure requires that the sample first be embedded in a substance of comparable hardness. In this work pieces of feather keratin were suspended in a 4% solution of purified cellulose nitrate (parlodion) in a 1:1 mixture of

ether and alcohol as solvent. The mass was then hardened by prolonged exposure to chloroform vapors. In separate experiments it was found that none of these solvents had any effect on the orientation of feather keratin fibers. Even with this rather elaborate technique it was difficult to prevent the feather keratin from breaking loose from the embedding material during the cutting operation, but several sections could usually be obtained before this would occur.

In general, the most highly oriented portion of the feather proved to be the flat (back) surface of the rachis, though as much variation was encountered among similar portions of different feathers as was found among different portions of the same feather.

The most highly oriented specimen of sea-gull feather keratin was finally obtained by manually cutting a section from the back side of the rachis of a sea-gull feather which had been in the possession of Professor Corey for several years. The specimen was approximately 0.5 mm. thick in the direction perpendicular to the surface of the rachis, 2 mm. wide, and 10 mm. long in the direction of the axis of the rachis. Its surface was carefully scraped with a scalpel blade to remove any α keratin present there. Possibly the orientation of the specimen could have been improved further by the microtoming and drying procedure described above, but the greatly reduced thickness of the resulting section would have necessitated much longer

exposure times to obtain sufficiently dense photographs.

Diffraction photographs of this specimen were then obtained with a larger cylindrical camera, which provided improved collimation of the incident x-ray beam and a specimen-to-film distance of 10 cm., thus giving still better definition. A typical x-ray diffraction photograph obtained with this specimen and camera is reproduced in figure 27. In preparing this photograph, the specimen was mounted vertically with the broad face parallel to the x-ray beam (edge-on to the beam). Copper K_{α} radiation, filtered through nickel foil, was employed and the exposure time was 21 hours. The camera was continuously flushed with helium during the exposure in order to reduce the background due to atmospheric scattering.

D) Meridional and equatorial interplanar spacings.

Table 14 shows the interplanar spacings and estimated intensities obtained from figure 27 and other similar diffraction photographs. The shorter meridional spacings were most satisfactorily measured on photographs taken with the fiber mounted horizontally. Calibration of the camera by Dr. H. Yakel indicated an average fiber-to-film distance of 9.98 cm. with less than 0.02 cm. deviation from this value at any point. The spacings reported by other investigators are also listed for comparison in table 14. A bracket connecting two or more reflections in this table indicates

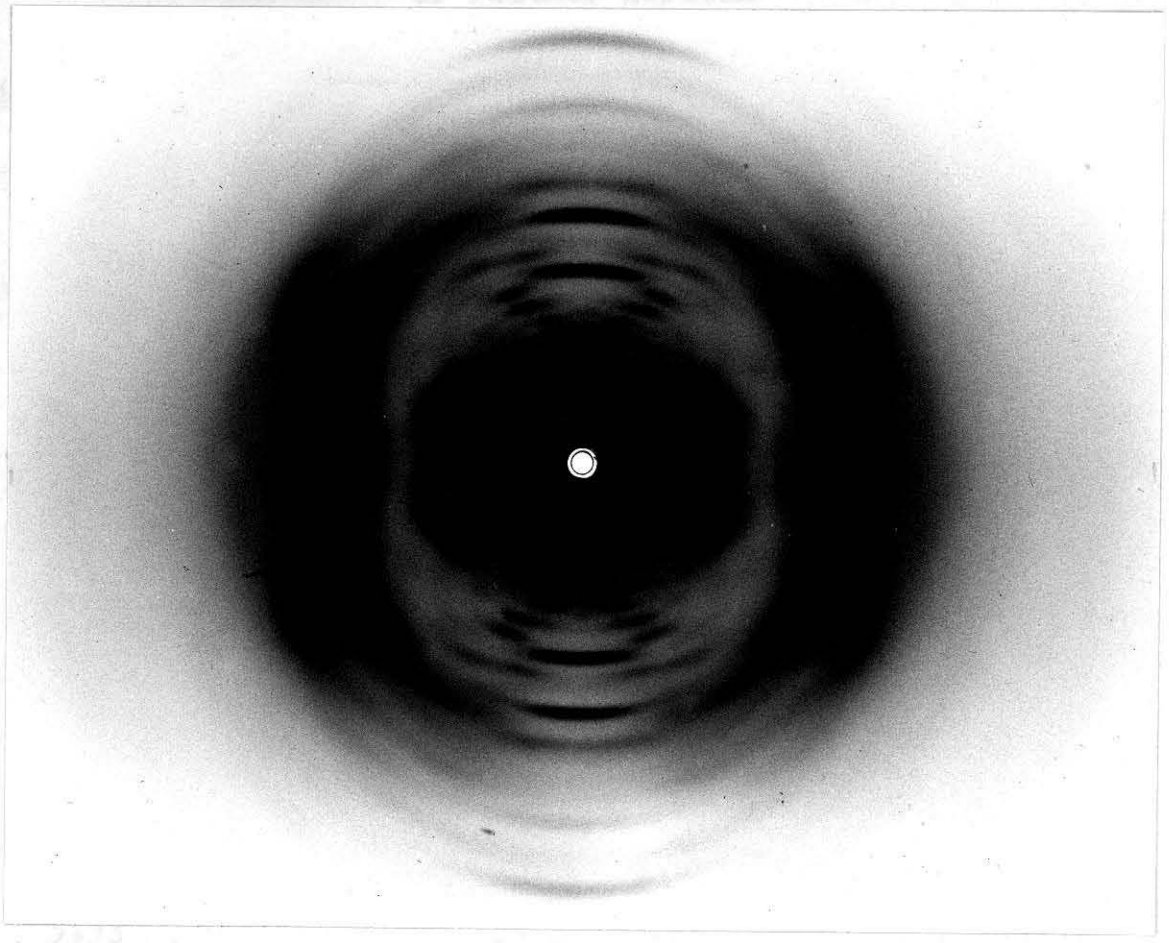

FIGURE 27

X-RAY DIFFRACTION DIAGRAM
OF
FEATHER KERATIN

Table 14 - Interplanar spacings of feather keratin

Meridian

Bear (55)	Corey and Wyckoff (47)	Astbury and Bell (54)	Rudall (53)	this study	inten-sity	ℓ	c_o
		47		50.7	sm	2	101.4
23.6	21.3	23.4	23.6	23.7	vs	4	94.8
	17.2						
				19.3	m	5	96.5
11.90			11.9	11.9	vw	8	95.1
10.46		10.4	10.45	10.4	w	9	93.5
	9.08	9.1					
				7.94	vw	12	95.3
6.30	6.20	6.26	6.30	6.26	sm	15	94.0
5.53			5.53	5.54	vvw	17	94.0
4.98	4.90	4.93	4.98	4.96	sm	19	94.3
4.45	4.37	4.42	4.45	4.45	m	21	93.5
	3.95			3.99	vvw	24	95.8
				3.80	vvw	25	95.0
	3.52	3.54	3.54	3.57	wm	27	96.3
				3.40	vvw	28	95.1
	3.22	3.29	3.29	3.25	vvw	29	94.3
	3.07	3.08	3.08	3.09	m	31	95.9

Table 14 - Interplanar spacings of feather keratin (continued)

Bear (55)	Corey and Wyckoff (47)	Astbury and Bell (54)	Rudall (53)	this study	intensity	l	c_0
		2.94	2.94	2.97	vw	32	95.0
		2.74	2.74	2.75	vw	35	96.3
				2.56	vvw	37	94.7
				2.34	vvw	41	95.9
				2.13	vvw	45	95.8
				2.04	vw	47	95.8
Equator							
	115	115					
	81.8	81.8					
	51	51		55	m	0	
	33.3	33.3	34	33.5	s	0	
	17.1	17.6	17.6	17.3	vw	0	
	11.0	11.3	11.3	11.2	sm	0	
	8.56	8.8	8.8	8.84	m	0	
		5.8	5.8	5.82	w	0	
				4.90	m	0	
	4.68	4.5	4.5	4.50	m	0	
				3.90	vw	0	
				3.50	w	0	
				3.25	w	0	
				2.28	vw	0	

that the reflections in this group were too vague and diffuse to permit very reliable determination of the position of each individual intensity maximum.

Bear (55) believes that the very long equatorial spacings of 115 A., 81.8 A., and 51 A. reported by Corey and Wyckoff and by Astbury and Bell are artifacts due to the strength of other small angle reflections*.

The intensities reported by the other investigators agreed substantially with those listed in table 14. The 17.2 A. and 9.08 A. meridional reflections reported by Corey and Wyckoff, which were not found on the present photographs, were both reported as weak by those authors. The 9.1 A. meridional reflection reported by Astbury and Bell was listed as very weak.

The mean value of c_o was computed to be 95.4 A. This is in good agreement with the value for c_o of 95 A. reported by Bear (55) and with 94.6 A. deduced by Pauling and Corey (51) from the data of Bear and of Corey and Wyckoff. It is possible, however, that when measurements of greater accuracy are made some multiple of 95 A. will have to be postulated as the true repeat distance to account for the spacings of some of the meridional reflections.

---

* Bear makes the observation that, "Both the fourth meridional order and the equatorial 34 A. arc are so strong that general radiation artifacts related to them (located within these spots and streaking toward the center) often confuse the central regions of the pattern. This is probably the source of the 51, 82, and 115 A. equatorial spacings reported by Corey and Wyckoff ....."

E) The Pauling-Corey structure for feather keratin.

1) Background.

The existence of the Pauling-Corey 3.7-residue helix (57) in synthetic polypeptides and α proteins is now widely accepted. The evidence for this structure has been summarized in reviews by Pauling and Corey (52) and by Low (58). However attention has been directed to two important discrepancies between experimental observations on proteins and predictions based on simple packing of such α helixes. The first is that the prominent meridional reflection at 5.1 A. observed on x-ray diffraction photographs of the α proteins can not be explained readily on the basis of this structure. Simple side-by-side packing of 3.7-residue helixes would give rise to a reflection at 5.4 A. instead of 5.1 A. The second discrepancy between prediction and observation is that the density calculated from an average amino acid residue weight of 117 gives a value of 1.1 gm./cm^3 whereas the actual density of the α proteins, and indeed of almost all proteins, has been observed to be 1.3 gm./cm^3.

These objections now seem to have been overcome by the additional hypothesis that the simple helixes are thrown into super-helical configurations by the interactions of their side chains (44). Thus the axis of the 3.7-residue helix itself may describe a helical course. As a result

it is possible for the compound helical configurations to combine into various kinds of ropes and cables. In particular, three-strand ropes could be formed from simple helixes constructed of repeating sequences of seven residues. These ropes would have their sense of twist opposite to that of the individual 3.7-residue helixes. Simple helixes with repeating sequences of fifteen amino acid residues would also form three-strand ropes, but with their sense of twist the same as that of the individual helixes. A seven-strand cable may be formed, on the other hand, from individual strands having repeating sequences of seven or fourteen residues. In the seven-strand cable six outer compound helixes twist about a central straight helix.

Pauling and Corey proposed that the structure of α keratin consists of such seven-strand cables packed together with single compound helixes in the interstices. In this way the 5.1 A. meridional reflection is interpreted as resulting from the second order of the seven-residue repeating sequence in the outer strands of the seven-strand cable. The density of the protein calculated for this structure is also in agreement with the experimentally observed density. Finally, an equatorial reflection at 27 A. is then explained as resulting from reflection from the 1·0·0 planes of the hexagonal unit of structure with a_0 equal to about 31 A.

In the same paper in which the compound helical configurations were proposed for the α-protein structures (44) Pauling and Corey suggested that these configurations may also provide an explanation of the x-ray diffraction diagram of feather keratin. They suggested a unit of structure containing one seven-strand cable and two three-strand ropes. The details of such a model will now be examined.

2) Details of the proposed structure.

The unit of structure of feather keratin is taken as hexagonal, with a seven-strand cable, designated AB_6, at the position $x_1 = 0$, $x_2 = 0$ and two three-strand ropes, designated $D_3(1)$ and $D_3(2)$, at the positions $x_1 = 1/3$, $x_2 = 2/3$ and $x_1 = 2/3$, $x_2 = 1/3$ respectively. Figure 28 illustrates cross-sectional views perpendicular to the fiber axis and at various heights in the unit cell; a) represents the plane at $z = 0$; b) shows the plane at that value of z at which the cross section of the AB_6 cable has rotated counter-clockwise by 1/24 th of a revolution and that of each D_3 rope has rotated clockwise by twice that amount, or 1/12 th of a revolution; at c) the cross section of the AB_6 cable has rotated counter-clockwise by 1/12 th of a revolution and that of each D_3 rope has rotated clockwise by 1/6 th of a revolution. It is clear from these diagrams that the lead of the seven-strand cable (the distance along the cable in which a

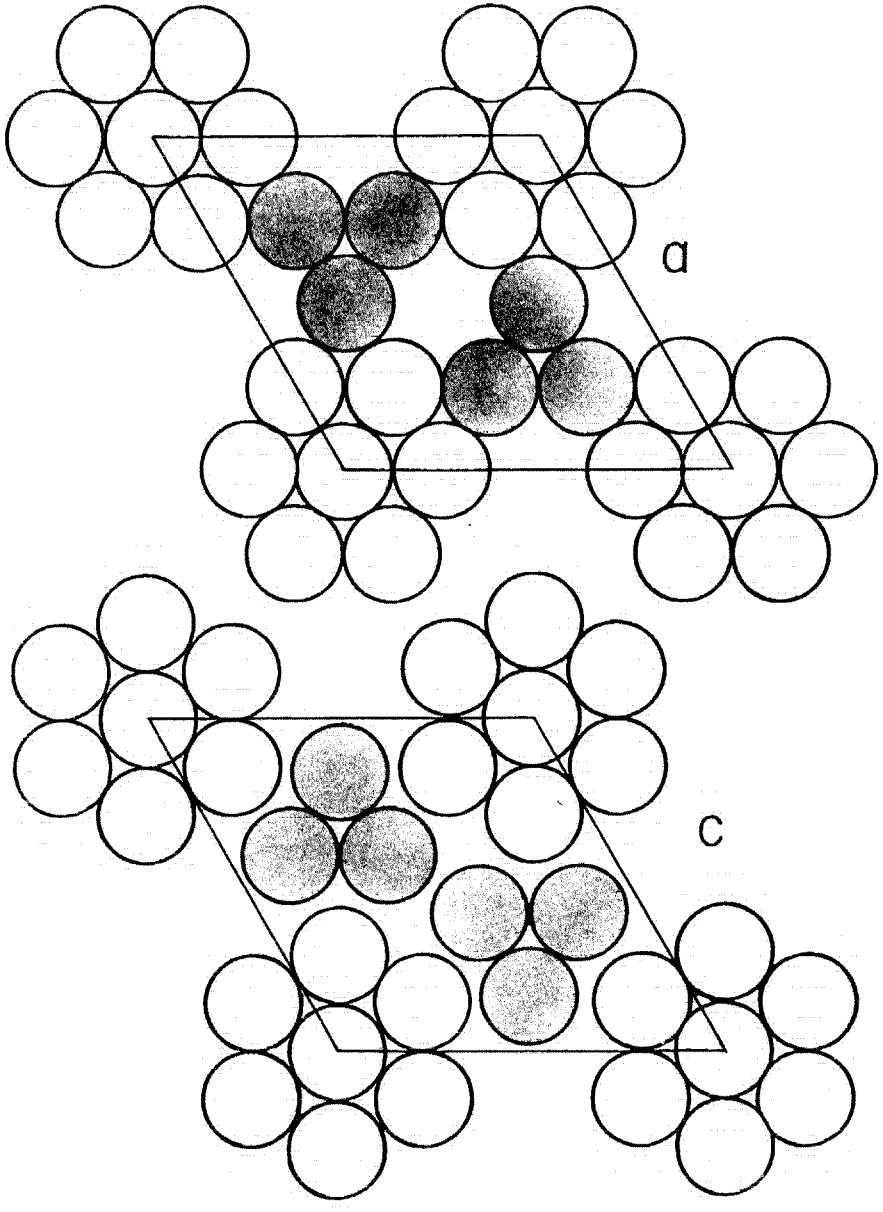

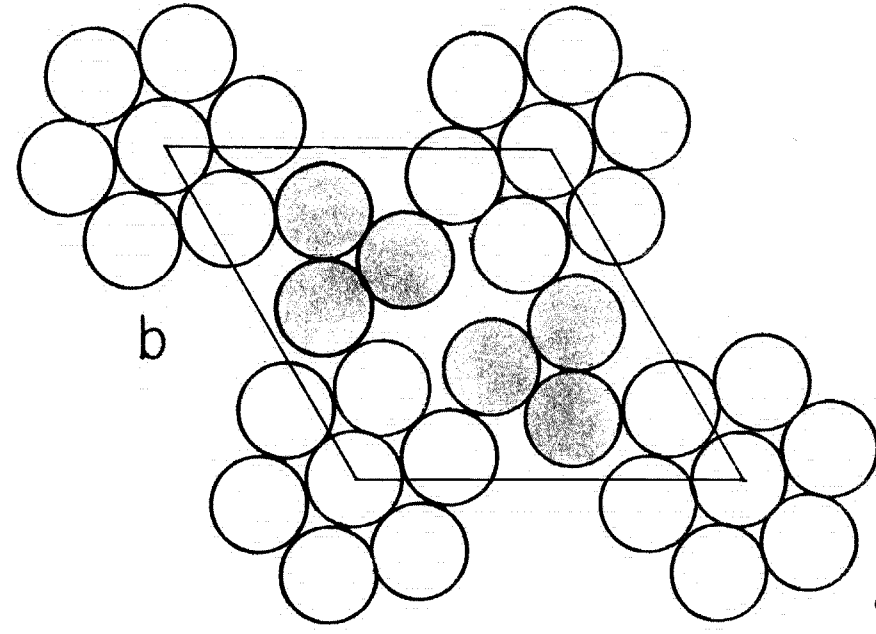

FIGURE 28

STRUCTURE PROPOSED
FOR
FEATHER KERATIN

particular strand returns to its original azimuthal position; the pitch of the individual strand) is twice the lead of the three-strand ropes. It also appears that their respective senses of rotation must be opposite.

In the AB_6 cable the distance from the center of the central α helix A to the center of an outer compound helix B is taken to be 9.94 A., and the distance from the center of either D_3 rope to the center of one of the D helixes is taken to be 5.97 A. For the purposes of the diagram all the helixes are considered to have the same cross-sectional diameter, about 10 A. From figure 28 a) it is seen that a_0 is equal to four diameters of the single helixes, or about 40 A. It is taken to be 38.7 A. so that the 1•0•0 interplanar spacing would be 38.7 sin 60° 33.5 A., the spacing of the prominent equatorial reflection. This value for a_0 also permits the remaining equatorial and near-equatorial reflections to be satisfactorily indexed.

On the basis of this unit of structure the density of feather keratin is calculated to be 1.30 by using 117 as the average residue weight and 1.5A as the vertical rise per residue. The density of feather keratin was experimentally determined by the author using the flotation method and found to be 1.28, in agreement with the predicted value.

3) Calculation of theoretical intensities.

The intensities of the reflections to be expected from the structure depicted in figure 28 may be estimated

by application of the theory presented by Cochran, Crick and Vand (59). According to their development, the Fourier transform (continuous structure factor) for a continuous helix with radius r and pitch P is given by

$$T(R,\psi,\zeta) = 0$$

$$T(R,\psi, n/P) = J_n(2\pi Rr) \exp\left\{in(\psi+\tfrac{\pi}{2})\right\} \qquad \text{XXIV}$$

R,ψ, and ζ are the cylindrical coordinates of Fourier space, with R the radial distance from the origin, ψ the azimuthal angle, and ζ the height. J_n is the n th order Bessel function. Thus $T(R,\psi,\zeta)$ is different from zero only when $\zeta = n/P$, n being zero or any integer. This implies that for a continuous helix scattering occurs only at layer lines with reciprocal-space height equal to n/P.

For the discontinuous helix consisting of like atoms arranged on a helix of pitch P and spaced at intervals of p along the vertical axis, Cochran, Crick and Vand obtain for the Fourier transform

$$F(R,\psi,l/c_0) = \sum_n T(R,\psi, n/P) \qquad \text{XXV}$$

where l is the layer line number and c_0 is the repeat distance along the fiber axis. The sum is taken over all n which satisfy the condition

$$an + bm = l$$

where m is any integer and a and b are the number of turns of the helix and the number of atoms, respectively, in the repeat distance c_o. That is, $aP = bp = c_o$.

Calculation of the structure factors for ropes or cables composed of compound α helixes is approached by means of the assumption that a compound helix has a structure factor which is the product of the structure factors for the simple α helix and that for the larger continuous helix which coincides with the axis of the α helix.

Regarding the larger helix as continuous is equivalent to assuming that the number of residues per repeat of the larger helix is great. The series of Bessel functions involved in the right-hand side of equation XXV applied to this helix can then be approximated by the first term, J_n, since the remaining terms consist of higher-order Bessel functions which are negligible at all values of their argument encountered.

Closer attention must be given to the structure factor for the α helix by which that for the continuous larger helix is to be multiplied. If the structure factor for the α helix in an undistorted state, computed from equation XXV, were to be used, the product would be zero everywhere in reciprocal space except where the non-zero portions of the two factors happened to coincide. It is probable that the factor to be used to represent the α helix should be, rather, a somewhat "smeared out" function derived from the ordinary structure factor for the α helix. The "smearing"

is due to the distortion of the α helix caused by constraining its axis to follow the course of the larger helix. When considering reflections which are sufficiently close to the equator the equatorial structure factor for the α helix may be used as an approximation to the "smeared" structure factor for the distorted α helix in forming the product. This discussion will be comfined to near-equatorial layer lines of the compound helical structures.

Finally, the structure factor for ropes and cables composed of these compound helixes may be obtained by adding together the structure factors for the individual strands (compound helixes), each with its appropriate relative azimuthal orientation in reciprocal space.

Particularizing the above general discussion to the problem of computing the structure factor of the seven-strand cable AB_6 for a near-equatorial layer line, one obtains for the contribution of an outer B compound helix to the n <u>th</u> layer line of the repeat distance P

$$F_B(\xi = n/P) = F_\alpha(\xi = 0) \cdot J_n(4\pi r \frac{\sin\theta}{\lambda}) e^{in\phi} \qquad \text{XXVI}$$

Here $F_\alpha(\xi = 0)$ represents the equatorial structure factor for an undistorted α helix. The argument of the Bessel function J_n may be transformed from $2\pi Rr$ as given in equation XXIV to $4\pi r \frac{\sin\theta}{\lambda}$ if it is recalled that for near-equatorial layer lines $R = 1/d = 2\frac{\sin\theta}{\lambda}$. In this case r is the distance from the center of the AB_6 cable to the center of an outer B compound helix. ϕ is the relative azimuthal angle in

Fourier space of the strand under consideration. It is arbitrarily taken as zero for the first B strand and as the appropriate multiple of $2\pi/6$ for the subsequent strands*.

To obtain the contribution made by the entire B_6 part of AB_6 the six terms of the form XXVI are added, each with the appropriate value of ϕ. This gives

$$F_{B_6}(\xi=n/P) = F_\alpha(\xi=0)\cdot J_n(4\pi r \frac{\sin\theta}{\lambda}) \sum_{j=0}^{j=5} \left(e^{\frac{2\pi i n}{6}}\right)^j \qquad \text{XXVII}$$

But, by the rule for summing geometrical series, we have

$$\sum_{j=0}^{j=5} \left(e^{\frac{2\pi i n}{6}}\right)^j = \frac{1-e^{2\pi i n}}{1-e^{\frac{2\pi i n}{6}}} \qquad \begin{cases} =0 \text{ if } n \neq 6\ell \\ =6 \text{ if } n = 6\ell \end{cases}$$

where ℓ is zero or any integer. Thus the B_6 part of AB_6 contributes only to layer lines with $\xi = 6\ell/P$ and will have there the structure factor

$$F_{B_\ell}(\xi=6\ell/P) = 6F_\alpha(\xi=0)\, J_{6\ell}(4\pi r \frac{\sin\theta}{\lambda}) \qquad \text{XXVIII}$$

Finally, the α helix A in AB_6 will contribute simply $F_\alpha(\xi=0)$ to the equator but nothing to the near-equatorial layer lines, making the total structure factor for AB_6

$$F_{AB_\ell}(\xi=6\ell/P) = 6F_\alpha(\xi=0)\, J_{6\ell}(125 \frac{\sin\theta}{\lambda})$$

or

$$F_{AB_\ell}(\xi=0) = F_\alpha(\xi=0)\left\{1 + 6J_0(125 \frac{\sin\theta}{\lambda})\right\} \qquad \text{XXIX}$$

where r has been given its value of 9.94 A.

---

* It is stated by Cochran, Crick and Vand that a rotation of the helix in real space results in the transform being rotated in Fourier space by the same amount and in the same direction.

It should be noted that the α helix A may contribute to layer lines to which no contribution is made by the rest of the AB_6 cable or by the D_3 ropes; however the scattering from this helix alone would be small, since it comprises only 1/13 th of the total mass of the unit cell.

A similar calculation may be made for the D_3 ropes. On the m th layer line defined by the D strand repeat distance P' --- that is, at m/P' --- the structure factor for an individual D compound helix may be approximated by the product of the structure factor for the α helix and that for the continuous helix with pitch P':

$$F_D(\zeta = m/P') = F_\alpha(\zeta = 0)\, J_m(4\pi r \frac{\sin\theta}{\lambda})\, e^{im\Phi} \qquad \text{XXX}$$

Adding structure factors of the form XXX for the three strands and taking account of the rotation of the subsequent strands, one obtains

$$F_{D_3}(\zeta = m/P') = F_\alpha(\zeta = 0)\, J_m(4\pi r \frac{\sin\theta}{\lambda}) \cdot e^{im\phi_0} \sum_{j=0}^{j=2} \left(e^{\frac{2\pi i m}{3}}\right)^j \qquad \text{XXXI}$$

Here ϕ_0 is the azimuthal angle of the first strand of the D_3 rope in Fourier space relative to that of the first strand of the AB_6 cable. It can not be arbitrarily set equal to zero since it is fixed by steric considerations.

The summation on the right-hand side of equation XXXI may be shown by the rule for geometrical series to

have the property

$$\sum_{j=0}^{j=2} \left(e^{\frac{2\pi i m}{3}}\right)^j = \frac{1 - e^{2\pi i m}}{1 - e^{\frac{2\pi i m}{3}}} \quad \begin{cases} = 0 \text{ if } m \neq 3\ell \\ = 3 \text{ if } m = 3\ell \end{cases}$$

Thus the D_3 ropes contribute only to those layer lines with $\zeta = 3\ell/P'$ and will have there the structure factor

$$F_{D_3}(\zeta = 3\ell/P') = 3F_\alpha\ (\zeta=0)\ J_{3\ell}\ (75\ \frac{\sin\theta}{\lambda})\ e^{13\ell\phi_0} \qquad \text{XXXII}$$

where r has been given the value appropriate to the three-strand rope, 5.97 A.

It was pointed out on page 132 that $P' = P/2$. Therefore expression XXXII shows that the D_3 ropes contribute to layer lines with $\zeta = 3\ell/P' = 6\ell/P$, coinciding with the layer lines to which the AB_6 cable contributes. Thus, the observed value of c_0 , 95.4 A., must represent the sixth order of the pitch P of the B compound helix; that is, $P/6 = c_0 = 95.4$ A., $P = 570$ A., and $P' = 285$ A. Hence, were the Pauling-Corey model correct, the lead of the AB_6 cable would be 570 A. and the lead of each D_3 rope would be 285 A.

Finally, the complete structure factor for the ℓ th near-equatorial layer line of the $c_0 = 95.4$ A. spacing is obtained by adding the contribution of the AB_6 cable (equation XXIX) and of each D_3 rope (equation XXXII) including the phase angle due to their positions in the unit cell:

$$F(h, k, \ell) = F_\alpha(\xi=0)\left[{}^{1}_{0} + 6J_{6\ell}\left(125\,\frac{\sin\theta}{\lambda}\right)\right] +$$
$$+ 3F_\alpha(\xi=0)\,J_{3\ell}\left(75\,\frac{\sin\theta}{\lambda}\right) e^{13\ell\,\phi_o(1)}\, e^{2\pi i(h/3 + 2k/3)} +$$
$$+ 3F_\alpha(\xi=0)\,J_{3\ell}\left(75\,\frac{\sin\theta}{\lambda}\right) e^{13\ell\,\phi_o(2)}\, e^{2\pi i(2h/3 + k/3)} \qquad \text{XXXIII}$$

where $\Phi_o(1)$ and $\phi_o(2)$ refer to the respective D_3 ropes. If we disignate

$$A_o \equiv F_\alpha(\xi=0)\left[1 + 6J_o\left(125\,\frac{\sin\theta}{\lambda}\right)\right]$$

$$A_{\ell\neq o} \equiv 6F_\alpha(\xi=0)\,J_{6\ell}\left(125\,\frac{\sin\theta}{\lambda}\right)$$

$$B_\ell \equiv 3F_\alpha(\xi=0)\,J_{3\ell}\left(75\,\frac{\sin\theta}{\lambda}\right)$$

it can be shown that

$$F(h, k, \ell)\cdot F^*(h, k, \ell) = A_\ell^2 + 4A_\ell B_\ell\,(-1)^{h+k}\cdot$$
$$\cdot\cos\left[\frac{3\ell}{2}\,(\phi_o(1) + \phi_o(2))\right]\cdot\cos\left[\frac{3\ell}{2}\,(\phi_o(1) - \phi_o(2)) + \right.$$
$$\left. + \frac{\pi}{3}(k - h)\right] + 4B_\ell^2\cos^2\left[\frac{3\ell}{2}\,(\phi_o(1) - \phi_o(2)) + \right.$$
$$\left. + \frac{\pi}{3}(k - h)\right] \qquad \text{XXXIV}$$

For the equatorial layer line with $\ell=0$ the dependance upon $\phi_o(1)$ and $\phi_o(2)$ is eliminated and one obtains

$$F(h, k, 0)\cdot F^*(h, k, 0) = \left[A_o + 2B_o(-1)^{h+k}\cdot\right.$$
$$\left.\cdot\cos\frac{\pi}{3}(k - h)\right]^2 \qquad \text{XXXV}$$

When $\ell \neq 0$, reference to figure 28 shows that one may take $\phi_o(1) = \pi/2$ and $\phi_o(2) = \pi/6$. Thus for near-equatorial layer lines equation XXXIV becomes

$$F(h, k, \ell)\, F^*(h, k, \ell) = A_\ell^2 + 4A_\ell B_\ell (-1)^{h+k} \cdot \cos\left[\frac{\pi}{3}(k - h + 3\ell)\right] \cos\left[\frac{\pi}{3}(k - h + 3\ell/2)\right] + 4B_\ell^2 \cos^2\left[\frac{\pi}{3}(k - h + 3\ell/2)\right] \qquad \text{XXXVI}$$

Pauling and Corey (60) have calculated $F_\alpha(\xi = 0)$ as a function of $\frac{\sin\theta}{\lambda}$ and tables of Bessel functions were used to evaluate J_n. Theoretical intensities were calculated from equations XXXV and XXXVI for each value of h, k and ℓ corresponding to reflections observed on the feather keratin diffraction photographs. These were multiplied by the number of equivalent sets of planes and contributions from planes with nearly the same spacings were included in calculating the total intensity to be expected at the given value of $\frac{\sin\theta}{\lambda}$. The results are compared with the observed intensities in table 15. No correction was made for the polarization or the Lorentz factors.

It is clear that the over-all agreement is quite poor, though this does not eliminate the Pauling-Corey structure for feather keratin as a possibility since it is clear that the lack of agreement may be due entirely to questionable assumptions in the derivation of the structure factor above. It may also be that a slight change in the values assumed for the radii of the compound helixes would change the

Table 15 - Comparison of calculated and observed intensities of reflections for feather keratin

h · k · l	$\frac{\sin\theta}{\lambda}$	m	F.F*	A_l	B_l	intensity calc.	intensity obs.
1 · 0 · 0	0.015	6	$(A_o - B_o)^2$	80	65.5	1260	s
2 · 0 · 0	0.029	6	$(A_o - B_o)^2$	-32.5	13.0	12400	vw
3 · 0 · 0	0.045	6	$(A_o + 2B_o)^2$	20.0	-18.5	1730	sm
4 · 0 · 0	0.057	6	$(A_o - B_o)^2$	43.6	-16.5	21700	m
5 · 0 · 0	0.073	6	$(A_o - B_o)^2$	3.50	-2.00	182	absent
6 · 0 · 0 4 · 3 · 0	0.086	6 12	$(A_o + 2B_o)^2$ $(A_o - B_o)^2$	-1.00	3.00	342	w
7 · 0 · 0 4 · 4 · 0 5 · 3 · 0	0.103	6 12 6	$(A_o - B_o)^2$ $(A_o + 2B_o)^2$ $(A_o - B_o)^2$	-2.25	-0.50	119	m
8 · 0 · 0 6 · 3 · 0	0.110	6 12	$(A_o - B_o)^2$ $(A_o + 2B_o)^2$	-4.63	-0.75	541	m
9 · 0 · 0 7 · 3 · 0	0.129	6 12	$(A_o + 2B_o)^2$ $(A_o - B_o)^2$	0.25	2.88	299	vw
10 · 0 · 0	0.144	6	$(A_o - B_o)^2$	-2.50	2.75	165	w
11 · 0 · 0	0.155	6	$(A_o - B_o)^2$	-10.0	1.13	740	w
13 · 0 · 0 7 · 8 · 0 6 · 9 · 0	0.189	6 12 12	$(A_o - B_o)^2$ $(A_o - B_o)^2$ $(A_o + 2B_o)^2$	-1.50	-2.00	364	absent
15 · 0 · 0 6 · 11 · 0	0.219	6 12	$(A_o + 2B_o)^2$ $(A_o - B_o)^2$	-2.75	1.38	204	vw
1 · 0 · 1	0.016	6	$A_1^2 + \sqrt{3}A_1B_1 + 3B_1^2$	0.22	3.50	228	vw
2 · 0 · 1	0.029	6	$A_1^2 + \sqrt{3}A_1B_1 + 3B_1^2$	5.00	11.75	3250	vm
3 · 0 · 1	0.044	6	A_1^2	22.0	20.8	2900	absent

Table 15 - Comparison of calculated and observed intensities of reflections for feather keratin (continued)

h · k · l	$\frac{\sin\theta}{\lambda}$	m	F · F*	A_l	B_l	intensity calc.	intensity obs.
1 · 0 · 2	0.019	6	$A_2^2+A_2B_2+B_2^2$	0.00	0.05	0.02	wm
2 · 0 · 2	0.031	6	$A_2^2-A_2B_2+B_2^2$	0.00	0.25	0.75	w
3 · 0 · 2	0.046	6	$A_2^2+4A_2B_2+4B_2^2$	0.06	1.38	11.4	sm
4 · 0 · 2	0.056	6	$A_2^2-A_2B_2+B_2^2$	0.50	2.88	42.4	sm
5 · 0 · 2	0.074	6	$A_2^2+A_2B_2+B_2^2$	1.30	4.13	145	absent
1 · 0 · 3	0.021	6	$A_3^2-\sqrt{3}A_3B_3+3B_3^2$	0.00	0.01	0.00	absent
1 · 0 · 4	0.025	6	$A_4^2-A_4B_4+B_4^2$	0.00	0.00	0.00	wm
2 · 0 · 4	0.036	6	$A_4^2+A_4B_4+B_4^2$	0.00	0.00	0.00	w
3 · 0 · 4	0.050	6	$A_4^2-4A_4B_4+4B_4^2$	0.00	0.00	0.00	wm
4 · 0 · 4	0.061	6	$A_4^2+A_4B_4+B_4^2$	0.00	0.00	0.00	m
5 · 0 · 4	0.076	6	$A_4^2-A_4B_4+B_4^2$	0.00	0.01	0.00	absent
1 · 0 · 5	0.030	6	$A_5^2+\sqrt{3}A_5B_5+3B_5^2$	0.00	0.00	0.00	wm
2 · 0 · 5	0.039	6	$A_5^2+\sqrt{3}A_5B_5+3B_5^2$	0.00	0.00	0.00	absent
1 · 0 · 6	0.035	6	$A_6^2+A_6B_6+B_6^2$	0.00	0.00	0.00	w
2 · 0 · 6	0.043	6	$A_6^2-A_6B_6+B_6^2$	0.00	0.00	0.00	absent
3 · 0 · 6	0.054	6	$A_6^2+4A_6B_6+4B_6^2$	0.00	0.00	0.00	wm

arguments of the Bessel functions in the structure factors sufficiently to cause improved agreement between prediction and observation.

F) Miscellaneous data on feather keratin.

1) Evidence for cylindrical symmetry of structure.

Fiber photographs of feather keratin taken with the surface of the rachis both perpendicular and parallel to the x-ray beam showed no difference in the positions or intensities of the reflections. The only evident effect was the broadening of the very strong 23.7 A. meridional reflection in the photograph taken with the surface of the rachis perpendicular to the beam. This was probably due to the fact that the fiber was of greater thickness parallel to this surface than perpendicular to it, introducing a higher degree of disorientation perpendicular to the x-ray beam in the first instance. Hence there is no evidence that the crystallites of feather keratin are oriented relative to the plane of the surface of the rachis.

2) Evidence for the presence of the 1.5 A. meridional reflection.

A prominent meridional reflection at about 1.5 A. has been found in the diffraction patterns of many α proteins and some synthetic polypeptides. It is considered to be good

evidence for the existence of the Pauling-Corey 3.7-residue helix in these substances, since 1.5 A. corresponds to the axial length of one residue of the helix. Perutz (61) has found this spacing in poly-γ-benzyl-L-glutamate, horse hair, porcupine quill, muscle fibers and hemoglobin. It has also been found in poly-γ-methyl-L-glutamate by H. Yakel (52). Perutz, however, failed to find the 1.5 A. reflection when he examined sea-gull feather keratin, and recently Bamford and coworkers (62) have reported that the 1.5 A. reflection is absent from diffraction photographs of swan quill. These investigators failed to find a reflection at 1.16 A. on the meridian, which is prominent, they report, in the diffraction patterns of β proteins and polypeptides.

On the other hand, Dr. John Leonard at this laboratory has obtained fiber photographs of feather keratin which show a diffuse but rather strong meridional reflection at 1.5 A. An attempt was made, therefore, to confirm his results.

The feather keratin fiber which had been employed to obtain figure 27 was mounted horizontally in the 10 cm. camera, with the fiber axis inclined to the x-ray beam at an angle of 59.1°. The fiber was allowed to oscillate through 6 degrees about this position. The radiation was nickel-filtered copper K_α and an exposure time of 48 hours was used. The camera was continuously flushed with helium. Examination of the resulting photograph revealed an extremely weak and rather diffuse arc at 1.47 A. on the meridian,

accompanied by at least two additional fainter arcs nearby. It is felt that the 1.47 A. reflection was too weak to be considered as conclusive evidence for the presence of α helixes in feather keratin, although it is possible that it is a true α-helix reflection which has been weakened by interference due to the arrangement of neighboring helixes. On the other hand, it is possible to explain the result (and that of Dr. Leonard) as due to incomplete removal of the surface layer of α keratin from the feather keratin specimen.

3) The powder pattern of feather keratin.

Riley and Arndt (63), (64), (65) have found that the three recognized classes of proteins, the alpha, beta and collagen classes, can be distinguished by differences between the x-ray diffraction patterns given by the proteins in the amorphous powdered state. Specifically, the α proteins show pronounced intensity peaks at values of $\frac{\sin \theta}{\lambda}$ corresponding to spacings of 10 A. and 4.5 A., a low maximum at 2.4 A. and a diffuse band at about 1.2 A. The collagen (and gelatin) class shows a sharp peak at 12 A. and at 2.85 A., and a broad maximum at 4.45 A. Chopped silk, a β protein, shows a radically different pattern containing details which are absent from the patterns of the other protein types.

In view of the indefinite place of feather keratin in

the above classification scheme, it was thought desirable to determine whether the x-ray powder pattern for this protein would show the characteristics of any particular class of proteins.

The required amorphous powder was obtained by pressing sea-gull feather quill against a rapidly turning power-operated rotary file. The resulting dust was drawn into a filter attached to an ordinary vacuum cleaner. The powder was compressed into a briquette approximately 27 x 14 x 2 mm. and the powder diagram obtained from it with the General Electric XRD-3 x-ray spectrometer. This diagram is compared with a powder diagram of fibrinogen in figure 29. The latter was obtained in a similar manner by Dr. R. E. Marsh. It is evident that there are peaks at $2\theta = 19.5^{\circ}$ in both diagrams, corresponding to the α-protein spacing of 4.5 A. The maximum at about $2\theta = 9^{\circ}$ in fibrinogen, corresponding to the 10 A. spacing of the α proteins, appears to be much less pronounced in feather keratin and displaced somewhat toward a higher value of 2θ.

In general, the x-ray scattering from powdered feather keratin shows the characteristics of that from the α proteins which have been examined at this laboratory, although the amplitudes of the maxima for feather keratin are lower than for the other proteins. Whether or not a structure consisting of α helixes is the only one which would give the diagram observed for powdered feather keratin is not known. However,

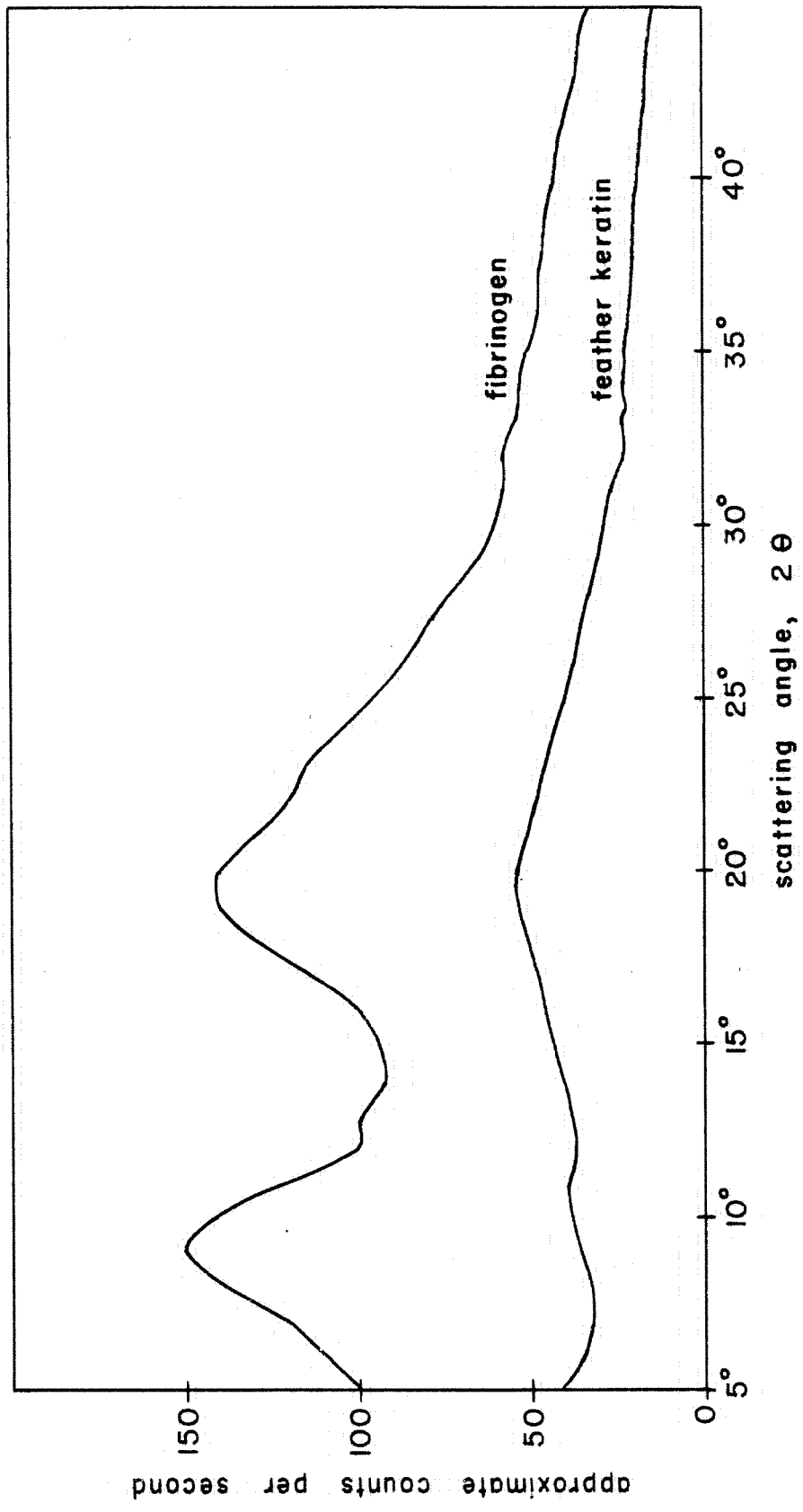

FIGURE 29

X-RAY SCATTERING

FOR POWDERED FIBRINOGEN AND FEATHER KERATIN

it seems fairly certain that on the basis of these data feather keratin is not to be classified with the β proteins and is probably similar to the class of α proteins in structure.

PART V - REFERENCES

1. P. Debye, J. Appl. Physics, 15, 338 (1944).

2. Lord Rayleigh, Phil. Mag., 41, 107, 274, 447 (1871).

3. A. Einstein, Ann. Physik, 33, 1275 (1910).

4. P. Doty and J. T. Edsall, Advances in Protein Chemistry, Academic Press Inc., New York, N. Y., 6, 37 (1951).

5. B. H. Zimm, R. S. Stein and P. Doty, Polymer Bull., 1, 90 (1945).

6. G. Oster, Chem. Rev., 43, 319 (1948).

7. J. T. Edsall and W. B. Dandliker, Fortschr. Chem. Forsch., 2, 1 (1951).

8. B. A. Brice, M. Halwer and R. Speiser, J. Opt. Soc. Am., 40, 768 (1950).

9. B. H. Zimm, J. Chem. Phys., 15, 1093 (1948).

9'. C. I. Carr and B. H. Zimm, J. Chem. Phys., 18, 1616 (1950).

10. P. Doty and R. F. Steiner, J. Chem. Phys., 18, 1211 (1950).

11. F. Buecha, P. Debye and W. M. Cashin, J. Chem. Phys., 19, 803 (1951).

12. H. Sheffer and J. C. Hyde, Can. J. Chem., 30, 817 (1952).

13. J. J. Hermans and S. Levinson, J. Opt. Soc. Am., 41 460 (1951).

14. W. F. H. M. Mommaerts, J. Colloid Sci., 7, 71 (1952).

15. J. Cabannes, "La Diffusion Moleculaire de la Lumiere", Presses Universitaires de France, Paris, France (1929).

16. R. S. Bear, Advances in Protein Chemistry, Academic Press Inc., New York, N. Y., 7, 69 (1952).

17. R. B. Corey and L. Pauling, Proc. Roy. Soc. (London), B 141, 30 (1952).

18. R. Cohen and R. Bear, J. Am. Chem. Soc., 75, 2783 (1953).

19. J. T. Randall, R. D. B. Fraser and A. C. T. North, Proc. Roy. Soc. (London), B 141, 621 (1952).

20. F. O. Schmitt, J. Gross and J. H. Highberger, Proc. Nat. Acad. Sci. U. S., 39, 459 (1953).

21. J. Thaureaux, Bull. soc. chim. biol., 27, 327 (1945).

22. S. E. Bresler, P. A. Finogenov and S. Y. Frenkel, Doklady Akad. Nauk S. S. S. R., 72, 555 (1950).

23. T. P. Salo, J. Am. Chem. Soc., 71, 2276 (1949).

24. H. Noda and R. W. G. Wyckoff, Biochim. et Biophys. Acta, 7, 494 (1951).

25. J. R. Loofbourow, B. S. Gould and I. W. Sizer, Arch. Biochem., 22, 406 (1949).

26. T. P. Salo, Arch. Biochem., 24, 25 (1949).

27. P. Doty and R. F. Steiner, J. Chem. Phys., 20, 85 (1952).

28. A. E. Alexander and P. Johnson, "Colloid Science", Oxford University Press, London (1949).

29. P. Doty and B. H. Bunce, J. Am. Chem. Soc., 74, 5029 (1952).

30. K. O. Pedersen, "The Ultracentrifuge", Oxford University Press, London, Part I, B (1940).

31. S. J. Singer and D. H. Campbell, J. Am. Chem. Soc., 74, 1794 (1952).

32. R. H. Ewart, C. P. Roe, P. Debye and J. R. McCartney, J. Chem. Phys., 14, 687 (1946).

33. P. Doty and S. Katz, Abstracts, Chicago Meeting A. C. S., September 1950.

34. K. H. Gustavson, Advances in Protein Chemistry, Academic Press Inc., New York, N. Y., 5, 253 (1949).

35. B. A. Brice, G. C. Nutting and M. Halwer, J. Am. Chem. Soc., 75, 824 (1953).

36. T. Svedberg, "The Ultracentrifuge", Oxford University Press, London, Part I, A (1940).

37. H. A. Scheraga and L. Mandelkern, J. Am. Chem. Soc., 75, 179 (1953).

38. B. R. Leonard, J. W. Anderegg, P. Kaesberg, S. Shulman and W. W. Beeman, J. Chem. Phys., 19, 793 (1951).

39. J. W. Anderegg, W. W. Beeman and S. Shulman, Phys. Rev., 37, 186 (1952).

40. J. Pouradier and A. M. Venet, J. chim. phys., 47, 11 (1950).

41. R. H. Blaker, Thesis, California Institute of Technology (1950).

42. P. Doty, Abstracts, Los Angeles Meeting A. C. S., March 1953.

43. G. Scatchard, J. L. Oncley, J. W. Williams and A. Brown, J. Am. Chem. Soc., 66, 1980 (1944).

44. L. Pauling and R. B. Corey, Nature, 171, 59 (1953).

45. W. T. Astbury, Ann. Repts. on Progr. Chem. (Chem. Soc. London), 322 (1931).

46. W. T. Astbury and T. C. Marwick, Nature, 130, 309 (1932).

47. R. B. Corey and R. W. G. Wyckoff, J. Biol. Chem., 114, 407 (1936).

48. W. T. Astbury and A. Street, Phil. Trans. Roy. Soc. (London), A 230, 75 (1931).

49. W. T. Astbury and R. Lomax, Nature, 133, 795 (1934).

50. W. T. Astbury, S. V. Perry, R. Reed and L. C. Spark, Biochim. et Biophys. Acta, 1, 379 (1947).

51. L. Pauling and R. B. Corey, Proc. Nat. Acad. Sci. U. S., 37, 256 (1951).

52. L. Pauling and R. B. Corey, Proc. Roy. Soc. (London), B 141, 21 (1953).

53. K. M. Rudall, Biochim. et Biophys. Acta, 1, 549 (1947).

54. W. T. Astbury and F. O. Bell, Tabulae Biologicae, 17, 90 (1939).

55. R. S. Bear, J. Am. Chem. Soc., 66, 2043 (1944).

56. K. M. Rudall, Progr. Biophys. and Biophys. Chem., Academic Press Inc., New York, N. Y., 1, 39 (1950).

57. L. Pauling, R. B. Corey and H. R. Branson, Proc. Nat. Acad. Sci. U. S., 37, 205 (1951).

58. B. W. Low, "The Proteins", Edited by H. Neurath and K. Bailey, Academic Press Inc., New York, N. Y., Vol. I, Part A, p. 235 (1953).

59. W. Cochran, F. H. C. Crick and V. Vand, Acta Cryst., 5, 581 (1952).

60. L. Pauling and R. B. Corey, Proc. Nat. Acad. Sci. U. S., 37, 235 (1951).

61. M. F. Perutz, Nature, 167, 1053 (1951).

62. C. H. Bamford, L. Brown, A. Elliott, W. E. Hanby and I. F. Trotter, Nature, 171, 1149 (1953).

63. D. P. Riley and U. W. Arndt, Proc. Roy. Soc. (London), B 141, 93 (1953).

64. D. P. Riley and U. W. Arndt, Nature, 169, 138 (1952).

65. D. P. Riley and U. W. Arndt, Nature, 171, 144 (1953).

PART VI - PROPOSITIONS

1. The relation connecting the contact angle of a liquid on a solid surface and the surface tensions of the phase interfaces involved is usually "proved" by means of a vector diagram of the acting surface forces. The relation may be written

$$\cos \theta = \frac{\gamma_{sg} - \gamma_{ls}}{\gamma_{lg}}$$

where θ is the angle of contact between the liquid and the solid, γ_{ij} is the surface tension of the interface between phases i and j, and s, g, and l represent the solid, gaseous and liquid phases respectively.

It is proposed that sufficient conditions for the proof of this equation by thermodynamic methods are that the liquid be incompressible and have the shape of a droplet with the form of a spherical segment.

It is further suggested that it may be possible to prove that these conditions are also necessary in order that the above relation be rigorously valid.

2. Sheffer and Hyde (1) have given a correction to be applied to light-scattering intensities when the incident beam is partially reflected at the exit face of the light-scattering cell. The corrected intensity of scattering is given by them as

$$I(\theta) = i(\theta) - R\, i(180 - \theta)$$

where $I(\theta)$ is the corrected scattering intensity at the angle θ, $i(\theta)$ is the apparent scattering intensity at the same angle, R is the fraction of the incident beam intensity reflected at the glass-air interface, and $i(180 - \theta)$ is the apparent scattering intensity at the angle supplementary to θ. The authors state that this is an approximation which neglects "second order" terms.

It is proposed that if multiple reflection of the incident beam is taken into account, the above equation is the exact solution for the corrected scattering intensity at the angle θ.

3. An amino-acid analysis of feathers reported by Graham, Waitkoff and Hier (2) shows that there are about 68 cysteine residues in 10^5 grams of feather keratin. With an average residue weight assumed to be 117, this analysis indicates a proportion of one cysteine per twelve residues.

Rudall (3) has taken x-ray diffraction photographs of feather keratin which had been treated with a solution of mercuric acetate. He reports that the intensity of the meridional reflection at 11.9 A. is enhanced by this treatment. Apparently this is the only meridional reflection thus affected.

W. L. Hughes has demonstrated (4) that mercuric ion is preferentially bound to the -SH groups of a protein

molecule.

In view of the above facts, and on the basis of the assumption that the cysteine residues of feather keratin are arranged along the fiber axis in a regular sequence, it is proposed that the maximum length per residue along the fiber axis is about 1 A. This suggests that the polypeptide chains in feather keratin are in a highly folded configuration.

4. The hydrodynamic properties of aqueous sucrose solutions have been interpreted on the basis of approximately spherical molecules with attached water of solvation (5). For example, Gosting and Morrison (6) state that the increased intrinsic viscosity of such a solution at lower temperatures is probably due to an increased solvation of the sucrose molecules, causing their effective specific volume to become greater.

If it is thus permissible to interpret the hydrodynamic behavior of solutions of small molecules in terms of a suspension of equivalent hydrodynamic ellipsoids in a continuous medium, the diffusion and viscosity data of Gosting and Morris may be treated in accordance with the suggestions of Scheraga and Mandelkern (7) for the treatment of similar data on protein solutions. The following table shows the axial ratios and specific volumes of the equivalent hydrodynamic ellipsoids thus obtained at two temperatures. The partial specific volumes of sucrose in water, also taken

from the data of Gosting and Morris, are included for comparison.

temperature, °C.	24.95	1.0
axial ratio	7	8
specific volume	0.29	0.28
$\bar{V}$ of sucrose	0.618	0.607

It is proposed, therefore, that the effective specific volume of the sucrose molecules in aqueous solution actually decreases slightly on lowering the temperature, and that if the above method of treatment is to be used the greater intrinsic viscosity at the lower temperature must be attributed to an increase in the axial ratio of the equivalent hydrodynamic ellipsoid representing the sucrose molecules.

Attention is also called to the fact that the effective volume per gram of the sucrose is less than one-half of the actual specific volume of sucrose in aqueous solution. This effect is probably due to the inappropriateness of the assumption that the solvent is a continuous medium.

5. Studies of the binding of metal cations to bovine serum albumin (8) and human serum albumin (9) have indicated that binding occurs at the imidazole groups of histidine residues, with one metal ion binding to each such group. The metals which have been thus far studied are copper, zinc, cadmium and lead.

It is proposed that the small-angle x-ray scattering of an albumin solution containing metal ions would show intensity maxima at spacings corresponding to the distances between imidazole groups in the molecule, providing that all the molecules have approximately the same configuration. If this is indeed the case, it may also be possible to study the swelling undergone by albumin molecules upon dissolving by comparing the result with powder diagrams given by the dry metal-protein complex. Furthermore, changes of configuration with denaturation could be investigated by examining the small-angle scattering from the heated solutions.

6. It is proposed that the energy of the hydrogen bonds in water can be approximately computed by considering the various physical processes occurring during the sublimation of ice, including the O-H bond shortening. The energies for all the processes are summed and equated to the energy of sublimation of ice. Reasonable values for the energies involved give a hydrogen bond energy of 4½ k. cal/mole, in agreement with the known value.

7. Pouradier and Venet (10) have found that the temperature at which a gelatin gel begins to melt depends upon the molecular weight of the gelatin. They report that fractions with molecular weights ranging from 46,000 to 207,000 have gel-fusion points of from 15.5° C. to 27.6° C.

It is proposed, therefore, that it may be possible to separate gelatin into molecular weight fractions by means of a partial gelation procedure. For example, a gelatin solution could be slowly cooled to the point at which the first signs of gelation were observed, then passed through a sintered-glass filter. The gel remaining on the filter should be composed of molecules with higher than average molecular weight.

This method, if workable, would have the advantage of avoiding the possibility of degradation at the higher temperatures which are used in other fractionation procedures.

8. An interesting and instructive experiment which might be performed by the freshman class would be to determine the molecular weight of sulfur and thus show that the molecule contains eight sulfur atoms. A suitable method for doing this would be to measure the depression of the freezing point of β-naphthol caused by a known molal concentration of sulfur dissolved in the melted compound. Since $K_f = 11.25$ for β-naphthol (11), about 200 mg. of sulfur dissolved in one gram of this compound should depress its freezing point by 8.8° C., reducing it from 122.5° C. to 113.7° C. (11), an easily measurable decrease. This concentration of sulfur is well within the limit of its solubility in β-naphthol, which is about 340 mg. of sulfur per gram of β-naphthol at 118° C. (12).

9. M. A. Lauffer and coworkers have determined the sedimentation constants of several proteins in solutions of varying sucrose concentration (13), (14), (15). By extrapolating the plot of ηs versus d to $\eta s = 0$ (where η is the solution viscosity, s is the sedimentation constant of the protein and d is the solution density) they obtain the effective density of the sedimenting molecule. The reciprocal of this effective density is always larger than the partial specific volume of the protein. Assuming this effect to be due to the preferential binding of water to the protein molecules, they compute the amount of water bound per gram of protein.

It is proposed that the assumption that water is bound to the protein in preference to sucrose is sufficiently doubtful to warrant its investigation before accepting this method for determining the solvation of proteins in solution. A study of the light scattering of the proteins in sucrose solutions is proposed as offering a suitable method for such an investigation. The interaction of nitrocellulose with various solvents was determined by Blaker and Badger (16) using this technique.

10. It is proposed that there is a simple, intuitive proof for Euler's relation connecting the number of faces, edges and vertices of a solid figure bounded by planes,

$$F = E - V + 2$$

It is based on the fact that, in order to add a face to such a figure, a new plane must be cut in such a way that parts of all the original planes remain as boundaries of the figure. To do so one must remove n vertices but only n - 1 edges. Then, since this relation holds for the simplest such figure, it also holds for any more complicated figure that can be carved from the simple one.

REFERENCES FOR PROPOSITIONS

1. H. Sheffer and J. C. Hyde, Can. J. Chem., 30, 817 (1952).

2. C. E. Graham, H. K. Waitkoff and S. W. Hier, J. Biol. Chem., 177, 529 (1949).

3. K. M. Rudall, Biochim. et Biophys. Acta, 1, 549 (1947).

4. W. L. Hughes, Jr., Cold Spring Harbor Symposia on Quantitative Biology, 14, 79 (1950).

5. A. E. Alexander and P. Johnson, "Colloid Science", Oxford University Press, London, p. 361 (1949).

6. L. J. Gosting and M. S. Morris, J. Am. Chem. Soc., 71, 1998 (1949).

7. H. A. Scheraga and L. Mandelkern, J. Am. Chem. Soc., 75, 179 (1953).

8. C. Tanford, J. Am. Chem. Soc., 74, 211 (1952).

9. F. R. N. Gurd and D. S. Goodman, J. Am. Chem. Soc., 74, 670 (1952).

10. J. Pouradier and A. M. Venet, J. chim. phys., 47, 391 (1950).

11. N. A. Lange, "Handbook of Chemistry", Handbook Publishers, Inc., Sandusky, Ohio, 6 th edition, p. 1366 (1946).

12. A. Seidell, "Solubilities of Inorganic and Metal-Organic Compounds", D. Van Nostrand Company, Inc., New York, N. Y., 3 rd edition, volume I, p. 1452 (1940).

13. M. A. Lauffer, N. W. Taylor and C. C. Wunder, Arch. Biochem. and Biophys., 40, 453 (1952).

14. M. A. Lauffer and N. W. Taylor, Arch. Biochem and Biophys., 42, 102 (1953).

15. M. A. Lauffer and N. W. Taylor, Arch. Biochem and Biophys., 43, 374 (1953).

16. R. H. Blaker and R. M. Badger, J. Am. Chem. Soc., 72, 3129 (1950).